# *ACKNOWLEDGEMENTS*

*The research work that I carried out in the department of Physics, Bangladesh University of Engineering & Technology (BUET), Dhaka, Bangladesh, is the result of lots of supports, collaboration, encouragement and friendship during the time while the research work was performed.*

*First of all I express all my admiration and devotion to the almighty Allah- Rabbul Alamin, the most beneficial who has enabled me to perform this research work and to submit this thesis.*

*I express my profound gratitude to my honourable supervisor Dr. A.K.M. Akther Hossain, Professor and Head, Department of Physics, BUET, for his constant direction, constructive criticism and inspiration in pursuing the whole investigation of the present research. Words are always insufficient to express his working capacities and unending enthusiasm for scientific rigorousness for innovative investigations. This always becomes the everlasting source of inspiration for his students. I am also deeply grateful to him for his kind permission to do this work. I am also grateful to BUET authority for providing the financial grant for this research.*

*I would like to express my gratitude to Professor Md. Abu Hashan Bhuiyan, Professor Dr. Nazma Zaman, Professor Dr. Jiban Podder, Professor Dr. Feroz Alam Khan, Professor Dr. Md. Mostak Hossain, Dr. Afia Begum, Dr. Rafi Uddin, Dr. Md. Forhad Mina, and all other teachers of Physics Department, for their cooperation.*

*I would like to give special thank to Dr. Bertrand Vilquin, Lyon Institute of Nanotechnology, France, for using their X-ray Diffractometer. I am grateful to the authority of BCSIR, Bangladesh especially Mr.Syed Farid Uddin Farhad, Industrial Physics Division, for help me measuring Frequency dependent permeability by using their Impedence Analyzer. I wish to thank specially my senior research workers and Ph.D students of the department of Physics, Hamidur Rahman Khan, Md. Farhad Alam, Md M.M. Shah and others for their cooperation throughout the study. I am also grateful to my friend and coresearcher Maruf Morshed (Department of the Physics, BUET) for his inspiration and encouragement. I am thankful to Mr. Khurshed Alam (Lecturer of Physics, BUET) for his kind help. I also gratefully acknowledge the wishes of my younger researchers Anis Munshi and Arif for their constant support.*

*Ultimately, I would mention a very special gratefulness for the moral support and sustaining inspiration provided by the members of my family. This dissertation would never have been possible without their love and affection.*

*The Author*

*Md. Abdur Rahman*

**pdfMachine**
**Is a pdf writer that produces quality PDF files with ease!**
Produce quality PDF files in seconds and preserve the integrity of your original documents. Compatible across nearly all Windows platforms, if you can print from a windows application you can use pdfMachine.
Get yours now!

M. Phil. Thesis

MD. ABDUR RAHMAN

BUET 2010

# STUDY OF MAGNETIC PROPERTIES OF $Li_xMg_{0.4}Ni_{0.6-2x}Fe_{2+x}O_4$ FERRITES


**MD. ABDUR RAHMAN**

**DEPARTMENT OF PHYSICS**

**BANGLADESH UNIVERSITY OF ENGINEERING & TECHNOLOGY**

**DHAKA 1000, BANGLADESH**


**November- 2010**


**pdfMachine - is a pdf writer that produces quality PDF files with ease!**
**Get yours now!**
"Thank you very much! I can use Acrobat Distiller or the Acrobat PDFWriter but I consider your product a lot easier to use and much preferable to Adobe's" A.Sarras - USA

M. Phil. Thesis

MD. ABDUR RAHMAN

BUET 2010

# STUDY OF MAGNETIC PROPERTIES OF $Li_xMg_{0.4}Ni_{0.6-2x}Fe_{2+x}O_4$ FERRITES


**MD. ABDUR RAHMAN**

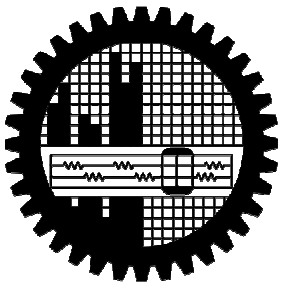

**DEPARTMENT OF PHYSICS**

**BANGLADESH UNIVERSITY OF ENGINEERING & TECHNOLOGY**

**DHAKA 1000, BANGLADESH**


**November- 2010**


**pdfMachine - is a pdf writer that produces quality PDF files with ease!**
**Get yours now!**
"Thank you very much! I can use Acrobat Distiller or the Acrobat PDFWriter but I consider your product a lot easier to use and much preferable to Adobe's" A.Sarras - USA

# STUDY OF MAGNETIC PROPERTIES OF $Li_xMg_{0.4}Ni_{0.6-2x}Fe_{2+x}O_4$ FERRITES


**SUBMITTED BY**

**Md. Abdur Rahman**


*A Dissertation Submitted to the Department of Physics, Bangladesh University of Engineering & Technology, Dhaka, in Partial Fulfillment of the Requirement for the Degree of Master of Philosophy in Physics*


**EXAMINATION ROLL NO. : 040814004F**
**REGISTRATION NO. : 040814004**
**SESSION : April 2008**


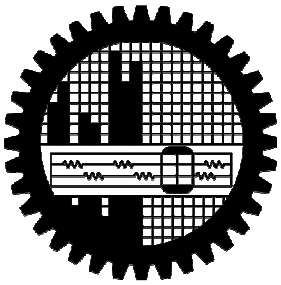


**DEPARTMENT OF PHYSICS**

**BANGLADESH UNIVERSITY OF ENGINEERING & TECHNOLOGY**

**DHAKA 1000, BANGLADESH**



**pdfMachine**
**A pdf writer that produces quality PDF files with ease!**
Produce quality PDF files in seconds and preserve the integrity of your original documents. Compatible across nearly all Windows platforms, simply open the document you want to convert, click "print", select the "Broadgun pdfMachine printer" and that's it! Get yours now!

# CHAPTER 1

# INTRODUCTION

## 1.1 Background of the Study

Spinel type ferrites are ceramic materials formed by reacting non-magnetic metal oxides to magnetic materials. According to their crystal structure, spinel-type ferrites are natural superlattices and have tetrahedral *A*-site and octahedral *B*-site in $AB_2O_4$ crystal structure. These materials show various magnetic properties depending on the chemical composition and cation distribution. Various cations can be placed in *A*-site and *B*-site to tune its magnetic properties. Depending on *A*-site and *B*-site cations, they can exhibit ferrimagnetic, antiferromagnetic, spin (cluster) glass, and paramagnetic behavior [1, 2]. Due to their remarkable magnetic and electric properties, these materials are subjects of intense theoretical and experimental investigation for technological application [2-4]. The polycrystalline spinel ferrites are widely used in many electronic devices. They are preferred because of their high permeability and saturation magnetization in the radio-frequency (RF) region, high electrical resistivity, mechanical hardness and chemical stability [5]. Ferrites are also useful to prevent and eliminate RF interference to audio systems [6]. Most other technologically useful magnetic materials such as iron and soft magnetic alloys have low electrical resistivity. This makes them difficult for applications at high frequencies. The low electrical resistivity of these materials allows eddy currents to flow within the materials themselves, thereby producing heat and waste energy [7-8].

In this thrust area of research on magnetic fine particles, lithium ferrite forms a very important group of materials. Lithium ferrite and mixed lithium ferrites have very high potential for microwave applications, especially as replacements for garnets, due to their low cost. The squareness of the hysteresis loop and superior temperature performance are other prominent advantages that have made them very promising candidates for application in microwave devices [9-11, 17, 27]. Effect of various substitutions in lithium ferrite exhibits very good relaxation and anisotropy properties than other type of ferrites [12, 13].

Studies on substituted *Li-Mg-Fe* spinels show that it can be useful in microwave applications having improved magnetic properties [14, 15]. Various researchers have

**pdfMachine**
**A pdf writer that produces quality PDF files with ease!**
Produce quality PDF files in seconds and preserve the integrity of your original documents. Compatible across nearly all Windows platforms, simply open the document you want to convert, click “print”, select the “Broadgun pdfMachine printer” and that’s it! Get yours now!

reported the study of *Ni* substitution which seems to enhance the magnetic properties as well [16-17] Besides studying on pure Lithium ferrite [9-11], *Li-Mg* and *Li-Ni* ferrite, many researchers have studied *Li-Zn* [18-19], *Li-Co* [20] and *Li-Ti* [21], *Li-Cd* [22], *Li-Cr*[23], *Li-Ce* [24] ferrites. However, no reports have been found in the literature so far about Li substituted $Li_xMg_{0.4}Ni_{0.6-2x}Fe_{2+x}O_4$ ferrites. In the present research the influence of *Li* substitution on structural and magnetic properties of $Li_xMg_{0.4}Ni_{0.6-2x}Fe_{2+x}O_4$ ferrites has been investigated.

## 1.2 Objectives of the Present Work

Ferrites are especially convenient for high frequency uses because of their high resistivity. The high frequency response of the complex permeability is therefore very useful in determining the convenient frequency range in which a particular ferrite material can be used. The mechanisms of eddy current losses and damping of domain wall motion can be understood from the relative magnitudes of the real and imaginary parts of the complex permeability. To understand these mechanisms the effect of composition and microstructure on the frequency response is very useful.

The main objectives of the present research are as follows:

- Preparation of various $Li_xMg_{0.4}Ni_{0.6-2x}Fe_{2+x}O_4$ (x=0.00, 0.05, 0.10, 0.15, 0.20, 0.25, 0.30) samples.
- Characterizations of crystalline structure, density, porosity and surface morphology (grain sizes) of the samples.
- Measurement of initial permeability as a function of frequency (300 *kHz*-110 *MHz*) for samples having various microstructures (e. g. grain size).
- Measurement of magnetization as a function of field, *M(H)*, at room temperature.

**pdfMachine**
**A pdf writer that produces quality PDF files with ease!**
Produce quality PDF files in seconds and preserve the integrity of your original documents. Compatible across nearly all Windows platforms, simply open the document you want to convert, click “print”, select the “Broadgun pdfMachine printer” and that’s it! Get yours now!

## 1.3 Outline of the Thesis

The summary of the thesis is as follows:

Chapter 1 of this thesis deals with the importance of ferrites and objectives of the present work.

Chapter 2 gives a brief overview of the materials, theoretical background as well as crystal structure of the spinel type ferrites.

Chapter 3 gives the details of the sample preparation and describes different measurement techniques that have been used in this research work.

Chapter 4 is devoted to the results of various investigations of the study and explanation of results in the light of existing theories.

The conclusions drawn from the overall experimental results and discussion are presented in Chapter 5.

## References:

[1] Peelamedu, R.,Grimes, C., Agrawal, D., and Roy, R., "Ultralow dielectric constant nickel-zinc ferrites using microwave sintering", J. Mater. Res., Vol-18(10), pp 2292-2295, 2003.

[2 Hossain, A. K. M. A., Mahmud, S. T., Seki, M., Kawai, T. and Tabata, H., "Structural, Electrical transport and Magnetic Properties of $Ni_{1-x}Zn_xFe_2O_4$", Journal of Magnetism and Magnetic Materials, Vol-312(1), pp 210-219, 2007.

[3] Valenzuela, R., "Magnetic Ceramics", Cambridge University Press, Cambridge, 1994.

[4] Schiessl, W., Potzel, W., Karzel H., Steiner, M. and Kalvius, G. M. ,"Magnetic properties of the $ZnFe_2O_4$ spinel", Physical Review B, Vol-53, No. 14, pp 9143-9152, 1996.

[5] Hasting, J. M. and Corliss, L. M., "An antiferromagnetic transition in zinc ferrite", Physical . Review., Vol-102, No. 6, pp 1460-1463, 1956.

[6] Hasting, J. M. and Corliss, L. M., "Neutron diffraction studies of zinc ferrite and nickel ferrite", Reviews of Modern Physics, Vol-25, No. 1, pp 114-118, 1953.

[7] Chukalkin, Yu. G. and Teplykh, A. E., "Magnetic state of nickel-zinc ferrites at high zinc concentrations", Physics of the Solid State, Vol-40, No. 8 , pp 1364-1365, 1998.

[8] Ahmed, M.A., Okasha, N., Salah L., "Influence of yttrium ions on the magnetic properties of Ni-Zn ferrites", Journal of Magnetism and Magnetic MaterialsVol-264, pp 241-250 ,2003.

[9] Argentina, G. M., and Baba, P.D., "Microwave Lithium Ferrites: An Overview", IEEE Transactions on Microwave Theory and Techniques, Vol - MTT-22, No. 6, pp 652-658, 1974.

**pdfMachine**
**A pdf writer that produces quality PDF files with ease!**
Produce quality PDF files in seconds and preserve the integrity of your original documents. Compatible across nearly all Windows platforms, simply open the document you want to convert, click "print", select the "Broadgun pdfMachine printer" and that's it! Get yours now!

[10] White , G.O. and Patton , C.E., "Magnetic Properties of Lithium Ferrite Microwave Materials", Journal of Magnetism and Magnetic Materials, Vol-9, pp 299, 1978.

[11] Andreev , N.M. and Kojoukharoff, V.I., "On some magnetic characteristics of a system of lithium ferrites for microwave applications", Journal of Magnetism and Magnetic Materials, Vol-54-57, No 3, pp 1605-1606, February 1986.

[12] Patton, C. E., Blankenbeckler, D. L., Brower, C. J., Dalton ,B. B. and Lucero, A. M., "Microwave Relaxation Properties of Substituted Lithium Ferrite", IEEE Transactions on Magnetics, Vol-17, Issue 6, pp 2976-2978, 1981.

[13] Brower, C. J. and Patton, C. E, "Determination of Anisotropy Field in Polycrystalline Lithium Ferrites from FMR linewidths", Journal of Applied Physics , Vol-53, pp 2104-2106, 1982.

[14] Kishan, P., Kumar, N., Prakash, C., Zaidi Z. H., "Studies on substituted *Li-Mg-Fe* spinels for microwave applications", Ferroelectrics Letters Section, Vol-18, Issue 3 & 4, pp 91-97, 1994.

[15] Widatallah, H.M., Johnson,C., Gismelseed, A. M., Al- Omari, I .A., Stewart, S. J., Al- Harthi, S.H., Thomas S. and Sitepu. H., "Structural and magnetic studies of nanocrystalline Mg-doped $Li_{0.5}Fe_{2.5}O_4$ particles prepared by mechanical milling", Journal of Physics D: Applied Physics, Vol-41, pp (165006)1-(165006) 10, 2008.

[16] Bhatu, S. S., Lakhani, V.K., Tanna, A.R., Vasoya , N. H., Buch, J.U., Sharma, P.U., Trivedi, U. N., Joshi ,H.H. and Modi ,K.B., "Effect of nickel substitution on structural, infrared and elastic properties of lithium ferrite", Indian Journal of Pure & Applied Physics, Vol-45, pp 597-608, 2007.

[17] Soibam I., Phanjoubam S., Prakash , C., "Magnetic and Mössbauer studies of Ni substituted Li-Zn ferrites", Journal of Magnetism and Magnetic Materials, Vol-321, pp 2779-2782, 2009

[18]. Patton, C. E., Edmonson , C.A., and Liu., Y. H., "Magnetic Properties of Lithium Zinc Ferrite", Journal of Applied Physics, Vol-53, pp 2431-2433, 1982.

[19] Rosenberg, M, Deppe, P., Dey, S., Janssen, U., Patton, C., Edmondson, C., "Mossbauer study of hyperfine field distributions and spin canting in lithium-zinc ferrites", IEEE Transactions on Magnetics, Vol-18, (6), pp 1616-1618, 1982.

[20] Abo El Ata, A.M., Attia, S.M., El Kony, D., Al-Hammadi, A. H., "Spectral, initial magnetic permeability and transport studies of $Li_{0.5-0.5x}Co_xFe_{2.5-0.5x}O_4$ spinel ferrite", Journal of Magnetism and Magnetic MaterialsVol-295, pp 28–36, 2005.

[21] Surzhikov, P., Pritulov, A. M., Ivanov, Yu. F., Shabardin, R. S., and Usmanov, R.U., "Electron-microscopic study of morphology and phase composition of Lithium-Titanium ferrites", Russian Physics Journal, Vol-44, No. 4, pp 420-423, 2001.

[22] Bellad, S. S. Watawe, S. C., Shaikh ,A.M., and Chougule, B. K., "Cadmium substituted high permeability lithium ferrite", Bulletin of Materials Science, Vol-23, No. 2, pp 83–85, 2000.

[23] Laishram, R., Prakash, C., "Magnetic properties of $Cr^{3+}$ substituted Li–Sb ferrites", Journal of Magnetism and Magnetic Materials., Vol-305, pp 35–39, 2006.

[24] Sun, C., Sun, K., "Preparation and microwave absorption properties of Ce-substituted lithium ferrite ", Solid State Communications, Vol-141, (5), pp 258-261, 2007.

**pdfMachine**
**A pdf writer that produces quality PDF files with ease!**
Produce quality PDF files in seconds and preserve the integrity of your original documents. Compatible across nearly all Windows platforms, simply open the document you want to convert, click "print", select the "Broadgun pdfMachine printer" and that's it! Get yours now!

# CHAPTER 1

# INTRODUCTION

## 1.1 Background of the Study

Spinel type ferrites are ceramic materials formed by reacting non-magnetic metal oxides to magnetic materials. According to their crystal structure, spinel-type ferrites are natural superlattices and have tetrahedral *A*-site and octahedral *B*-site in $AB_2O_4$ crystal structure. These materials show various magnetic properties depending on the chemical composition and cation distribution. Various cations can be placed in *A*-site and *B*-site to tune its magnetic properties. Depending on *A*-site and *B*-site cations, they can exhibit ferrimagnetic, antiferromagnetic, spin (cluster) glass, and paramagnetic behavior [1, 2]. Due to their remarkable magnetic and electric properties, these materials are subjects of intense theoretical and experimental investigation for technological application [2-4]. The polycrystalline spinel ferrites are widely used in many electronic devices. They are preferred because of their high permeability and saturation magnetization in the radio-frequency (RF) region, high electrical resistivity, mechanical hardness and chemical stability [5]. Ferrites are also useful to prevent and eliminate RF interference to audio systems [6]. Most other technologically useful magnetic materials such as iron and soft magnetic alloys have low electrical resistivity. This makes them difficult for applications at high frequencies. The low electrical resistivity of these materials allows eddy currents to flow within the materials themselves, thereby producing heat and waste energy [7-8].

In this thrust area of research on magnetic fine particles, lithium ferrite forms a very important group of materials. Lithium ferrite and mixed lithium ferrites have very high potential for microwave applications, especially as replacements for garnets, due to their low cost. The squareness of the hysteresis loop and superior temperature performance are other prominent advantages that have made them very promising candidates for application in microwave devices [9-11, 17, 27]. Effect of various substitutions in lithium ferrite exhibits very good relaxation and anisotropy properties than other type of ferrites [12, 13].

Studies on substituted *Li-Mg-Fe* spinels show that it can be useful in microwave applications having improved magnetic properties [14, 15]. Various researchers have

**pdfMachine**
**A pdf writer that produces quality PDF files with ease!**
Produce quality PDF files in seconds and preserve the integrity of your original documents. Compatible across nearly all Windows platforms, simply open the document you want to convert, click “print”, select the “Broadgun pdfMachine printer” and that’s it! Get yours now!

reported the study of *Ni* substitution which seems to enhance the magnetic properties as well [16-17] Besides studying on pure Lithium ferrite [9-11], *Li-Mg* and *Li-Ni* ferrite, many researchers have studied *Li-Zn* [18-19], *Li-Co* [20] and *Li-Ti* [21], *Li-Cd* [22], *Li-Cr*[23], *Li-Ce* [24] ferrites. However, no reports have been found in the literature so far about Li substituted $Li_xMg_{0.4}Ni_{0.6-2x}Fe_{2+x}O_4$ ferrites. In the present research the influence of *Li* substitution on structural and magnetic properties of $Li_xMg_{0.4}Ni_{0.6-2x}Fe_{2+x}O_4$ ferrites has been investigated.

## 1.2 Objectives of the Present Work

Ferrites are especially convenient for high frequency uses because of their high resistivity. The high frequency response of the complex permeability is therefore very useful in determining the convenient frequency range in which a particular ferrite material can be used. The mechanisms of eddy current losses and damping of domain wall motion can be understood from the relative magnitudes of the real and imaginary parts of the complex permeability. To understand these mechanisms the effect of composition and microstructure on the frequency response is very useful.

The main objectives of the present research are as follows:

- Preparation of various $Li_xMg_{0.4}Ni_{0.6-2x}Fe_{2+x}O_4$ (x=0.00, 0.05, 0.10, 0.15, 0.20, 0.25, 0.30) samples.
- Characterizations of crystalline structure, density, porosity and surface morphology (grain sizes) of the samples.
- Measurement of initial permeability as a function of frequency (300 *kHz*-110 *MHz*) for samples having various microstructures (e. g. grain size).
- Measurement of magnetization as a function of field, *M(H)*, at room temperature.

**pdfMachine**
**A pdf writer that produces quality PDF files with ease!**
Produce quality PDF files in seconds and preserve the integrity of your original documents. Compatible across nearly all Windows platforms, simply open the document you want to convert, click “print”, select the “Broadgun pdfMachine printer” and that’s it! Get yours now!

## 1.3 Outline of the Thesis

The summary of the thesis is as follows:

Chapter 1 of this thesis deals with the importance of ferrites and objectives of the present work.

Chapter 2 gives a brief overview of the materials, theoretical background as well as crystal structure of the spinel type ferrites.

Chapter 3 gives the details of the sample preparation and describes different measurement techniques that have been used in this research work.

Chapter 4 is devoted to the results of various investigations of the study and explanation of results in the light of existing theories.

The conclusions drawn from the overall experimental results and discussion are presented in Chapter 5.

## References:

[1] Peelamedu, R.,Grimes, C., Agrawal, D., and Roy, R., "Ultralow dielectric constant nickel-zinc ferrites using microwave sintering", J. Mater. Res., Vol-18(10), pp 2292-2295, 2003.

[2 Hossain, A. K. M. A., Mahmud, S. T., Seki, M., Kawai, T. and Tabata, H., "Structural, Electrical transport and Magnetic Properties of $Ni_{1-x}Zn_xFe_2O_4$", Journal of Magnetism and Magnetic Materials, Vol-312(1), pp 210-219, 2007.

[3] Valenzuela, R., "Magnetic Ceramics", Cambridge University Press, Cambridge, 1994.

[4] Schiessl, W., Potzel, W., Karzel H., Steiner, M. and Kalvius, G. M. ,"Magnetic properties of the $ZnFe_2O_4$ spinel", Physical Review B, Vol-53, No. 14, pp 9143-9152, 1996.

[5] Hasting, J. M. and Corliss, L. M., "An antiferromagnetic transition in zinc ferrite", Physical . Review., Vol-102, No. 6, pp 1460-1463, 1956.

[6] Hasting, J. M. and Corliss, L. M., "Neutron diffraction studies of zinc ferrite and nickel ferrite", Reviews of Modern Physics, Vol-25, No. 1, pp 114-118, 1953.

[7] Chukalkin, Yu. G. and Teplykh, A. E., "Magnetic state of nickel-zinc ferrites at high zinc concentrations", Physics of the Solid State, Vol-40, No. 8 , pp 1364-1365, 1998.

[8] Ahmed, M.A., Okasha, N., Salah L., "Influence of yttrium ions on the magnetic properties of Ni-Zn ferrites", Journal of Magnetism and Magnetic MaterialsVol-264, pp 241-250 ,2003.

[9] Argentina, G. M., and Baba, P.D., "Microwave Lithium Ferrites: An Overview", IEEE Transactions on Microwave Theory and Techniques, Vol - MTT-22, No. 6, pp 652-658, 1974.

**pdfMachine**
**A pdf writer that produces quality PDF files with ease!**
Produce quality PDF files in seconds and preserve the integrity of your original documents. Compatible across nearly all Windows platforms, simply open the document you want to convert, click "print", select the "Broadgun pdfMachine printer" and that's it! Get yours now!

[10] White , G.O. and Patton , C.E., "Magnetic Properties of Lithium Ferrite Microwave Materials", Journal of Magnetism and Magnetic Materials, Vol-9, pp 299, 1978.

[11] Andreev , N.M. and Kojoukharoff, V.I., "On some magnetic characteristics of a system of lithium ferrites for microwave applications", Journal of Magnetism and Magnetic Materials, Vol-54-57, No 3, pp 1605-1606, February 1986.

[12] Patton, C. E., Blankenbeckler, D. L., Brower, C. J., Dalton ,B. B. and Lucero, A. M., "Microwave Relaxation Properties of Substituted Lithium Ferrite", IEEE Transactions on Magnetics, Vol-17, Issue 6, pp 2976-2978, 1981.

[13] Brower, C. J. and Patton, C. E, "Determination of Anisotropy Field in Polycrystalline Lithium Ferrites from FMR linewidths", Journal of Applied Physics , Vol-53, pp 2104-2106, 1982.

[14] Kishan, P., Kumar, N., Prakash, C., Zaidi Z. H., "Studies on substituted *Li-Mg-Fe* spinels for microwave applications", Ferroelectrics Letters Section, Vol-18, Issue 3 & 4, pp 91-97, 1994.

[15] Widatallah, H.M., Johnson,C., Gismelseed, A. M., Al- Omari, I .A., Stewart, S. J., Al- Harthi, S.H., Thomas S. and Sitepu. H., "Structural and magnetic studies of nanocrystalline Mg-doped $Li_{0.5}Fe_{2.5}O_4$ particles prepared by mechanical milling", Journal of Physics D: Applied Physics, Vol-41, pp (165006)1-(165006) 10, 2008.

[16] Bhatu, S. S., Lakhani, V.K., Tanna, A.R., Vasoya , N. H., Buch, J.U., Sharma, P.U., Trivedi, U. N., Joshi ,H.H. and Modi ,K.B., "Effect of nickel substitution on structural, infrared and elastic properties of lithium ferrite", Indian Journal of Pure & Applied Physics, Vol-45, pp 597-608, 2007.

[17] Soibam I., Phanjoubam S., Prakash , C., "Magnetic and Mössbauer studies of Ni substituted Li-Zn ferrites", Journal of Magnetism and Magnetic Materials, Vol-321, pp 2779-2782, 2009

[18]. Patton, C. E., Edmonson , C.A., and Liu., Y. H., "Magnetic Properties of Lithium Zinc Ferrite", Journal of Applied Physics, Vol-53, pp 2431-2433, 1982.

[19] Rosenberg, M, Deppe, P., Dey, S., Janssen, U., Patton, C., Edmondson, C., "Mossbauer study of hyperfine field distributions and spin canting in lithium-zinc ferrites", IEEE Transactions on Magnetics, Vol-18, (6), pp 1616-1618, 1982.

[20] Abo El Ata, A.M., Attia, S.M., El Kony, D., Al-Hammadi, A. H., "Spectral, initial magnetic permeability and transport studies of $Li_{0.5-0.5x}Co_xFe_{2.5-0.5x}O_4$ spinel ferrite", Journal of Magnetism and Magnetic MaterialsVol-295, pp 28–36, 2005.

[21] Surzhikov, P., Pritulov, A. M., Ivanov, Yu. F., Shabardin, R. S., and Usmanov, R.U., "Electron-microscopic study of morphology and phase composition of Lithium-Titanium ferrites", Russian Physics Journal, Vol-44, No. 4, pp 420-423, 2001.

[22] Bellad, S. S. Watawe, S. C., Shaikh ,A.M., and Chougule, B. K., "Cadmium substituted high permeability lithium ferrite", Bulletin of Materials Science, Vol-23, No. 2, pp 83–85, 2000.

[23] Laishram, R., Prakash, C., "Magnetic properties of $Cr^{3+}$ substituted Li–Sb ferrites", Journal of Magnetism and Magnetic Materials., Vol-305, pp 35–39, 2006.

[24] Sun, C., Sun, K., "Preparation and microwave absorption properties of Ce-substituted lithium ferrite ", Solid State Communications, Vol-141, (5), pp 258-261, 2007.

**pdfMachine**
**A pdf writer that produces quality PDF files with ease!**
Produce quality PDF files in seconds and preserve the integrity of your original documents. Compatible across nearly all Windows platforms, simply open the document you want to convert, click "print", select the "Broadgun pdfMachine printer" and that's it! Get yours now!

# CHAPTER 2

# LITERATURE REVIEW

## 2.1 Overview of the Materials

Ferrites commonly expressed by the general chemical formula $MeO.Fe_2O_3$, where *Me* represents divalent metals, first commanded the public attention when Hilpert (1909) focused on the usefulness of ferrites at high frequency [1]. A systematic investigation was launched by Snoek (1936) at Philips Research Laboratory [2]. At the same time Takai (1937) in Japan was seriously engaged in the research work on the same materials [1]. Snoek's extensive works on ferrites unveiled many mysteries regarding magnetic properties of ferrites. He was particularly looking for high permeability materials of cubic structure. This particular structure for symmetry reasons supports low crystalline anisotropy. He found suitable materials in the form of mixed spinels of the type $MeZnFe_2O_4$, where *Me* stands for metals like *Cu, Mg, Ni, Co* or *Mn*, for which permeability were found to be up to 4000 [1-2 ,3]. Here after starts the story of *Li*-ferrites. Lithium ferrites became commercially important as computer memory core materials in the early 1960's. The high Curie temperature, leading to unparalleled thermal stability, the excellent hysteresis loop properties, and the high saturation magnetization all prompted this commercial interest. For many of the same reasons there was considerable development effort aimed at providing micro-wave quality lithium ferrites [4-7]. The principal interest in microwave lithium ferrites is a low-cost replacement for the rare earth-iron garnets, offering competitive or improved temperature performance. Lithium ferrites with magnetizations comparable to the garnets are very refractory due to the high concentration and nature of the substituent elements, which requires relatively high sintering temperatures. This type of heat treatment causes the volatility of $Li_2O$ [8, 9] which results in some reduction of iron. For this reason lithium ferrites were considered difficult to prepare with low dielectric loss. In addition, these lower magnetization lithium ferrites were characterized by high porosities, and as a result, high coercive forces and broad resonance line-widths were experienced [10].

The structural and elastic properties of *Li-Ni* ferrite was studied by Bhatu *et al.* [11]. The observed increase in magnitude of elastic constants, elastic wave

**pdfMachine**
**A pdf writer that produces quality PDF files with ease!**
Produce quality PDF files in seconds and preserve the integrity of your original documents. Compatible across nearly all Windows platforms, simply open the document you want to convert, click "print", select the "Broadgun pdfMachine printer" and that's it! Get yours now!

velocities and infrared spectral analysis is found easier, valid and suitable for spinel ferrite.

The effect of magnetic properties of *Ni* concentration in *Li-Zn* ferrite was studied by I. Soibam *et al.*[12]. From their investigation of saturation magnetization, Curie temperature and Mossbaur studies, it has been observed that *Ni* substitution greatly affects the magnetic properties of the *Li-Zn* ferrite system. The value of saturation magnetization and Curie temperature was observed to decrease with increase in the *Ni* concentration in their system. Magnetic studies of cobalt substituted lithium zinc ferrites was also studied by I. Soibam. Magnetisation measurement indicated that cobalt shows anomalous behaviour when substituted in lithium ferrites in the presence of *Zn*.[13]

The structure and magnetic properties of spinel-related *Mg*-doped $Li_{0.5}Fe_{2.5}O_4$ nano-crystalline particles prepared by milling a pristine sample, $Li_{0.41}Fe_{2.41}Mg_{0.17}O_4$ for different times were investigated by H M Widatallah *et al* [14]. The saturation magnetization and Curie temperature were found to decrease and the material increasingly turned super-paramagnetic as milling proceeded. The coercivity and the magnetization increased initially and later decreased at higher milling times.

The sintering process is considered to be one of the most vital steps in ferrite preparation and often plays a dominant role in many magnetic properties. Tasaki *et al.* [15] studied the effect of sintering atmosphere on permeability of sintered ferrite. They found that high density is one of the factors, which contribute to greater permeability. However, permeability decreased in an atmosphere without $O_2$ at high sintering temperature where high density was expected. This decrease in permeability is attributed to the variation of chemical composition caused by volatilization of *Zn*. At low sintering temperature a high permeability is obtained in an atmosphere without $O_2$ because densification and stoichiometry plays a principal role in increasing permeability. At high sintering temperature the highest permeability is obtained in the presence of $O_2$ because the effect of decrease of *Zn* content can then be neglected.

Studying the electromagnetic properties of ferrites, Nakamura [16] suggested that both the sintering density and the average grain size increased with sintering temperature. These changes were responsible for variations in magnetization, initial permeability and electrical resistivity.

**pdfMachine**
**A pdf writer that produces quality PDF files with ease!**
Produce quality PDF files in seconds and preserve the integrity of your original documents. Compatible across nearly all Windows platforms, simply open the document you want to convert, click “print”, select the “Broadgun pdfMachine printer” and that’s it! Get yours now!

High permeability attainment is certainly affected by the microstructure of the ferrites. Roess showed that [17] the very high permeability is restricted to certain temperature ranges and the shapes of permeability versus temperature curves are strongly affected by any inhomogeneity in the ferrite structure.

Leung *et al.* [18] performed a Low-temperature Mössbauer study of a nickel-zinc ferrite: $Zn_{1-x}Ni_xFe_2O_4$. They found that for $x \leq 0.5$ the resultant *A*- and *B*- site *Fe*-spin moments have a collinear arrangement, whereas for $x > 0.5$ a non-collinear arrangement of *A*- and *B*-site *Fe*-spin moments exist. An explanation based on the relative strength of the exchange constant $J_{AB}$ and $J_{BB}$ is given to account for this difference.

Rezlescu *et al.* [19][1 reported that the sintering behaviour and microstructure of the ferrites samples largely affected by *PbO* addition. *PbO* significantly reduced the sintering temperatures, thus energy consumption is minimized and material loss by evaporation is minimized [20].

There are two mechanisms in the phenomenon of permeability; spin rotation in the magnetic domains and wall displacements. The uncertainty of contribution from each of the mechanisms makes the interpretation of the experimental results difficult. Globus [21] shows that the intrinsic rotational permeability $\mu_r$ and $180^0$ wall permeability $\mu_w$ may be written as: $\mu_r = 1 + 2\pi M_s^2 / K$ and $\mu_w = 1 + 3\pi M_s^2 D / 4\gamma$, where $M_s$ is the saturation magnetization, $K$ is the total anisotropy, $D$ is the grain diameter and $\gamma \equiv K\delta_w$ is the wall energy.

El-Shabasy [22] studied the DC electrical resistivity of $Zn_xNi_{1-x}Fe_2O_4$ ferrites. He shows that the ferrite samples have semiconductor behaviour where DC electrical resistivity decreases on increasing the temperature. $\rho(T)$ for all samples follows $\rho(T) = \rho_0 \exp(E/k_BT)$, where $E$ is the activation energy for electric conduction and $\rho_0$ is the pre-exponential constant or resistivity at infinitely high temperature. The DC resistivity, $\rho(T)$, decreases as the *Zn* ion substitution increases. It is reported that *Zn* ions prefer the occupation of tetrahedral (*A*) sites, *Ni* ions prefer the occupation of octahedral (*B*) sites while *Fe* ions partially occupy the *A* and *B* sites. On increasing *Zn* substitution (at *A* sites), the *Ni* ion concentration (at *B* sites) will decrease. This lead to the migration of some *Fe* ions from *A* sites to *B* sites to substitute the reduction in *Ni* ion concentration at *B* sites. As a result, the number of ferrous and ferric ions at *B* sites

**pdfMachine**
**A pdf writer that produces quality PDF files with ease!**
Produce quality PDF files in seconds and preserve the integrity of your original documents. Compatible across nearly all Windows platforms, simply open the document you want to convert, click “print”, select the “Broadgun pdfMachine printer” and that’s it! Get yours now!

(which is responsible for electric conduction in ferrites) increases. Consequently $\rho$ decreases on *Zn* substitution. Another reason for the decrease in $\rho$ on increasing *Zn* ion substitution is that, zinc is less resistive ($\rho = 5.92\ \mu\Omega cm$) than nickel ($\rho = 6.99\ \mu\Omega cm$). The main conductivity mechanism in ferrites is attributed to electron hopping between $Fe^{3+}$ and $Fe^{2+}$ in octahedral sites. Resistivity in spinels is very sensitive to stoichiometry; a small variation of *Fe* content in $Zn_{0.7}Ni_{0.3}Fe_{2+x}O_{4-y}$ results in resistivity variations of $\sim 10^7$. Excess *Fe* can easily dissolve in spinel phase by a partial reduction of *Fe* from $3Fe_2^{3+}O_3$ to $2Fe^{2+}Fe_2^{3+}O_4$ (and $1/2O_2 \uparrow$) [2].

## 2.2 Magnetic Ordering

The onset of magnetic order in solids has two basic requirements:

(i) Individual atoms should have magnetic moments (spins),

(ii) Exchange interactions should exist that couple them together.

Magnetic moments originate in solids as a consequence of overlapping of the electronic wave function with those of neighbouring atoms. This condition is best fulfilled by some transition metals and rare-earths. The exchange interactions depend sensitively upon the inter-atomic distance and the nature of the chemical bonds, particularly of nearest neighbour atoms. When the positive exchange dominates, which corresponds to parallel coupling of neighbouring atomic moments (spins), the magnetic system becomes ferromagnetic below a certain temperature $T_C$ called the Curie temperature. The common spin directions are determined by the minimum of magneto-crystalline anisotropy energy of the crystal. Therefore, ferromagnetic substances are characterized by spontaneous magnetization. But a ferromagnetic material in the demagnetized state displays no net magnetization in zero field because in the demagnetized state a ferromagnetic of macroscopic size is divided into a number of small regions called domains, spontaneously magnetized to saturation value and the directions of these spontaneous magnetization of the various domains are such that the net magnetization of the specimen is zero. The existence of domains is a consequence of energy minimization. The size and formation of these domains is in a complicated manner dependent on the shape of the specimen as well as its magnetic and thermal history. When negative exchange dominates, adjacent atomic moments (spins) align antiparallel

**pdfMachine**
**A pdf writer that produces quality PDF files with ease!**
Produce quality PDF files in seconds and preserve the integrity of your original documents. Compatible across nearly all Windows platforms, simply open the document you want to convert, click “print”, select the “Broadgun pdfMachine printer” and that’s it! Get yours now!

to each other, and the substance is said to be anti-ferromagnetic below a characteristic temperature, $T_N$, called the Néel temperature. In the simplest case, the lattice of an anti-ferromagnet is divided into two sublattices with the magnetic moments of these in anti-parallel alignment. This result is zero net magnetization. A special case of anti-ferromagnetism is ferrimagnetism. In ferrimagnetism, there are also two sublattices with magnetic moments in opposite directions, but the magnetization of the sublattices are of unequal strength resulting in a non-zero magnetization and therefore has net spontaneous magnetization. At the macroscopic level of domain structures, ferromagnetic and ferrimagnetic materials are therefore similar.

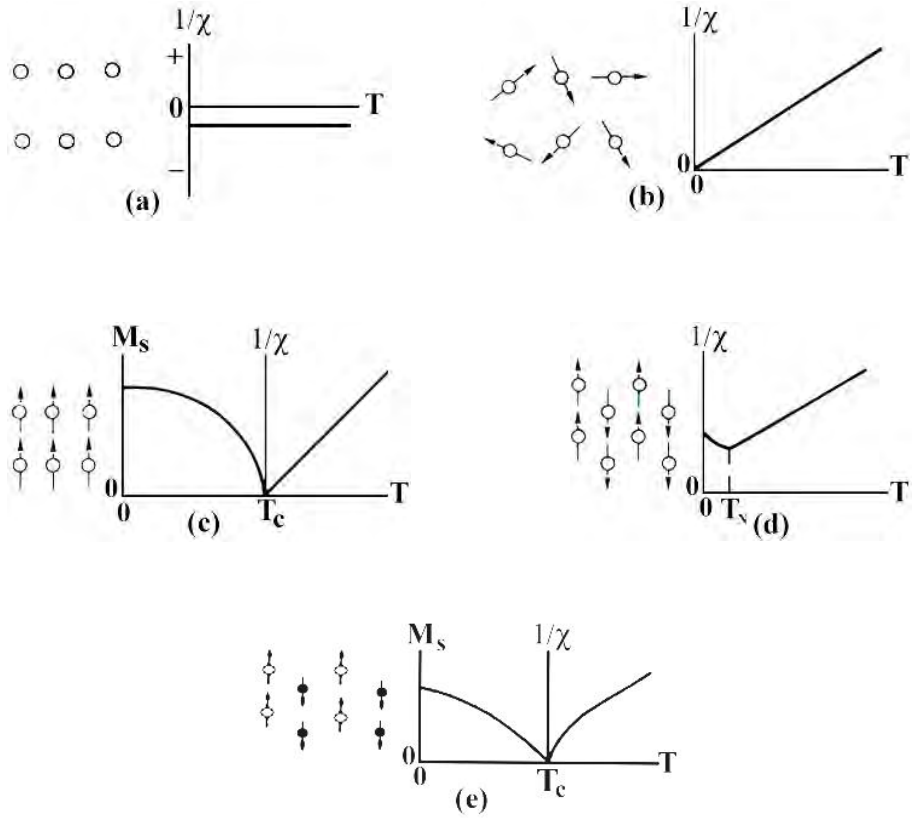


**Fig. 2.1.** Temperature dependence of the inverse susceptibility for: (a) a diamagnetic material; (b) a paramagnetic material, showing Curie's law behaviour; (c) a ferromagnetic material, showing a spontaneous magnetization for $T<T_C$ and Curie-Weiss behaviour for $T>T_C$; (d) an antiferromagnetic material; (e) a ferrimagnetic material, showing a net spontaneous magnetization for $T<T_C$ and non linear behaviour for $T>T_C$.

**pdfMachine**
**A pdf writer that produces quality PDF files with ease!**
Produce quality PDF files in seconds and preserve the integrity of your original documents. Compatible across nearly all Windows platforms, simply open the document you want to convert, click "print", select the "Broadgun pdfMachine printer" and that's it! Get yours now!

The Curie and Néel temperatures characterize a phase transition between the magnetically ordered and disordered (paramagnetic) states. From these simple cases of magnetic ordering various types of magnetic order exists, particularly in metallic substances. Because of long-range order and oscillatory nature of the exchange interaction, mediated by the conduction electrons, structures like helical, conical and modulated patterns might occur. *A* useful property for characterizing the magnetic materials is the magnetic susceptibility,$\chi$, defined as the magnetization, *M*, divided by the applied magnetic field, *H* i.e. $\chi = M / H$. The temperature dependence of susceptibility or, more accurately, inverse of susceptibility is a good characterization parameter for magnetic materials, Fig. 2.1. Fig. 2.1(e) shows that in the paramagnetic region, the variation of the inverse susceptibility with temperature of a ferrite material is decidedly non-linear. Thus the ferrite materials do not obey the Curie-Weiss law, $\chi = C /(T - T_C)$ [2, 27].

## 2.3 Crystal Structure of Spinel Ferrites

### 2.3.1 Ionic Charge Balance and Crystal Structure of Cubic Spinel Ferrite:

The spinel lattice is composed of a close-packed oxygen arrangement in which 32 oxygen ions form a unit cell that is the smallest repeating unit in the crystal network. Between the layers of oxygen ions, if we simply visualize them as spheres, there are interstices that may accommodate the metal ions. Now, the interstices are not all the same; some which are called *A* sites are surrounded by or coordinated with 4 nearest neighbouring oxygen ions whose lines connecting their centers form a tetrahedron. Thus, *A* sites are called tetrahedral sites (Fig. 2.2 (a)). The other type of site (*B* sites) is coordinated by 6 nearest neighbor oxygen ions whose center connecting lines describe an octahedron. The *B* sites are called octahedral sites (Fig. 2.2(b)). In the unit cell of 32 oxygen ions, there are 64 tetrahedral sites and 32 octahedral sites. If all of these were filled with metal ions, of either *+2* or +3 valence, the positive charge would be very much greater than the negative charge and so the structure would not be electrically neutral. It turns out that of the 64 tetrahedral sites, only 8 are occupied and out of 32 octahedral sites, only 16 are occupied. If, as in the mineral, spinel, the tetrahedral sites are occupied by divalent ions and the octahedral sites are occupied by the trivalent ions, the total positive charge would be 8x (+2) = +16 plus the 16x (+3) =+48 or a total of

**pdfMachine**
**A pdf writer that produces quality PDF files with ease!**
Produce quality PDF files in seconds and preserve the integrity of your original documents. Compatible across nearly all Windows platforms, simply open the document you want to convert, click “print”, select the “Broadgun pdfMachine printer” and that’s it! Get yours now!

+64 which is needed to balance the 32x (-2) = -64 for the oxygen ions. There would then be eight formula units of $MO.Fe_2O_3$ or $MFe_2O_4$ in a unit cell. *A* spinel unit cell contains two types of subcells . The two types of subcells alternate in a three- dimensional array so that each fully repeating unit cell requires eight subcells.

The crystallographic environments of the *A* and *B* sites are distinctly different. The unit cell contains so many ions that a two-dimensional drawing of the complete cell would not be very informative. Instead we can consider a unit cell of edge *a*, to be divided into eight octants, each of edge *a*/2, as shown in Fig. 2.2(c). The four shaded octants have identical contents, and so do the four unshaded octants. The contents of the two lower-left octants in Fig. 2.2(c) are shown in Fig. 2.2(d). One tetrahedral site occurs at the center of the right octant of Fig. 2.2(d), and other tetrahedral sites are at some but not all octant corners. Four octahedral sites occur in the left octant; one is connected by dashed lines to six oxygen ions, two of which, shown dotted, are in adjacent octants behind and below. The oxygen ions are arranged in the same way, in tetrahedra, in all octants. Not all of the available sites are actually occupied by metal ions. Only one-eighth of the *A* sites and one-half of the *B* sites are occupied, as shown in Table 2.1 [2]. In the mineral spinel, $MgO.Al_2O_3$, the $Mg^{2+}$ ions are in *A* sites and the $Al^{3+}$ ions are in *B* sites.

Some ferrites $MO.Fe_2O_3$ have exactly this structure, with $M^{2+}$ in *A* sites and $Fe^{3+}$ in *B* sites. This is called the normal spinel structure. If 8 divalent (*M*) ions occupy the *A*-site i.e., tetrahedral site and 16 tetravalent ions ($Fe^{3+}$) occupy the *B*-site i.e., octahedral site, the structure is said to be Normal spinel.

If *B*-site i.e., octahedral site is occupied half by divalent metal ion and half by trivalent iron ions, generally distributed in random and *A*-site i.e., tetrahedral site by trivalent iron ions, the structure is said to be Inverse spinel. Both zinc and cadmium ferrite have this structure and they are both nonmagnetic, i.e., paramagnetic. Many other ferrites, however, have the inverse spinel structure, in which the divalent ions are on *B* sites, and the trivalent ions are equally divided between *A* and B sites. The divalent and trivalent ions normally occupy the B sites in a random fashion, i.e., they are disordered. Iron, cobalt, and nickel ferrites have the inverse structure, and they are all ferrimagnetic.

The normal and inverse structures are to be regarded as extreme cases, because X-ray and neutron diffraction show that intermediate structures can exist. Thus

**pdfMachine**
**A pdf writer that produces quality PDF files with ease!**
Produce quality PDF files in seconds and preserve the integrity of your original documents. Compatible across nearly all Windows platforms, simply open the document you want to convert, click “print”, select the “Broadgun pdfMachine printer” and that’s it! Get yours now!

manganese ferrite is almost, but not perfectly, normal; instead of all the $Mn^{2+}$ ions being on *A* sites, a fraction 0.8 is on A sites and 0.2 on B sites. Similarly, magnesium ferrite is not quite inverse; a fraction 0.9 of the $Mg^{2+}$ ions is on B sites and 0.1 on A sites. The distribution of the divalent ions on A and B sites in some ferrites can be altered by heat treatment; it may depend, for example, on whether the material is quenched from a high temperature or slowly cooled.

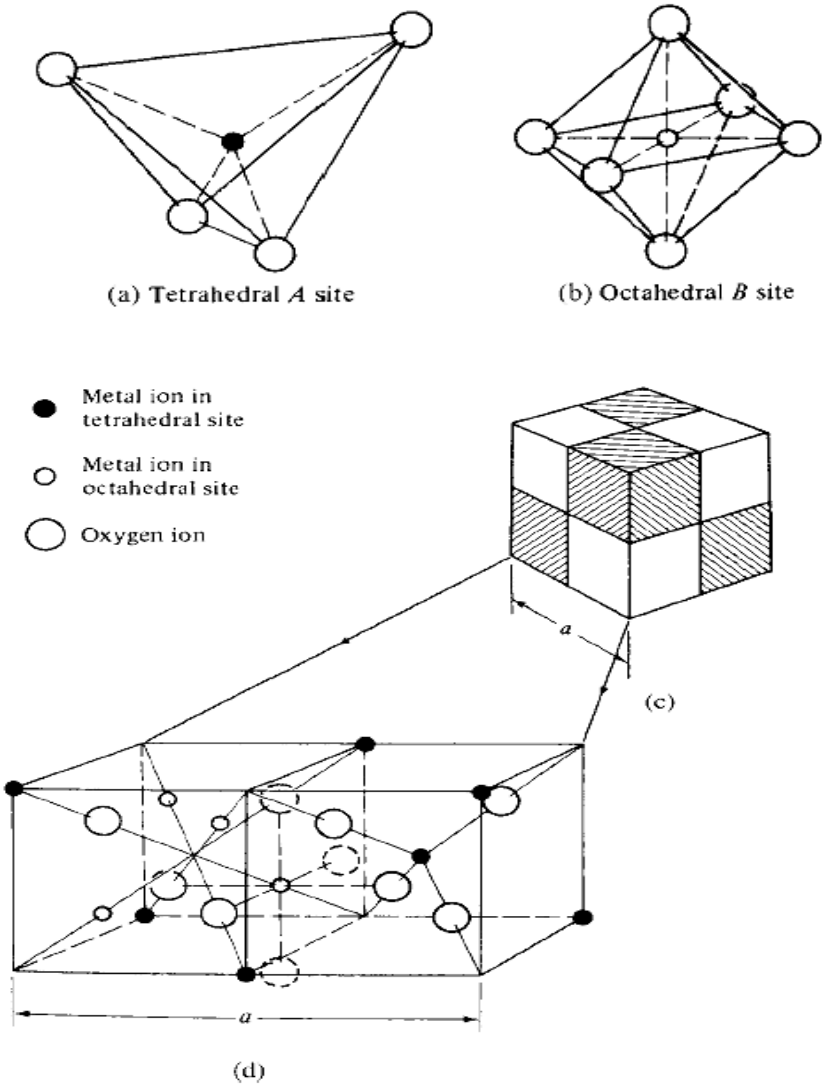


**Fig.2.2**. Crystal structure of a cubic ferrite [27].

**pdfMachine**
**A pdf writer that produces quality PDF files with ease!**
Produce quality PDF files in seconds and preserve the integrity of your original documents. Compatible across nearly all Windows platforms, simply open the document you want to convert, click "print", select the "Broadgun pdfMachine printer" and that's it! Get yours now!

**Table 2.1** Arrangements of Metal Ions in the Unit Cell of a Ferrite $MO.Fe_2O_3$ [27]

.

| Kind of Site | Number Available | Number Occupied | Occupants | |
|---|---|---|---|---|
| | | | Normal Spinel | Inverse Spinel |
| Tetrahedral (A) | 64 | 8 | $8M^{2+}$ | $8\ Fe^{3+}$ |
| Octahedral (B) | 32 | 16 | $16\ Fe^{3+}$ | $8\ Fe^{3+}$<br>$8\ M^{2+}$ |

The positions of the ions in the spinel lattice are not perfectly regular (as the packing of hard spheres) and some distortion does occur. The tetrahedral sites are often too small for the metal ions so that the oxygen ions move slightly to accommodate them. The oxygen ions connected with the octahedral sites move in such a way as to shrink the size the octahedral cell by the same amount as the tetrahedral site expands. The movement of the tetrahedral oxygen is reflected in a quantity called the oxygen parameter, which is the distance between the oxygen ion and the face of the cube edge along the cube diagonal of the spinel subcell. This distance is theoretically equal to $3/8a_o$ where $a_o$ is the lattice constant [1].

### 2.3.2 Site Preferences of the Ions

The preference of the individual ions for the two types of lattice sites is determined by;

1. The ionic radii of the specific ions
2. The size of the interstices
3. Temperature
4. The orbital preference for specific coordination

The most important consideration would appear to be the relative size of the ion compared to the size of the lattice site. The divalent ions are generally larger than the trivalent (because the larger charge produces greater electrostatic attraction and so pulls the outer orbits inward). The octahedral sites are also larger than the tetrahedral [28]. Therefore, it is reasonable that the trivalent ions such as $Fe^{3+}$ would go into the tetrahedral sites and the divalent ions would go into the octahedral. Two exceptions are found in $Zn^{2+}$ and $Cd^{2+}$ which prefer tetrahedral sites because the electronic

**pdfMachine**
**A pdf writer that produces quality PDF files with ease!**
Produce quality PDF files in seconds and preserve the integrity of your original documents. Compatible across nearly all Windows platforms, simply open the document you want to convert, click "print", select the "Broadgun pdfMachine printer" and that's it! Get yours now!

configuration is favorable for tetrahedral bonding to the oxygen ions. Thus *Zn* takes preference for tetrahedral sites over the $Fe^{3+}$ ions. $Zn^{2+}$ and $Co^{2+}$ have the same ionic radius but *Zn* prefers tetrahedral sites and $Co^{2+}$ prefers octahedral sites because of the configurationally exception. $Ni^{2+}$ and $Cr^{3+}$ have strong preferences for octahedral sites, while other ions have weaker preferences [28].

### 2.3.3 Unit Cell Dimensions

The dimensions of the unit cell are given in Angstrom Units which are equivalent to $10^{-8}$ cm. If we assume that the ions are perfect spheres and we pack them into a unit cell of measured (X-ray diffraction) dimensions we find certain discrepancies that show that the packing is not ideal. The positions of the ions in the spinel lattice are not perfectly regular (as the packing of hard spheres) and some distortion does occur. The tetrahedral sites are often too small for the metal ions so that the oxygen ions move slightly to accommodate them. The oxygen ions connected with the octahedral sites move in such a way as to shrink the size of the octahedral cell by the same amount as the tetrahedral site expands .The movement of the tetrahedral oxygen is reflected in a quantity called the oxygen parameter which is the distance between the oxygen ion and the face of the cube edge along the cube diagonal of the spinel subcell. This distance is theoretically equal to $3/8a_o$. The unit cell length of *Li*-Ferrite, *Ni* ferrite and *Mg* Ferrite are observed to be 8.33 Å, 8.3390 Å and 8.36 Å respectively [2].

## 2.4 Cation Distribution of Spinel Ferrites

In spinel structure the distribution of cations over the tetrahedral or *A* sites and octahedral or *B* sites can be present in a variety of ways. If all the $Me^{2+}$ ions in $Me^{2+}Me_2^{3+}O_4$ are in tetrahedral and all $Me^{3+}$ ions in octahedral positions, the spinel is then called normal spinel. Another cation distribution in spinel exists, where one half of the cations $Me^{3+}$ are in the *A* positions and the rest, together with the $Me^{2+}$ ions are randomly distributed among the *B* positions. The spinel having the latter kind of cation distribution is known as inverse spinel. The distribution of these spinels can be summarized as [2, 25-26]

1) Normal spinels, i.e. the divalent metal ions are on *A*-sites: $Me^{2+}[Me_2^{3+}]O_4$,
2) Inverse spinels, i.e. the divalent metal ions are on *B*-sites: $Me^{3+}[Me^{2+}Me_2^{3+}]O_4$.

**pdfMachine**
**A pdf writer that produces quality PDF files with ease!**
Produce quality PDF files in seconds and preserve the integrity of your original documents. Compatible across nearly all Windows platforms, simply open the document you want to convert, click “print”, select the “Broadgun pdfMachine printer” and that’s it! Get yours now!

A completely normal or inverse spinel represents the extreme cases. There are many spinel oxides which have cation distributions intermediate between these two extreme cases and are called mixed spinels.

The general cation distribution for the spinel can be indicated as:

$$(Me_x^{2+}Me_{1-x}^{3+})[Me_{1-x}^{2+}Me_{1+x}^{3+}]O_4$$

where the first and third brackets represent the A and B sites respectively. For normal spinel $x$=1, for inverse spinel $x$=0. The quantity x is a measure of the degree of inversion. In the case of some spinel oxides x depends upon the method of preparation.

The cation distributions of *Li*-Ferrite, *Mg*-Ferrite and *Ni*-Ferrite are shown below:

Li Ferrite : $(Fe^{3+})[Li_{0.5}Fe_{1.5}^{3+}]O_4$ [2,10]

Ni Ferrite : $(Fe^{3+})[Ni^{2+}Fe^{3+}]O_4$ [2, 42]

Mg Ferrite : $(Mg_{1-x}Fe^{3+})[Mg_xFe_{2-x}^{3+}]O_4$ [2, 43]

where x is the degree of inversion.

Both Li ferrite and Ni-Ferrite is a inverse spinel and Mg –Ferrite is a mixed ferrite.

The cation distribution of various $Li_xMg_{0.4}Ni_{0.6-2x}Fe_{2+x}O_4$ ferrite assumed as

$$(Fe_{0.9}^{3+})[Li_x^{1+}Mg_{0.4}^{2+}Ni_{0.6-2x}^{2+}Fe_{1.1+x}^{3+}] \quad [31]$$

The basic magnetic properties of the ferrites are very sensitive functions of their cation distributions. Mixed ferrites having interesting and useful magnetic properties are prepared by mixing two or more different types of metal ions

Spinel oxides are ionic compounds and hence the chemical bonding occurring in them can be taken as purely ionic to a good approximation. The total energy involved, however, consists of the Coulomb energy, the Born repulsive energy, the polarization and the magnetic interaction energy. The energy terms are all dependent on lattice constant, oxygen position parameter and the ionic distribution. In principle the equilibrium cation distribution can be calculated by minimizing the total energy with respect to these variables. But the only energy that can be written with any accuracy is the Coulomb energy. The individual preference of some ions for certain sites resulting from their electronic configuration also play an important role. The divalent ions are generally larger than the trivalent (because the larger charge produces greater electrostatic attraction and so pulls the outer orbits inward). The octahedral sites are also

**pdfMachine**
**A pdf writer that produces quality PDF files with ease!**
Produce quality PDF files in seconds and preserve the integrity of your original documents. Compatible across nearly all Windows platforms, simply open the document you want to convert, click “print”, select the “Broadgun pdfMachine printer” and that’s it! Get yours now!

larger than the tetrahedral. Therefore, it would be reasonable that the trivalent ions $Fe^{3+}$ (0.73Å) would go into the tetrahedral sites and the divalent ions $Fe^{2+}$ (0.86Å) go into the octahedral. Two exceptions are found in $Zn^{2+}$ and $Cd^{2+}$ which prefer tetrahedral sites because the electronic configuration is favourable for tetrahedral bonding to the oxygen ions. It is known that $Li^{1+}$(0.82Å), $Ni^{2+}$(0.73Å) and $Mg^{2+}$(0.80Å) ions occupy B sites [6]. Hence the factors influencing the distribution the cations among the two possible lattice sites are mainly their ionic radii of the specific ions, the size of the interstices, temperature, the matching of their electronic configuration to the surrounding anions and the electrostatic energy of the lattice, the so-called Madelung energy, which has the predominant contribution to the lattice energy under the constrain of overall energy minimization and charge neutrality.

## 2.5 Interaction Between Magnetic Moments on Lattice Sites

Spontaneous magnetization of spinels (at 0K) can be estimated on the basis of their composition, cation distribution, and the relative strength of the possible interaction. Since cation-cation distances are generally large, direct (ferromagnetic) interactions are negligible. Because of the geometry of orbital involved, the strongest superexchange interaction is expected to occur between octahedral and tetrahedral cations. The strength of interaction or exchange force between the moments of the two metal ions on different sites depends on the distances between these ions and the oxygen ion that links them and also on the angle between the three ions. The nearest neighbours of a tetrahedral, an octahedral and an anion site are shown in Fig. 2.3. The interaction is greatest for an angle of $180^0$ and also where the interionic distances are the shortest.

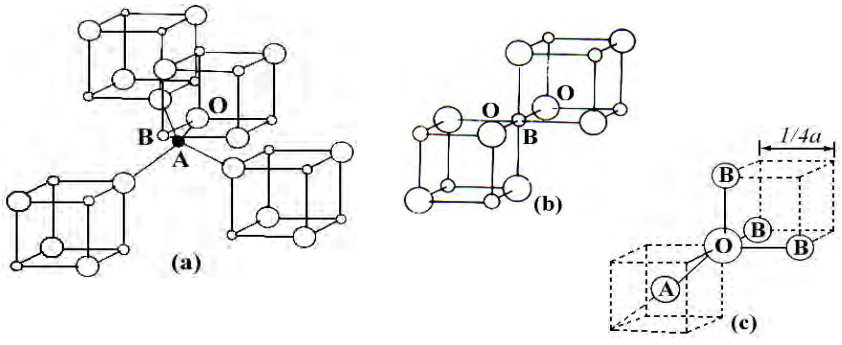


**Fig. 2.3.** Nearest neighbours of (a) a tetrahedral site, (b) an octahedral site and (c) an anion site.

**pdfMachine**
**A pdf writer that produces quality PDF files with ease!**
Produce quality PDF files in seconds and preserve the integrity of your original documents. Compatible across nearly all Windows platforms, simply open the document you want to convert, click "print", select the "Broadgun pdfMachine printer" and that's it! Get yours now!

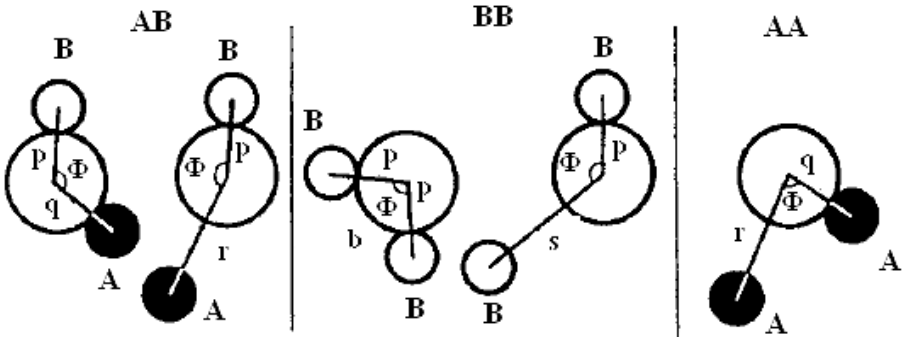


**Fig. 2.4.** Interionic distances and angles in the spinel structure for the different type of lattice site interactions [28, 29].

| **Distances M-O** | **Distances M-M** |
|---|---|
| $p = a(\frac{1}{2} - u)$ | $b = (a/4)\sqrt{2}$ |
| $q = a(u - \frac{1}{4})\sqrt{3}$ | $c = (a/8)\sqrt{11}$ |
| $r = a(1+u)\sqrt{11}$ | $d = (a/4)\sqrt{3}$ |
| $s = a(\frac{1}{3}u + 8)\sqrt{3}$ | $e = (3a/8)\sqrt{3}$ |
| | $f = (a/4)\sqrt{6}$ |

Fig. 2.4 shows the inter-atomic distances and the angles between the ions for the different types of interactions. In the A-A and B-B cases, the angles are too small or the distances between the metal ions and the oxygen ions are too large. The best combinations of distances and angles are found in the A-B interactions. For an undistorted spinel, the A-O-B angles are about 125˚ and 154˚ [1-2, 24]. The B-O-B angles are 90˚ and 125˚ but in the latter, one of the B-O distances is large. In the A-A case the angle is about 80˚. Therefore, the interaction between moments on the A and B sites is strongest. The B-B interaction is much weaker and the most unfavorable situation occurs in the A-A interaction. By examining the interactions involving the major contributor, or the A-B interaction which orients the unpaired spins of these ions antiparallel, Néel was able to explain the ferrimagnetism of ferrites The interaction between the tetrahedral and octahedral sites is shown in Fig. 2.4. An individual A site is interacted with a single B site, but each A site is linked to four such units and each B site is linked to six such units. Thus, to be consistent throughout the crystal, all A sites and all B sites act as unified blocks and are coupled antiparallel as blocks [28].

**pdfMachine**
**A pdf writer that produces quality PDF files with ease!**
Produce quality PDF files in seconds and preserve the integrity of your original documents. Compatible across nearly all Windows platforms, simply open the document you want to convert, click “print”, select the “Broadgun pdfMachine printer” and that’s it! Get yours now!

## 2.6 Magnetism in Spinel Ferrite

The magnetic moment of a free atom is associated with the orbital and spin motions of electrons in an incomplete sub-shell of the electronic structure of the atom. In crystals the orbital motions are quenched, that is the orbital planes may be considered to be fixed in space relative to the crystal lattice, and in such a way that in bulk the crystal has no resultant moment from this source. Moreover this orbital-lattice coupling is so strong that the application of a magnetic field has little effect upon it. The spin axes are not tightly bound to the lattice as are the orbital axes. The anions surrounding a magnetic cation subject it to a strong inhomogeneous electric field and influence the orbital angular momentum. However, the spin angular momentum remains unaffected. For the first transition group elements this crystal field effect is intense partly due to the large radius of the 3d shell and partly due to the lack of any outer electronic shell to screen the 3d shell whose unpaired electrons only contribute to the magnetic moment. We have originally defined the magnetic moment in connection with permanent magnets. The electron itself may well be called the smallest permanent magnet [1]. For an atom with a resultant spin quantum number *S*, the spin magnetic moment will be

$$\mu = g\sqrt{S(S+1)}\mu_B$$

Where $g$ is the Landé splitting factor and $\mu_B$, known as the Bohr magneton, is the fundamental unit of magnetic moment. The value of $g$ for pure spin moment is $2$ and the quantum number associated with each electron spin is $\pm 1/2$. The direction of the moment is comparable to the direction of the magnetization (from South to North poles) of a permanent magnet to which the electron is equivalent.

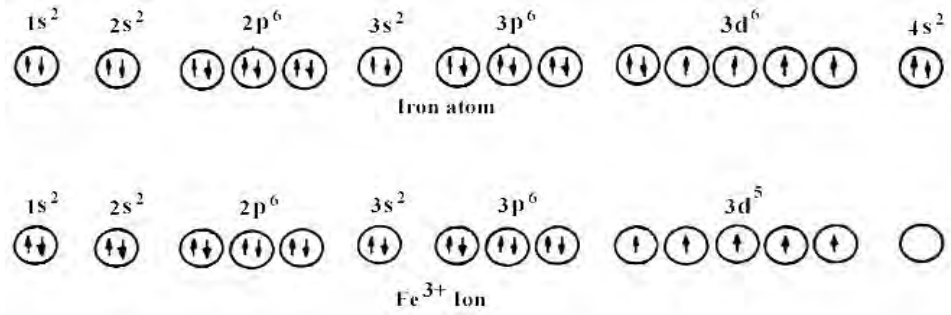


**Fig. 2.5.** Electronic configuration of atoms and ions [28].

**pdfMachine**
**A pdf writer that produces quality PDF files with ease!**
Produce quality PDF files in seconds and preserve the integrity of your original documents. Compatible across nearly all Windows platforms, simply open the document you want to convert, click "print", select the "Broadgun pdfMachine printer" and that's it! Get yours now!

Fig. 2.5 illustrates the electronic configuration of *Fe* atoms and $Fe^{3+}$ ions. *Fe* atom has four unpaired electrons and $Fe^{3+}$ ion has five unpaired electrons. Each unpaired electron spin produced 1 Bohr magneton. In compounds, ions and molecules, account must be taken of the electrons used for bonding or transferred in ionization. It is the number of unpaired electrons remaining after these processes occur that gives the net magnetic moment [1]. According to the Hund's rules the moment of *Fe* atom and $Fe^{3+}$ ion are $4\mu_B$ and $5\mu_B$ respectively. Similarly the moment of $Fe^{2+}$ and $Ni^{2+}$ ion are $4\mu_B$ and $\mu_B$ respectively.

### 2.6 .1 Magnetic Moments of Some Spinels Ferrites:

#### 2.6.1.1 Inverse Spinels

In the nickel ferrite it was observed that the moments of the eight $Ni^{2+}$ ions on the octahedral sites. The value of moment per $Ni^{2+}$ ion is $2\mu_B$ or $16\ \mu_B$ for a unit cell containing eight formula units. The magnetic moments of the other inverse spinels can be predicted in a similar manner. These predicted values are listed in Table 2.2 along with the measured values [28]. Because the effect of thermal agitation on the magnetic moments will lower the magnetic moment, the correlation of the moment to Bohr magnetons is always referred to the value at absolute zero or 0˚K. This is usually done by extrapolation of the values at very low temperatures. The deviations from the theoretical values can be attributed to several factors, namely:

- The ion distribution on the various sites may not be as perfect as predicted.
- The orbital magnetic contribution may not be zero as assumed.
- The directions of the spins may not be antiparallel in the interactions. In other words, they may be canted.

#### 2.6.1.2 Normal versus Inverse Spinels

Although some spinels are either normal or inverse, it is possible to get different mixtures of the two. Often, the ratio of the two will depend on the method of preparation. Some of the first ferrites studied by Neel (1948) were ones that contained *Mg* and *Cu* which by thermal treatment reduced the $Fe^{3+}$ on the tetrahedral A sites of the inverse spinel. As a result, there was an imbalance of the $Fe^{3+}$ ions on the two sites and

**pdfMachine**
**A pdf writer that produces quality PDF files with ease!**
Produce quality PDF files in seconds and preserve the integrity of your original documents. Compatible across nearly all Windows platforms, simply open the document you want to convert, click "print", select the "Broadgun pdfMachine printer" and that's it! Get yours now!

thus a magnetic moment. Even *Zn* ferrite, *Zn [Fe₂] O₄,* with a higher than 50 mole percentage of $Fe_2O_3$ and a special firing can have a small moment [28].

From the Table 2.2, it is observed that experimental magnetic moment of $Li_{0.5}Fe_{2.5}O_4$, $MgFe_2O_4$ and $NiFe_2O_4$ are 2.6, 1.1 and 2.3 respectively.

**Table 2.2**. Magnetic moment of Some Simple Ferrite [28].

| Ferrite | Magnetic Moment ($\mu_B$) | |
|---|---|---|
| | Experimental | Theoretical |
| $MnFe_2O_4$ | 4.6 | 5 |
| $FeFe_2O_4$ | 4.1 | 4 |
| $CoFe_2O_4$ | 3.7 | 3 |
| $NiFe_2O_4$ | 2.3 | 2 |
| $CuFe_2O_4$(Quenched) | 2.3 | 1 |
| $MgFe_2O_4$ | 1.1 | 0 |
| $Li_{0.5}Fe_{2.5}O_4$ | 2.6 | 2.5 |
| $\gamma$-$Fe_2O_3$ | 2.3 | 2.5 |

## 2.6.2 Exchange Interactions in Spinel

The intense short-range electrostatic field, which is responsible for the magnetic ordering, is the exchange force that is quantum mechanical in origin and is related to the overlapping of total wave functions of the neighbouring atoms. The total wave function consists of the orbital and spin motions. Usually the net quantum number is written as *S*, because the magnetic moments arise mostly due to the spin motion as described above. The exchange interactions coupling the spins of a pair of electrons are proportional to the scalar product of their spin vectors [23, 26, 30]

$$V_{ij} = -2J_{ij}\vec{S}_{i.}.\vec{S}_j \qquad (2.1)$$

where $J_{ij}$ is the exchange integral given in a self explanatory notation by

**pdfMachine**
**A pdf writer that produces quality PDF files with ease!**
Produce quality PDF files in seconds and preserve the integrity of your original documents. Compatible across nearly all Windows platforms, simply open the document you want to convert, click "print", select the "Broadgun pdfMachine printer" and that's it! Get yours now!

$$J_{ij} = \int \psi_i^*(1)\psi_j^*(2)\left[\frac{1}{r_{12}} + \frac{1}{r_{ij}} - \frac{1}{r_{i1}} - \frac{1}{r_{j2}}\right]\psi_i(2)\psi_j(2)dv_1 dv_2 \qquad (2.2)$$

In this expression $r$ 's are the distances, subscripts $i$ and $j$ refer to the atoms, 1 and 2 refers to the two electrons. If the $J$ in equation (2.1) is positive, we achieve ferromagnetism. A negative $J$ may give rise to anti-ferromagnetism or ferrimagnetism.

Magnetic interactions in spinel ferrites as well as in some ionic compounds are different from the one considered above because the cations are mutually separated by bigger anions (oxygen ions). These anions obscure the direct overlapping of the cation charge distributions, sometimes partially and sometimes completely making the direct exchange interaction very weak. Cations are too far apart in most oxides for a direct cation-cation interaction. Instead, super-exchange interactions appear, i.e., indirect exchange via anion *p*-orbitals that may be strong enough to order the magnetic moments. Apart from the electronic structure of cations this type of interactions strongly depends on the geometry of arrangement of the two interacting cations and the intervening anion. Both the distance and the angles are relevant. Usually only the interactions with in first coordination sphere (when both the cations are in contact with the anion) are important. In the Neél theory of ferrimagnetism the interactions taken as effective are inter- and intra-sublattice interactions *A-B*, *A-A* and *B-B*. The type of magnetic order depends on their relative strength.

The super-exchange mechanism between cations that operate via the intermediate anions was proposed by Kramer for such cases and was developed by Anderson and Van Vleck [23, 26]. A simple example of superexchange is provided by *MnO* which was chosen by Anderson. From the crystal structure of *MnO* it will be seen that the anti-parallel manganese ions are collinear with their neighbouring oxygen ions. The $O^{2-}$ ions each have six *2p* electrons in three anti-parallel pairs. The outer electrons of the $Mn^{2+}$ ions are in *3d* sub-shells which are half filled with five electrons in each. The phenomenon of super-exchange is considered to be due to an overlap between the manganese 3*d* orbits and the oxygen *2p* orbits with a continuous interchange of electrons between them. It appears that, for the overall energy of the system to be a minimum, the moments of the manganese ions on either side of the oxygen ion must be

**pdfMachine**
**A pdf writer that produces quality PDF files with ease!**
Produce quality PDF files in seconds and preserve the integrity of your original documents. Compatible across nearly all Windows platforms, simply open the document you want to convert, click "print", select the "Broadgun pdfMachine printer" and that's it! Get yours now!

anti-parallel. The manganese magnetic moments are thus, in effect, coupled through the intervening oxygen ion. The idea is illustrated in Fig. 2.6.

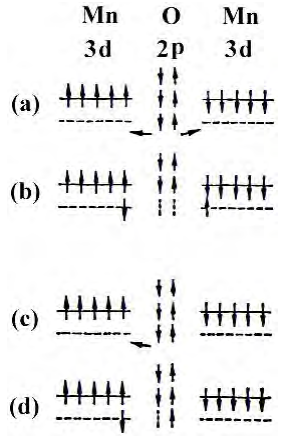


**Fig. 2.6.** Illustrating super-exchange in *MnO*.

In Fig. 2.6 (a) and Fig. 2.6 (c) the outer electrons in a pair of $Mn^{2+}$ ions, and in an intervening $O^{2-}$ ion in the unexcited state, are shown by the arrows. One suggested mode of coupling is indicated in Fig. 2.6 (b). The two electrons of a pair in the oxygen ion are simultaneously transferred, one to the left and the other to the right. If their directions of spin are unchanged then, by Hund's rules, the moments of the two manganese ions must be anti-parallel as shown. Another possibility is represented in Fig. 2.6(d). One electron only has been transferred to the manganese ion on the left. The oxygen ion now has a moment of $1\mu_B$ and if there is negative interaction between the oxygen ion and the right-hand manganese ion then again the moments of the manganese ions will be anti-parallel. If these ideas are accepted then the oxygen ions play an essential part in producing anti-ferromagnetism in the oxide. Moreover, because of the dumbbell shape of the *2p* orbits, the coupling mechanism should be most effective when the metal ions and the oxygen ions lie in one straight line, that is, the angle between the bonds is 180˚, and this is the case with *MnO*.

In the case of spinel ferrites the coupling is of the indirect type which involves overlapping of oxygen wave functions with those of the neighbouring cations. Consider two transition metal cations separated by an *O*, Fig. 2.7.

**pdfMachine**
**A pdf writer that produces quality PDF files with ease!**
Produce quality PDF files in seconds and preserve the integrity of your original documents. Compatible across nearly all Windows platforms, simply open the document you want to convert, click "print", select the "Broadgun pdfMachine printer" and that's it! Get yours now!

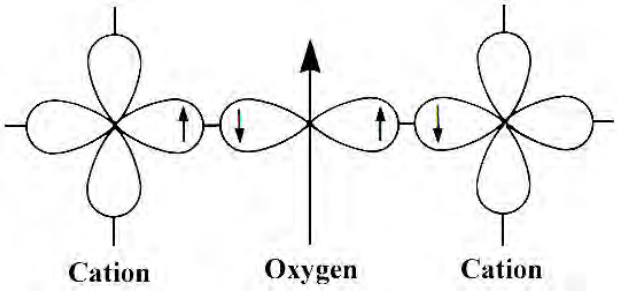


**Fig. 2.7.** Schematic representation of the superexchange interaction in the magnetic oxides. The *p* orbital of an anion (center) interact with the *d* orbitals of the transitional metal cations.

The $O^{2-}$ has no net magnetic moment since it has completely filled shells, with *p*-type outermost orbitals. Orbital $p_x$ has two electrons: one with spin up, and the other with spin down, consistent with pauli's exclusion principle. The essential point is that when an oxygen *p* orbital overlaps with a cation *d* orbital, one of the *p* electrons can be accepted by the cations. When one of the transition-metal cations is brought close the $O^{2-}$, partial electron overlap (between a *3d* electron from the cation and a *2p* electron form the $O^{2-}$) can occur only for anti-parallel spins, because electrons with the same spin are repelled. Empty *3d* states in the cation are available for partial occupation by the $O^{2-}$ electron, with an anti-parallel orientation. Electron overlap between the other cation and the $O^{2-}$ then occurs resulting in anti-parallel spins and therefore anti-parallel order between the cations. Since the *p* orbitals are linear, the strongest interaction is expected to take place for cation–$O^{2-}$–cation angles close to $180^{\circ}$ [2].

### 2.6.3 Néel Theory of Ferrimagnetism

If we consider the simplest case of a two-sublattice system having antiparallel and non-equal magnetic moments, the inequality may be due to:

1) different elements in different sites,
2) same element in different ionic states, and
3) different crystalline fields leading to different effective moments for ions having the same spin.

The spins on one sub-lattice are under the influence of exchange forces due to the spins on the second sub-lattice as well as due to other spins on the same sub-lattice. The molecular fields acting on the two sub-lattices A and B can be written as [2, 23-27]

**pdfMachine**
**A pdf writer that produces quality PDF files with ease!**
Produce quality PDF files in seconds and preserve the integrity of your original documents. Compatible across nearly all Windows platforms, simply open the document you want to convert, click "print", select the "Broadgun pdfMachine printer" and that's it! Get yours now!

$$\vec{H}_A = \lambda_{AA}\vec{M}_A + \lambda_{AB}\vec{M}_B,$$

$$\vec{H}_B = \lambda_{AB}\vec{M}_A + \lambda_{BB}\vec{M}_B$$

where $\vec{M}_A$ and $\vec{M}_B$ are the magnetizations of the two sub-lattices and $\lambda$'s are the Weiss constants. Since the interaction between the sub-lattices is anti-ferromagnetic, $\lambda_{AB}$ must be negative, but $\lambda_{AA}$ and $\lambda_{BB}$ may be negative or positive depending on the crystal structure and the nature of the interacting atoms. Probably, these interactions are also negative, though they are in general quite small.

Assuming all the exchange interactions to be negative the molecular fields will be then given by

$$\vec{H}_A = -\lambda_{AA}\vec{M}_A - \lambda_{AB}\vec{M}_B,$$

$$\vec{H}_B = -\lambda_{AB}\vec{M}_A - \lambda_{BB}\vec{M}_B$$

Since in general, $\lambda_{AA}$ and $\lambda_{BB}$ are small compared to $\lambda_{AB}$, it is convenient to express the strengths of these interactions relative to the dominant $\lambda_{AB}$ interaction.

Let $\lambda_{AA} = \alpha\lambda_{AB}$

and $\lambda_{BB} = \beta\lambda_{AB}$

In an external applied field $\vec{H}$, the fields acting on *A* and *B* sites are

$$\vec{H}_A = \vec{H} - \lambda_{AB}(\alpha\vec{M}_A - \vec{M}_B),$$

$$\vec{H}_B = \vec{H} - \lambda_{AB}(\vec{M}_A - \beta\vec{M}_B)$$

At temperatures higher than the transition temperature, $T_N$, $\vec{H}_A$, $\vec{M}_A$ and $\vec{M}_B$ are all parallel and we can write

$$\vec{M}_A = \frac{C_A}{T}[\vec{H} - \lambda_{AB}(\alpha\vec{M}_A - \vec{M}_B)], \qquad (2.3)$$

$$\vec{M}_B = \frac{C_B}{T}[\vec{H} - \lambda_{AB}(\vec{M}_A - \beta\vec{M}_B)] \qquad (2.4)$$

where $C_A$ and $C_B$ are the Curie constants for the two sublattices.

Here, $C_A = N_A g\mu_B^2 S_A(S_A+1)/3K$ and $C_B = N_B g\mu_B^2 S_B(S_B+1)/3K$

$N_A$ and $N_B$ denote the number of magnetic ions on *A* and *B* sites respectively and $S_A$ and $S_B$ are their spin quantum numbers. Solving for the susceptibility, $\chi$, one gets [2,27]

**pdfMachine**
**A pdf writer that produces quality PDF files with ease!**
Produce quality PDF files in seconds and preserve the integrity of your original documents. Compatible across nearly all Windows platforms, simply open the document you want to convert, click "print", select the "Broadgun pdfMachine printer" and that's it! Get yours now!

$$\frac{1}{\chi} = \frac{T}{C} - \frac{1}{\chi_0} - \frac{b}{T-\theta}$$

$$\frac{1}{\chi} = \frac{T + (C/\chi_0)}{C} - \frac{b}{T-\theta} \qquad (2.5)$$

Where $C$, $\chi_0$, $b$ and $\theta$ are constants for particular substance and are given by

$$C = C_A + C_B$$

$$\frac{1}{\chi_0} = -\frac{1}{C^2}[C_A^2\lambda_{AA} + C_B^2\lambda_{BB} + 2C_AC_B\lambda_{AB}]$$

$$b = \frac{C_AC_B}{C^3}[C_A^2(\lambda_{AA} - \lambda_{BB})^2 + C_B^2(\lambda_{BB} - \lambda_{AB})^2$$

$$- 2C_AC_B\{\lambda_{AB}^2 - (\lambda_{AA} + \lambda_{BB})\lambda_{AB} + \lambda_{AA}\lambda_{BB}\}]$$

$$\theta = -\frac{C_AC_B}{C}(\lambda_{AB} + \lambda_{BB}) - 2\lambda_{AB}$$

Equation (2.5) represents a hyperbola, and the physically meaning part of it is plotted in Fig. 2.9. This curvature of the plot of $1/\chi$ versus $T$ is a characteristics feature of a ferrimagnet. It cuts the temperature axis at $T_C$, called the Ferrimagnetic Curie point. At high temperatures the last term of equation (2.5) become negligible, and reduces to a Curie-Weiss law:

$$\chi = \frac{C}{T + (C/\chi_0)}$$

This is the equation of straight line, shown dashed in Fig. 2.9, to which the $1/\chi$ versus $T$ curve becomes asymptotic at high temperatures.

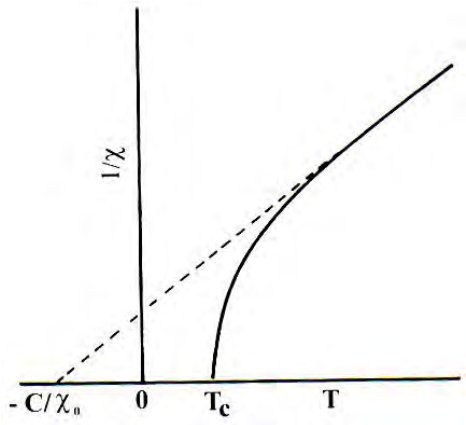


**Fig. 2.8.** The temperature dependence of the inverse susceptibility for ferrimagnets.

**pdfMachine**
**A pdf writer that produces quality PDF files with ease!**
Produce quality PDF files in seconds and preserve the integrity of your original documents. Compatible across nearly all Windows platforms, simply open the document you want to convert, click "print", select the "Broadgun pdfMachine printer" and that's it! Get yours now!

The Ferrimagnetic Curie temperature $T_C$ is obtained from equations (2.3) and (2.4) with $H = 0$ and setting the determinant of the coefficients of $M_i$ equal to zero. This gives

$$T_C = \frac{1}{2}[C_A\lambda_{AA} + C_B\lambda_{BB} + \{(C_A\lambda_{AA} - C_B\lambda_{BB})^2 + 4C_AC_B\lambda_{AB}^2\}^2] \qquad (2.6)$$

Equation (2.5) is in good agreement with the experiment, except near the Curie point. The experimental Curie temperature, the temperature at which the susceptibility becomes infinite and spontaneous magnetization appears, is lower than the theoretical Curie temperature [27]. This disagreement between theory and experiment in the region of Curie point is presumably due to the short-range spin order (spin clusters) at temperatures above experimental $T_C$ [2, 27].

The sub-lattice magnetizations will in general have different temperature dependences because the effective molecular fields acting on them are different. This suggests the possibility of having anomaly in the net magnetization versus temperature curves, Fig. 2.9. For most ferrimagnets the curve is similar to that of ferromagnets, but in a few cases there be a compensation point in the curve, Fig. 2.9(c) [1, 27]. At a point below the Curie temperature point, the two sub-lattice magnetizations are equal and thus appear to have no moment. This temperature is called the compensation point. Below this temperature one sub-lattice magnetization is larger and provides the net moment. Above this temperature the other magnetization does dominates and the net magnetization reverses direction.

The essential requisite for Néel configuration is a strong negative exchange interaction between *A* and *B* sub-lattices which results in their being magnetized in opposite directions below the transition point. But there may be cases where intra-sublattice interactions are comparable with inter-sublattice interaction. Neel's theory predicts paramagnetism for such substances at all temperatures. This is unreasonable since strong *AA* or *BB* interaction may lead to some kind of ordering especially at low temperature. In the cases of no *AB* interaction, antiferromagnetic ordering may be expected either in the *A* or in the *B* sub-lattice. Under certain conditions there may be non-collinear spin arrays of still lower energy.

**pdfMachine**
**A pdf writer that produces quality PDF files with ease!**
Produce quality PDF files in seconds and preserve the integrity of your original documents. Compatible across nearly all Windows platforms, simply open the document you want to convert, click “print”, select the “Broadgun pdfMachine printer” and that’s it! Get yours now!

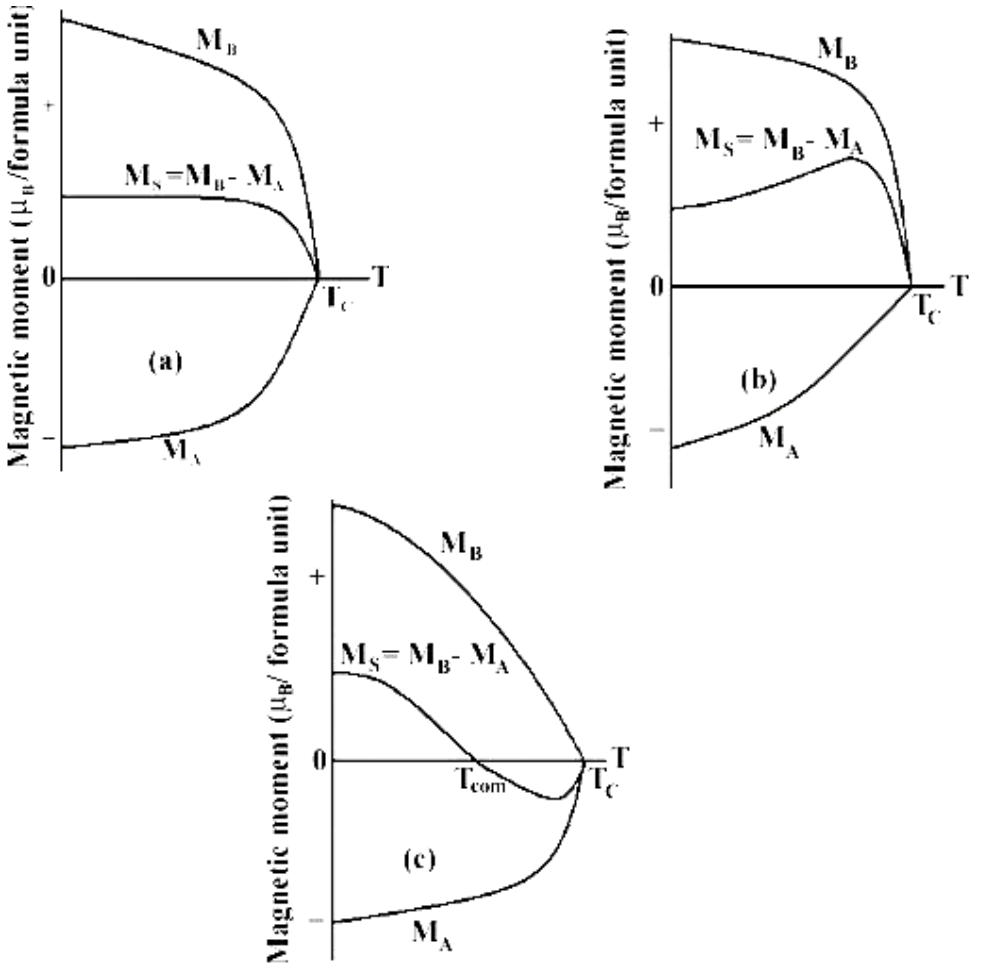


**Fig. 2.9.** Superposition of various combinations of two opposing sublattice magnetizations producing differing resultants including one with a compensation point (schematic).

### 2.6.4 Effect of Magnetic Moments in $Li_xMg_{0.4}Ni_{0.6-2x}Fe_{2+x}O_4$ Spinel Ferrites

$Fe_3O_4$ has ferromagnetic properties because of its inverse structure which leads to the formation of domains. A unit cell of $Fe_3O_4$ contains eight formula units each of which may be written in the form $Fe^{3+}[Fe^{2+}Fe^{3+}]O_4^{2-}$ [25]. Snoek and his co-workers found that oxides of inverse structure could be artificially produced in which the divalent ions of another element, for example *Mn*, *Ni*, *Co*, *Mg* or *Cu*, could be substituted for the divalent $Fe^{2+}$ ions in $Fe_3O_4$. An extensive range of ferrites could thus be made having the general formula $\vec{Fe}^{3+}[\overleftarrow{M}^{2+}\overleftarrow{Fe}^{3+}]O_4^{2-}$, where arrows indicate spin

pdfMachine
A pdf writer that produces quality PDF files with ease!
Produce quality PDF files in seconds and preserve the integrity of your original documents. Compatible across nearly all Windows platforms, simply open the document you want to convert, click "print", select the "Broadgun pdfMachine printer" and that's it! Get yours now!

ordering. Since the trivalent iron ions are equally distributed on *A* and *B* sites they cancel each other out magnetically, and the magnetic moment per formula unit is then theoretically the same as the magnetic moment of the divalent ion. The *Ni* ferrite has a moment of $2.3\mu_B$ compared with a theoretical value of $2\mu_B$ [1].

*Li* ferrite is a inverse spinel, with $Li^{1+}$ ions having no 3d shell's electron in *A* sites have zero magnetic moment; $Fe^{3+}$ ions in *B* sites have a magnetic moment $5\mu_B$. The cation distribution can be written as $\vec{Fe}^{3+}[\overleftarrow{Li}^{1+}\ \overleftarrow{Fe}^{3+}]O_4^{2-}$, where spin ordering is indicated by arrows. Again, *Ni* ferrites have inverse spinel structure and its formula may be written as $\vec{Fe}^{3+}[\overleftarrow{Ni}^{2+}\ \overleftarrow{Fe}^{3+}]O_4^{2-}$. On the other hand Mg ferrites have inverse spinel structure and its formula may be written as $Mg^{2+}{}_{1-x}\ \vec{Fe}^{3+}[Mg^{2+}{}_x\ \overleftarrow{Fe}^{3+}{}_{2-x}]O_4^{2-}$, where x is the degree of inversion.

The magnetic spins on each of the sites are antiparallel; so, the octahedral site is dominant. For reduction of magnetization a nonmagnetic ion (or magnetic ion having fewer spins than $Fe^{3+}$) is introduced on the octahedral sites as a replacement for $Fe^{3+}$.To increase the magnetization, a non magnetic ion is introduced on the tetrahedral site. In either case, the octahedral site normally remains dominant [10].

Theoretical aspect of magnetic moment in *Zn* substituted *Ni* Ferrite is explained by Velenzuala [2]. The zero magnetic moment of $Zn^{2+}$ ions leaves trivalent iron ions on *B* sites with a negative *BB* interaction between equal ions. Therefore *Zn* ferrite is not ferromagnetic. Zinc ferrite therefore be expected to be antiferromagnetic and thus to have a Néel point, though measurements show it to be paramagnetic only [1, 2, 25, 27]

Magnetic properties can be modified widely by cation substitution. In the present case An illustrative case is substituion of *Ni* by *Zn* in *Co* ferrite to form solid solutions $Ni_{1-x}Zn_xFe_2O_4$. The cation distribution can be written as $(Zn_x^{2+}Fe_{1-x}^{3+})[Ni_{1-x}^{2+}Fe_{1+x}^{3+}]O_4^{2-}$ [2]. $Zn^{2+}$ is diamagnetic and its main effect is to break linkages between magnetic cations. Another effect is to increase interaction distance by expanding the unit cell, since it has an ionic radious larger than the *Ni* and *Fe* radii. The most remarkable effect is that substitution of this diamagnetic cation (*Zn*) results in a significant increase in magnetic moment in a number of spinel solid solutions, Fig. 2.10.

**pdfMachine**
**A pdf writer that produces quality PDF files with ease!**
Produce quality PDF files in seconds and preserve the integrity of your original documents. Compatible across nearly all Windows platforms, simply open the document you want to convert, click "print", select the "Broadgun pdfMachine printer" and that's it! Get yours now!

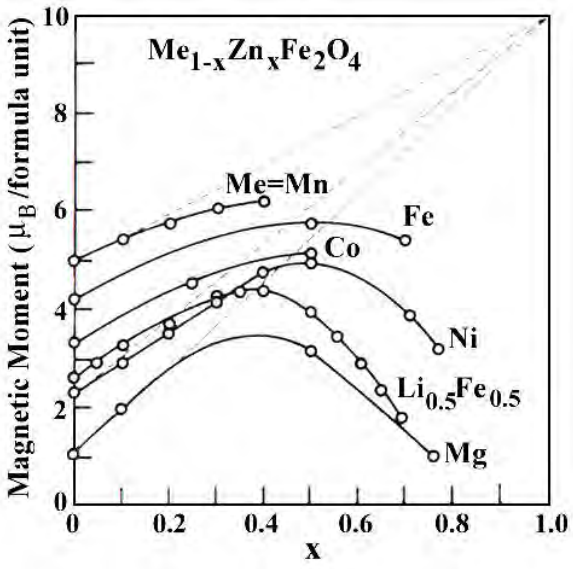


**Fig. 2.10.** Variation of Magnetic moment (in Bohr magnetons per formula unit) with increasing zinc substitution [1, 2].

Magnetic moment as a function of *Zn* content in *Li*-Ferrite, *Mg*-Ferrite and *Ni*-Ferrite shows an increase for small substitutions goes through a maximum for intermediate values, decreases and finally vanishes for high *Zn* contents. For *Zn* substituted *Li*-Ferrite it is observed that the magnetic moment increases up *Zn* content , $x$= 0.4 then it started to decrease. In *Zn* substituted *Ni* ferrite and *Mg* ferrite the magnetic moment increases up to *Zn* content , $x$= 0.5, then it decreases .

A simple analysis shows that this increase can be expected for an antiparallel alignment. As the *Zn* content increases, magnetic moments decreases in sublattice *A* and increase in sublattice *B*. If the magnetic moment of *Fe* and *Ni* are 5 and ~2.3 $\mu_B$/ion, respectively, then, per formula unit, the total moment in Bohr magnetons on *B* sublattice is $2.3(1-x)+5(1+x)$ and on *A* sublattice the total antiparallel moment is $5(1-x)$. If the resultant moment per formula unit is $M_S(0)$, then by taking the difference of *A* and *B* moments [26],

$$M_S(0) = 2.3(1-x)+5(1+x)-5(1-x)$$
$$= x(10-2.3)+2.3$$

A linear relationship is obtained with a slope of 7.7, predicting a moment value of $10\mu_B$ per formula unit for *Zn* substitution $x=1$, as shown by the broken lines in Fig. 2.10. This relationship is not followed over the entire composition range. However, as the *Zn* content increases, $A-O-B$ interactions become too weak and $B-O-B$ interactions

**pdfMachine**
**A pdf writer that produces quality PDF files with ease!**
Produce quality PDF files in seconds and preserve the integrity of your original documents. Compatible across nearly all Windows platforms, simply open the document you want to convert, click "print", select the "Broadgun pdfMachine printer" and that's it! Get yours now!

begin to dominate. That is, the average distance between the interacting spins gets larger. As a consequence, the system becomes frustrated causing a perturbation to the magnetically ordered spins as large number of *B* sites spins gets non-magnetic impurity atoms as their nearest neighbours.

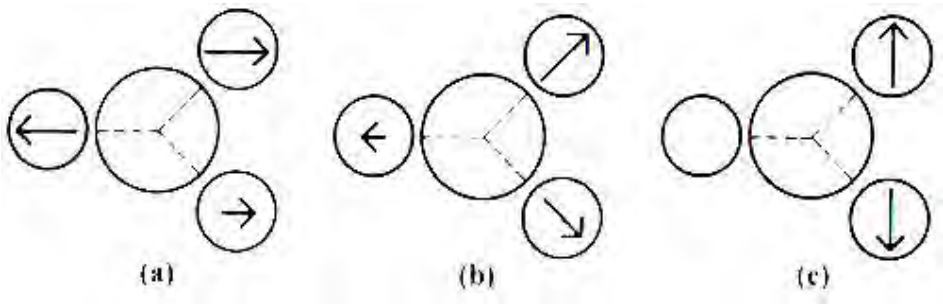


**Fig. 2.11.** Schematic representation of spin arrangements in $Ni_{1-x}Zn_xFe_2O_4$: (a) ferrimagnetic (for $x \leq 0.5$); (b) triangular or Yafet-Kittel (for $x > 0.5$); and (c) antiferromagnetic for $x \approx 1$.

The *B* spins are no longer held in place due to this weak anti-ferromagnetic *A*-*B* interaction leading to non-collinearity or canting among the *B* sublattice. Thus for $x > 0.5$ *Zn* content, instead of a collinear antiparallel alignment, canted structure appears, where spins in *B* sites are no longer parallel [2, 32], Fig. 2.11. Evidence of this triangular structure has been observed by neutron diffraction [22]; a theoretical analysis showed that departure from collinear order depends on the ratio of the $A-O-B$ to $B-O-B$ molecular field coefficients, $\lambda_{AB}/\lambda_{BB}$ [33]. For high *Zn* concentration, $B-O-B$ interactions dominant and the ferrite become antiferromagnetic for $x=1$ [2].

The theoretical aspect of the variation of magnetic moment in present ferrite system , $Li_xMg_{0.4}Ni_{0.6-2x}Fe_{2+x}O_4$ ferrite, increasing *Li* content can be explained as below from the cation distribution as stated in section

It is known that $Li^{1+}$, $Ni^{2+}$ and $Mg^{2+}$ ions occupy B sites, although Fe ions exist at both A and B sites [12]. The cation distribution of various $Li_xMg_{0.4}Ni_{0.6-2x}Fe_{2+x}O_4$ ferrite assumed as $(Fe^{3+}_{0.9})_A\,[Li^{1+}_xMg^{2+}_{0.4}Ni_{0.6-2x}\,Fe^{3+}_{1.1+x}]_B$ [31]

where the term within the square bracket indicates the octahedral (B) sites and the first term is tetrahedral (A) sites. When $Li^{1+}$ ions are introduced at the cost of $Ni^{2+}$ions, $Fe^{3+}$ ions concentration at B sites increases. As $Li^{1+}$ and $Mg^{2+}$ are non-magnetic, the magnetic moment of B site will depend on the $Ni^{2+}$ and $Fe^{3+}$ ion. Progressive substitution of $Li^+$ ion increases $Fe^{3+}$ ion and decreases $Ni^{2+}$ ion concentration at B sites.

**pdfMachine**
**A pdf writer that produces quality PDF files with ease!**
Produce quality PDF files in seconds and preserve the integrity of your original documents. Compatible across nearly all Windows platforms, simply open the document you want to convert, click "print", select the "Broadgun pdfMachine printer" and that's it! Get yours now!

The $Fe^{3+}$ content is increased by $2+x$ as the *Li* content increases As a result, the magnetic moments of B sublattice increases for small *Li* content.

## 2.7 Microstructure

A polycrystal is much more than many tiny crystals bonded together. The interfaces between the crystals, or the grain boundaries which separate and bond the grains, are complex and interactive interfaces. The whole set of a given material's properties (mechanical, chemical and especially electrical and magnetic) depend strongly on the nature of the microstructure.

In the simplest case, the grain boundary is the region, which accommodates the difference in crystallographic orientation between the neighbouring grains. For certain simple arrangements, the grain boundary is made of an array of dislocations whose number and spacing depends on the angular deviation between the grains. The ionic nature of ferrites leads to dislocation patterns considerably more complex than in metals, since electrostatic energy accounts for a significant fraction of the total boundary energy [2].

For low-loss ferrite, Ghate [1] states that the grain boundaries influence properties by

1) creating a high ressistivity intergranular layer,
2) acting as a sink for impurities which may act as a sintering aid and grain growth modifiers,
3) providing a path for oxygen diffusion, which may modify the oxidation state of cations near the boundaries.

In addition to grain boundaries, ceramic imperfections can impede domain wall motion and thus reduce the magnetic property. Among these are pores, cracks, inclusions, second phases, as well as residual strains. Imperfections also act as energy wells that pin the domain walls and require higher activation energy to detach. Stresses are microstructural imperfections that can result from impurities or processing problems such as too rapid a cool. They affect the domain dynamics and are responsible for a much greater share of the degradation of properties than would expect [1].

Grain growth kinetics depends strongly on the impurity content. A minor dopant can drastically change the nature and concentration of defects in the matrix, affecting

**pdfMachine**
**A pdf writer that produces quality PDF files with ease!**
Produce quality PDF files in seconds and preserve the integrity of your original documents. Compatible across nearly all Windows platforms, simply open the document you want to convert, click "print", select the "Broadgun pdfMachine printer" and that's it! Get yours now!

grain boundary motion, pore mobility and pore removal [2, 41]. The effect of a given dopant depends on its valence and solubility with respect to host material. If it is not soluble at the sintering temperature, the dopant becomes a second phase which usually segregates to the grain boundary.

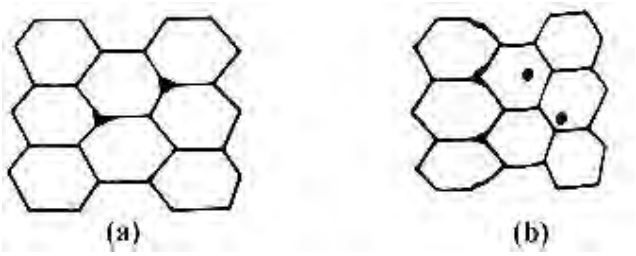


**Fig. 2.12.** Porosity character: (a) intergranular, (b) intragranular.

The porosity of ceramic samples results from two sources, intragranular porosity and intergranular porosity, Fig. 2.12. An undesirable effect in ceramic samples is the formation of exaggerated or discontinuous grain growth which is characterized by the excessive growth of some grains at the expense of small, neighbouring ones (Fig. 2.13). When this occurs, the large grain has a high defect concentration. Discontinuous growth is believed to result from one or several of the following: powder mixtures with impurities; a very large distribution of initial particle size; sintering at excessively high temperatures; in ferrites containing *Zn* and /or *Mn*, a low $O_2$ partial pressure in the sintering atmosphere. When a very large grain is surrounded by smaller ones, it is called 'duplex' microstructure.

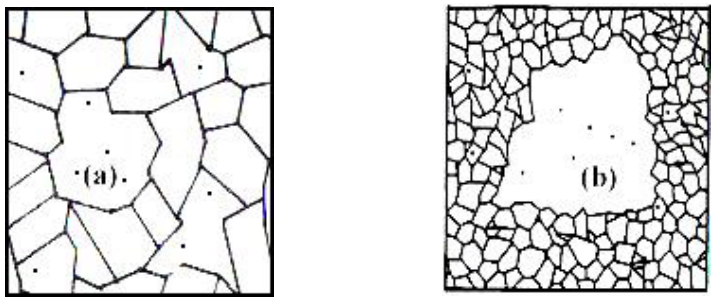


**Fig. 2.13.** Grain growth (a) discontinuous, (b) duplex (schematic).

**pdfMachine**
**A pdf writer that produces quality PDF files with ease!**
Produce quality PDF files in seconds and preserve the integrity of your original documents. Compatible across nearly all Windows platforms, simply open the document you want to convert, click "print", select the "Broadgun pdfMachine printer" and that's it! Get yours now!

## 2.8 Theories of Permeability

Permeability is defined as the proportionality constant between the magnetic field induction $B$ and applied field intensity $H$ [2, 24, 34]:

$$B = \mu H \tag{2.7}$$

If the applied field is very low, approaching zero, the ratio will be called the initial permeability, Fig. 2.15 and is given by

$$\mu_i = \frac{\Delta B}{\Delta H}_{(\Delta H \to 0)}$$

This simple definition needs further sophistications. A magnetic material subjected to an ac magnetic field can be written as

$$H = H_0 e^{i\omega t} \tag{2.8}$$

It is observed that the magnetic flux density $B$ lag behind $H$. This is caused due to the presence of various losses and is thus expressed as

$$B = B_0 e^{i(\omega t-\delta)} \tag{2.9}$$

Here $\delta$ is the phase angle that marks the delay of $B$ with respect to $H$. The permeability is then given by

$$\mu = \frac{B}{H} = \frac{B_0 e^{i(\omega t-\delta)}}{H_0 e^{i\omega t}} = \frac{B_0 e^{-i\delta}}{H_0} = \frac{B_0}{H_0}\cos\delta - i\frac{B_0}{H_0}\sin\delta = \mu^{/} - i\mu^{//} \tag{2.10}$$

where $$\mu^{/} = \frac{B_0}{H_0}\cos\delta \tag{2.11}$$

and $$\mu^{//} = \frac{B_0}{H_0}\sin\delta \tag{2.12}$$

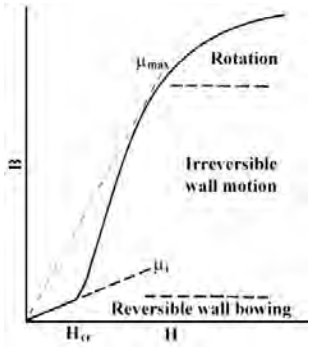


**Fig. 2.14.** Schematic magnetization curve showing the important parameter: initial permeability, $\mu_i$ (the slope of the curve at low fields) and the main magnetization mechanism in each magnetization range [2].

**pdfMachine**
**A pdf writer that produces quality PDF files with ease!**
Produce quality PDF files in seconds and preserve the integrity of your original documents. Compatible across nearly all Windows platforms, simply open the document you want to convert, click "print", select the "Broadgun pdfMachine printer" and that's it! Get yours now!

The real part ($\mu'$) of complex permeability ($\mu$), as expressed in equation (2.10) represents the component of *B* which is in phase with *H*, so it corresponds to the normal permeability. If there are no losses, we should have $\mu = \mu'$. The imaginary part $\mu''$ corresponds to that of *B*, which is delayed by phase angle 90° from *H* [23, 30]. The presence of such a component requires a supply of energy to maintain the alternating magnetization, regardless of the origin of delay. The ratio of $\mu''$ to $\mu'$, as is evident from equation (2.12) and (2.11) gives

$$\frac{\mu''}{\mu'} = \frac{\frac{B_0}{H_0}\sin\delta}{\frac{B_0}{H_0}\cos\delta} = \tan\delta \tag{2.13}$$

This $\tan\delta$ is called loss factor.

The quality factor is defined as the reciprocal of this loss factor, i.e.

$$\text{Quality factor} = \frac{1}{\tan\delta} \tag{2.14}$$

$$\text{And the relative quality factor, } Q = \frac{\mu'}{\tan\delta} \tag{2.15}$$

The curves that show the variation of both $\mu'$ and $\mu''$ with frequency are called the magnetic spectrum or permeability spectrum of the material [27]. The variation of permeability with frequency is referred to as dispersion. The measurement of complex permeability gives us valuable information about the nature of domain wall and their movements. In dynamic measurements the eddy current loss is very important. This occurs due to the irreversible domain wall movements. The permeability of a ferrimagnetic substance is the combined effect of the wall permeability and rotational permeability mechanisms.

### 2.8.1 Mechanisms of Permeability

The mechanisms can be explained as follows: A demagnetized magnetic material is divided into number of Weiss domains separated by Bloch walls. In each domain all the magnetic moments are oriented in parallel and the magnetization has its saturation value $M_s$. In the walls the magnetization direction changes gradually from the direction of magnetization in one domain to that in the next. The equilibrium positions

**pdfMachine**
**A pdf writer that produces quality PDF files with ease!**
Produce quality PDF files in seconds and preserve the integrity of your original documents. Compatible across nearly all Windows platforms, simply open the document you want to convert, click "print", select the "Broadgun pdfMachine printer" and that's it! Get yours now!

of the walls result from the interactions with the magnetization in neighbouring domains and from the influence of pores; crystal boundaries and chemical inhomogeneities which tend to favour certain wall positions.

### 2.8.1.1 Wall Permeability

The mechanism of wall permeability arises from the displacement of the domain walls in small fields. Lets us consider a piece of material in the demagnetized state, divided into Weiss domains with equal thickness $L$ by means of 180˚ Bloch walls (as in the Fig. 2.15).

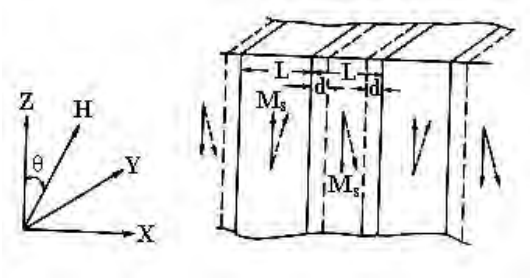


**Fig 2.15.** Magnetization by wall motion and spin rotation.

The walls are parallel to the $YZ$ plane. The magnetization $M_s$ in the domains is oriented alternately in the $+Z$ or $-Z$ direction. When a field $H$ with a component in the $+Z$ direction is applied, the magnetization in this direction will be favoured. A displacement $dx$ of the walls in the direction shown by the dotted lines will decrease the energy density by an amount [35, 36]:

$$\frac{2M_s H_z dx}{L}$$

This can be described as a pressure $M_s H_z$ exerted on each wall. The pressure will be counteracted by restoring forces which for small deviations may assume to be $kdx$ per unit wall surface. The new equilibrium position is then given by

$$d = \frac{M_s H_z dx}{L}$$

From the change in the magnetization

$$\Delta M = \frac{2M_s d}{L},$$

**pdfMachine**
**A pdf writer that produces quality PDF files with ease!**
Produce quality PDF files in seconds and preserve the integrity of your original documents. Compatible across nearly all Windows platforms, simply open the document you want to convert, click “print”, select the “Broadgun pdfMachine printer” and that’s it! Get yours now!

the wall susceptibility $\chi_w$ may be calculated. Let $H$ makes the angle $\theta$ with $Z$ direction. The magnetization in the $\theta$ direction becomes

$$(\Delta M)_\theta = \frac{2M_s d}{L}\cos\theta \text{, And with } H_z = H\cos\theta \text{ and } d = \frac{2M_s H_z}{K}$$

we obtain

$$\chi_w = \frac{(\Delta M)_\theta}{H} = \frac{4M_s^2\cos^2\theta}{KL} \tag{2.16}$$

### 2.8.1.2 Rotational Permeability

The rotational permeability mechanism arises from rotation of the magnetization in each domain. The direction of $M$ can be found by minimizing the magnetic energy $E$ as a function of the orientation. Major contribution to $E$ comes from the crystal anisotropy energy. Other contributions may be due to the stress and shape anisotropy. The stress may influence the magnetic energy via the magnetostriction. The shape anisotropy is caused by the boundaries of the sample as well as by pores, nonmagnetic inclusions and inhomogeneities. For small angular deviations, $\alpha_x$ and $\alpha_y$ may be written as

$$\alpha_x = \frac{M_x}{M_s} \text{ and } \alpha_y = \frac{M_y}{M_s}.$$

For equilibrium $Z$-direction, $E$ may be expressed as [36]

$$E = E_0 + \frac{1}{2}\alpha_x^2 E_{xx} + \frac{1}{2}\alpha_y^2 E_{yy}$$

where it is assumed that $x$ and $y$ are the principal axes of the energy minimum. Instead of $E_{xx}$ & $E_{yy}$, the anisotropy field $H_x^A$ and $H_y^A$ are often introduced. Their magnitude is given by

$$H_x^A = \frac{E_{xx}}{2M_s} \text{ and } H_y^A = \frac{E_{yy}}{2M_s},$$

$H_x^A$ & $H_y^A$ represent the stiffness with which the magnetization is bound to the equilibrium direction for deviations in $x$ and $y$ direction, respectively. The rotational susceptibilities $\chi_{r,x}$ and $\chi_{r,y}$ for fields applied along $x$ and $y$ directions, respectively are

pdfMachine
A pdf writer that produces quality PDF files with ease!
Produce quality PDF files in seconds and preserve the integrity of your original documents. Compatible across nearly all Windows platforms, simply open the document you want to convert, click "print", select the "Broadgun pdfMachine printer" and that's it! Get yours now!

$$\chi_{r,x} = \frac{M_s}{H_x^A} \text{ and } \chi_{r,y} = \frac{M_s}{H_y^A}.$$

For cubic materials it is often found that $H_x^A$ and $H_y^A$ are equal. For $H_x^A = H_y^A = H^A$ and a field $H$ which makes an angle $\theta$ with the $Z$ direction (as shown in Fig. 2.15) the rotational susceptibility, $\chi_{r,c}$ in one crystallite becomes

$$\chi_{r,c} = \frac{M_s}{H^A} \sin^2 \theta \tag{2.17}$$

A polycrystalline material consisting of a large number of randomly oriented grains of different shapes, with each grain divided into domains in a certain way. The rotational susceptibility $\chi_r$ of the material has to be obtained as a weighted average of $\chi_{r,c}$ of each crystallite, where the mutual influence of neighbouring crystallites has to be taken into account. If the crystal anisotropy dominates other anisotropies, then $H^A$ will be constant throughout the material, so only the factor $\sin^2 \theta$ (equation 2.17) has to be averaged. Snoek [36] assuming a linear averaging of $\chi_{r,c}$ and found

$$\chi_r = \frac{2M_s}{3H^A}$$

The total internal susceptibility

$$\chi = \chi_w + \chi_r = \frac{4M_s^2 \cos^2 \theta}{KL} + \frac{2M_s}{3H^A} \tag{2.18}$$

If the shape and stress anisotropies cannot be neglected, $H^A$ will be larger. Any estimate of $\chi_r$ will then be rather uncertain as long as the domain structure, and the pore distribution in the material are not known. A similar estimate of $\chi_w$ would require knowledge of the stiffness parameter $k$ and the domain width $L$. These parameters are influenced by such factors as imperfection, porosity and crystallite shape and distribution which are essentially unknown.

### 2.8.2 Frequency dependent Permeability Curve :

The techniques of impedance spectroscopy, widely used in dielectrics have been applied to magnetic materials [28]. In this method, impedance measurements as a function of frequency are modified by means of an equivalent circuit and its elements are associated with the physical parameters of the material. The complex permeability,

pdfMachine
A pdf writer that produces quality PDF files with ease!
Produce quality PDF files in seconds and preserve the integrity of your original documents. Compatible across nearly all Windows platforms, simply open the document you want to convert, click "print", select the "Broadgun pdfMachine printer" and that's it! Get yours now!

$\mu^*$, is determined from the complex impedance ,$Z^*$, by :

$$\mu^* = (jk/\omega)Z^* \qquad (2.19)$$

where $k$ is the geometric constant relating to inductance , $l$, to the permeability. The equivalent circuit for domain wall bowing (applied field lower than critical field) is a parallel *RL* arrangement; for wall displacement, additional Warbarg-type impedance element is required (Irvine *et al*.) [37].

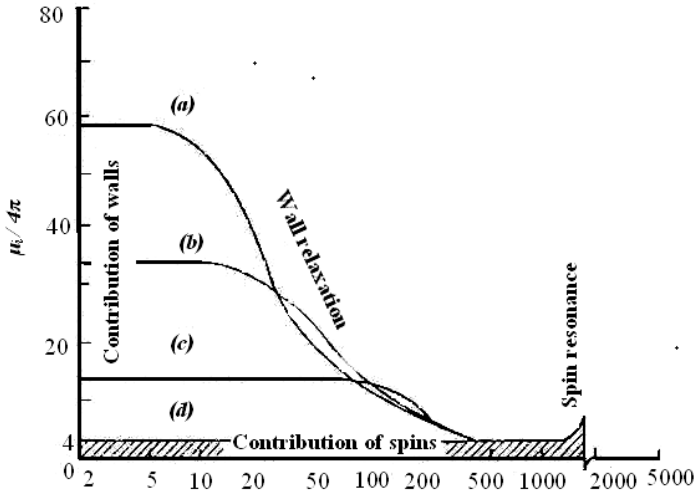


**Fig. 2.16.** Permeability spectra of $NiFe_2O_4$ samples with different grain size: (a)11µm;(b) 5µm;(c)2 µm (d)size <0.2 µm( single domain behaviour) [2]

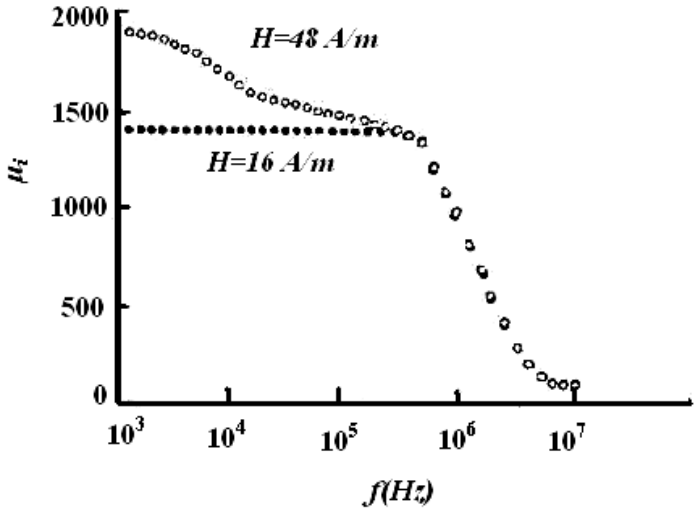


**Fig. 2.17.** Permeability spectrum of a *Ni-Zn* sample at fields above (open circles) and below (filled circles) the critical field [38].

**pdfMachine**
**A pdf writer that produces quality PDF files with ease!**
Produce quality PDF files in seconds and preserve the integrity of your original documents. Compatible across nearly all Windows platforms, simply open the document you want to convert, click "print", select the "Broadgun pdfMachine printer" and that's it! Get yours now!

Many of the specific applications of ferrites depend on their behaviour at high frequencies. When subjected to an ac field, ferrite permeability shows several dispersions; as the field frequency increases, the various magnetization mechanisms become unable to follow the field. The dispersion frequency for each mechanism is different time constants, Fig. 2.16. The low frequency dispersions are associated with domain wall dynamics and the high frequency dispersion, with spin resonance. The spin resonance phenomena occur usually in the GHz range. The two main magnetization mechanisms are wall bowing and wall displacement as discussed before in section 2.8. Any field results in a bowing of pinned walls, and if this field has higher value than the corresponding critical field, walls are unpinned and displaced. Otherwise, bowed walls remain pinned to material defects. Measurements at low fields therefore show only one wall dispersion. Measurements at high fields, several, complex dispersions are observed, such as those in Fig. 2.17. Wall displacement dispersion occurs at lower frequencies than wall bowing, since hysteresis is a more complex phenomenon of wall bowing, unpinning, displacement and pinning steps.

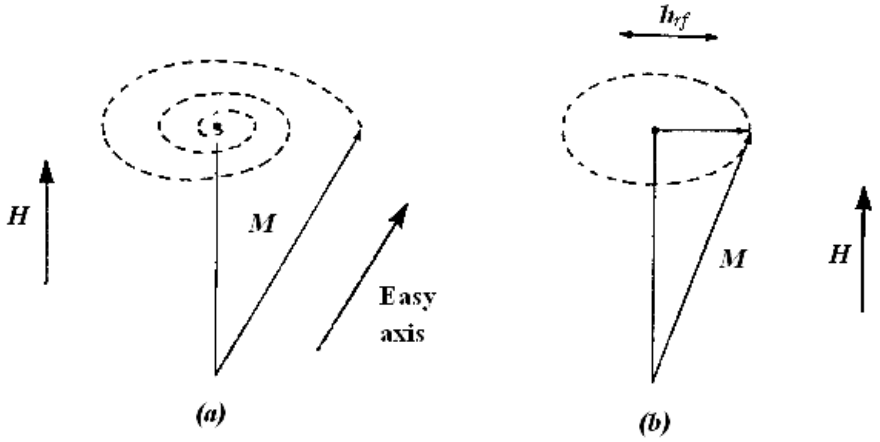


**Fig. 2. 18.** (a) Schematic representation of the spin deviation from an easy axis by precessional spiralling into the field direction, (b) Precession is maintained by a perpendicular rf field, $h_{rf}$ [2].

At very high frequencies, domain walls are unable to follow the field and the only remaining megnetisation mechanism is spin rotation within domains. This mechanism eventually also shows a dispersion, which always takes the form of a resonance. Spins are subjected to the anisotropy field, representing spin-lattice coupling; as an external field is applied (out of the spins' easy direction), spins experience a

**pdfMachine**
**A pdf writer that produces quality PDF files with ease!**
Produce quality PDF files in seconds and preserve the integrity of your original documents. Compatible across nearly all Windows platforms, simply open the document you want to convert, click "print", select the "Broadgun pdfMachine printer" and that's it! Get yours now!

torque. However, the response of spins is not instantaneous; spins precess around the field direction for a certain time (the relaxation time, $\tau$) before adopting the new orientation, Fig. 2.18.

The frequency of this precession is given by the Larmor frequency:

$$\omega_L = \gamma \mu_o H_T \qquad (2.20)$$

where $H_T$ is the total field acting on the spin.

$H_T = H_K + H + H_d + \ldots\ldots$, where $H_K$, $H$, $H_d$ are the anisotropy and the external and demagnetization fields, respectively. If an ac field of angular frequency $\omega_L$ is applied to the sample, a resonant absorption (ferromagnetic resonance) occurs. The Larmour frequency is independent of the precession amplitude.

## 2.9 Magnetization Mechanism

### 2.9.1 Concept of Magnetic Domain and Domain Wall (Weiss Domain Structure)

In 1907 Pierre Weiss in his paper "Hypothesis of the molecular field" [29, 39] postulated that a ferromagnetic material rather than be uniformly magnetized, is divided into a number of regions of domains, each of which is magnetized to saturation level but the direction of magnetization from domain to domain need not be parallel. The magnetization vectors are parallel to preferred direction such that the demagnetization field, and hence the demagnetization energy ($W_{dem.} = 1/8\pi\ H^2_D$) is as small as possible. The total magnetization is then given by the vector summation of individual magnetization over all domains. The demagnetized state of the magnet is from the view point of an observer outside the material. In ferromagnetic materials, the atomic magnetic moments aligned in parallel fashion, while in ferrite domain, the net moments of the anti ferromagnetic interaction are spontaneously oriented parallel to each other (even without applied magnetic field) [40]. The applied field serves as a control in changing the balance of potential energy within the, magnetic material. These uniformly magnetized domains are separated by a thin layer in which the magnetization gradually changes from one orientation to another. This transition boundary is called domain wall or Bloch wall.

The domain structure are found basically to reduce the magnetostatic energy i.e.,

**pdfMachine**
**A pdf writer that produces quality PDF files with ease!**
Produce quality PDF files in seconds and preserve the integrity of your original documents. Compatible across nearly all Windows platforms, simply open the document you want to convert, click "print", select the "Broadgun pdfMachine printer" and that's it! Get yours now!

the magnetic potential energy contained in the field lines (or flux lines) connecting north and south poles outside of the material. This concept can be understood by considering a simple case, as shown in Fig. 2.19, in which (a) to (e) represents a cross section of a ferromagnetic single crystal. In Fig. 2.19 (a) a single domain crystal is shown, the value of magnetostatic energy is high. The arrow indicates the direction of magnetization and hence the direction of spin alignment in the domain. If the crystal is divided into two domains (Fig. 2.19 (b), the magnetic energy will be reduced by roughly one half of the single domain case. This splitting process continues to lower the energy of the system until more energy is required to form the domain boundary. When a large domain is split into *n* domains, as shown in Fig. 2.19 (c) the magnetic energy will be reduced to approximately *1/n* of the magnetic energy of that of type (a). For the domain structure configuration in Fig. 2.19 (d) and (e), the magnetic energy is zero as the flux circuit is completed within a crystal, (i.e., flux path never leaves the boundary of the material). These triangular domains are callled closure domains. Therefore the magnetostatic energy is reduced. This type of structure may also be found at the surface of the material.

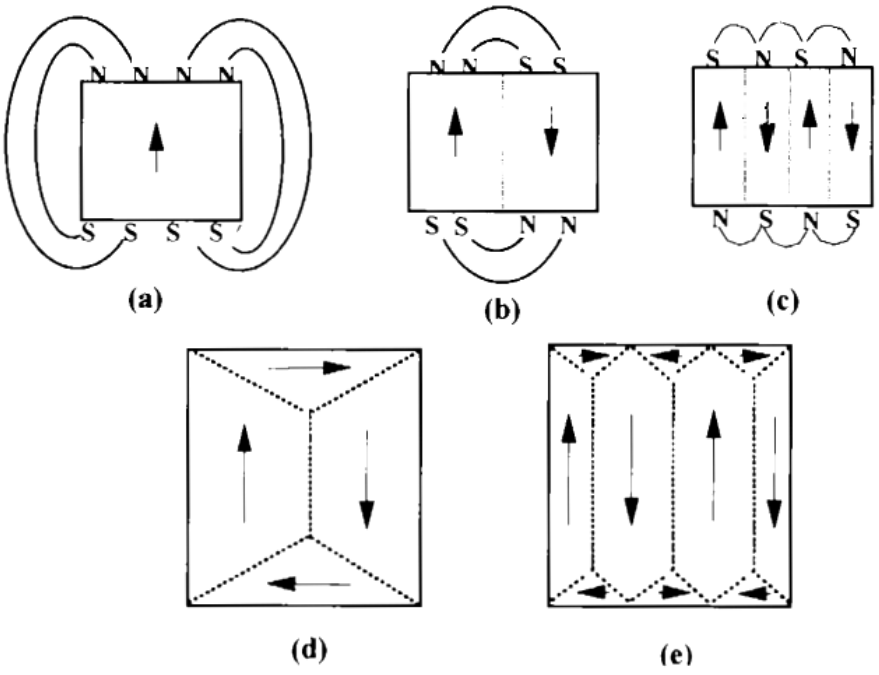


**Fig. 2.19.** Possible domain structures showing progressively low energy .Each part is representing a cross-section of a ferromagnetic single crystal [2, 28].

**pdfMachine**
**A pdf writer that produces quality PDF files with ease!**
Produce quality PDF files in seconds and preserve the integrity of your original documents. Compatible across nearly all Windows platforms, simply open the document you want to convert, click “print”, select the “Broadgun pdfMachine printer” and that’s it! Get yours now!

The boundaries between the domains, are not sharp on atomic scale but are spread over a finite thickness within which the direction of the spin changes gradually from one domain to the next [39]. The spin within a domain wall as shown in Fig. 2.20, are pointing in necessary directions, so that the crystal anisotropy energy within the wall is higher than it is in the adjacent domains. The exchange energy tries to align the spin in a direction parallel to the direction in the domain while the anisotropy energy tries to make the wall thin to minimize misalignment within the easy directions. The actual thickness of the domain wall is determined by the counterbalance of the exchange energy and anisotropy energy.

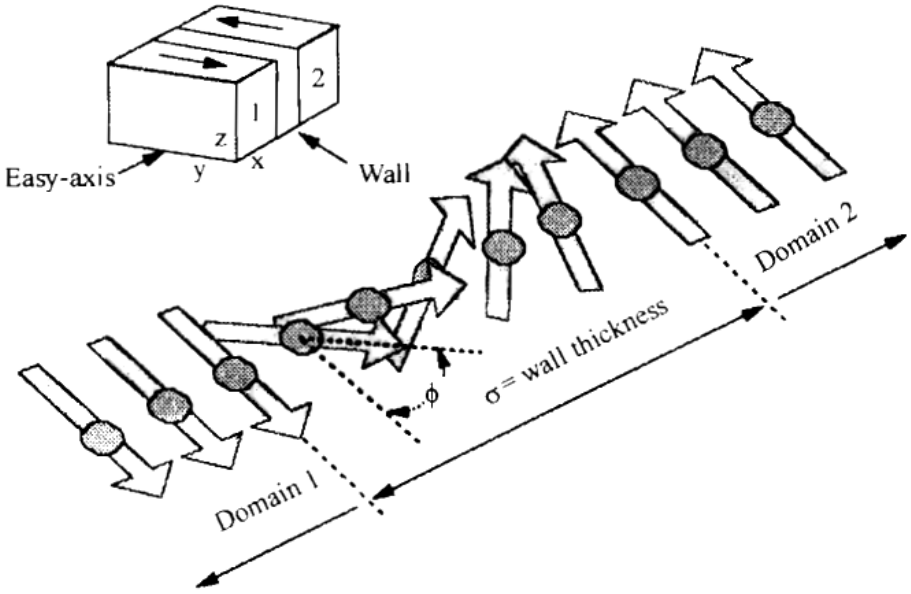


**Fig. 2.20.** Schematic representation of a domain wall. All spins, within the wall thickness are in non-easy direction [27].

### 2.9.2 The dynamic behaviour of Domains

Two general mechanisms are involved in changing the magnetization in a domain and, therefore, changing the magnetization in a sample. The first mechanism acts by rotating the magnetization towards the direction of the field. Since this may involve rotating the magnetization from an axis of easy magnetization in a crystal to one

**pdfMachine**
**A pdf writer that produces quality PDF files with ease!**
Produce quality PDF files in seconds and preserve the integrity of your original documents. Compatible across nearly all Windows platforms, simply open the document you want to convert, click “print”, select the “Broadgun pdfMachine printer” and that’s it! Get yours now!

of more difficult magnetization, a certain amount of anisotropy energy is required. The rotations can be small as indicated in Figure 2.21(a) or they can be almost the equivalent of a complete 180˚ reversal or flip if the crystal structure is uniaxial and if the magnetizing field is opposite to the original magnetization direction of the domain. The other mechanism for changing the domain magnetization is one in which the direction of magnetization remains the same, but the volumes occupied by the different domains may change. In this process, the domains whose magnetizations are in a direction closest to the field direction grow larger while those that are more unfavorably oriented shrink in size. Fig. 2.21(b) shows this process which is called domain wall motion.

The mechanism for domain wall motion starts in the domain wall. Present in the wall is a force (greatest with the moments in the walls that are at an angle of 90˚ to the applied field) that will tend to rotate those moments in line with the field. As a result, the center of the domain wall will move towards the domain opposed to the field. Thus, the area of the domain with favorable orientation will grow at the expense of its neighbour.

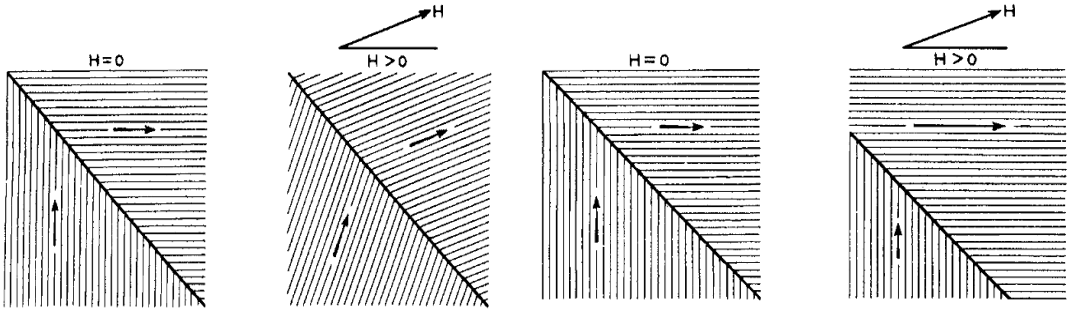


*(a)Volume constant , directions changed* *b)Volume changed , directions constant*

**Fig. 2.21.** (a) Change of domain magnetization by domain wall movement and (b) Change of domain magnetization by domain rotation [28].

### 2.9.3 Bulk Material Magnetization

Although domains are not physical entities such as atoms or crystal lattices and can only be visualized by special means, for the purpose of magnetic structure they are important in explaining the process of magnetization. A material that has strongly oriented moments in a domain often has no resultant bulk material magnetization. Non-magnetic material can be transformed into a strongly magnetic body by domain dynamics discussed above. If the material has been demagnetized, the domains point in

**pdfMachine**
**A pdf writer that produces quality PDF files with ease!**
Produce quality PDF files in seconds and preserve the integrity of your original documents. Compatible across nearly all Windows platforms, simply open the document you want to convert, click “print”, select the “Broadgun pdfMachine printer” and that’s it! Get yours now!

all random directions so that there is complete cancellation and the resultant magnetization is zero (Fig. 2.22). The possible steps to complete orientation of the domains or magnetization of the material are also shown in Fig. 2.22 [28].

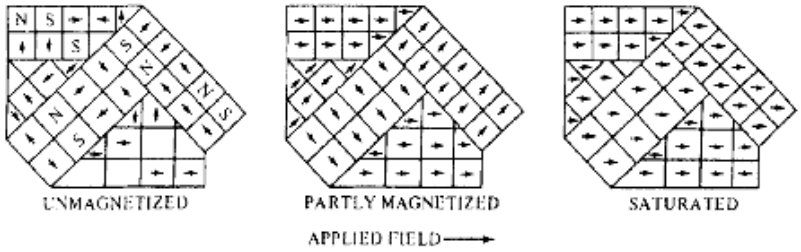


**Fig. 2.22.** Stages in Magnetization of a sample containing several crystals [28].

### 2.9.4 The Magnetization Curve

For unmagnetized bulk material, there is a zero net magnetic moment. It can be predicted that there will be an infinite number of degree of magnetization between the unmagnetized and saturation condition, when the material is subjected to an external magnetic field. These extreme situation correspond respectively, to random orientation of domains complete alignment in one direction with elimination of domain walls. It can be started with the a demagnetized specimen and increase the applied magnetic field and then the bulk material will be progressively magnetized by the domain dynamics. The magnetization of the sample will follow the course as shown in Fig. 2.23 (a) [28]. The slope from the origin to a point on the curve or the ratio *M/H* is defined as magnetic susceptibility. This curve is called Magnetization Curve. This curve is generally percieved as being made of three major portions.

The first, the lower section, is the initial susceptibility region and is characterized by reversible domain wall movements and rotations. By reversible means that after the magnetization slightly with an increase in field the original magnetization conditions can be reversed if the field is reduced to initial value. The contribution of the displacement walls to an initial permeability is entirely dependent on the sort of material studied.

In the second stage magnetization curve, if the field is increased, the intensity of the magnetization increases more drastically, is called the irreversible magnetization range. This range is obtained mainly by the irreversible domain wall motion from one stable state to another.

**pdfMachine**
**A pdf writer that produces quality PDF files with ease!**
Produce quality PDF files in seconds and preserve the integrity of your original documents. Compatible across nearly all Windows platforms, simply open the document you want to convert, click “print”, select the “Broadgun pdfMachine printer” and that’s it! Get yours now!

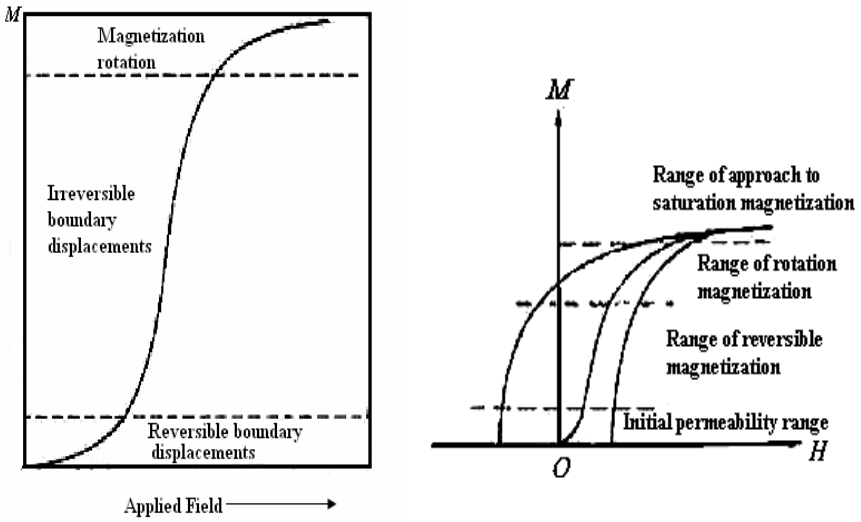


(a) (b)

**Fig. 2.23.** Domain dynamics during various parts of the magnetization curve [28].

If the field is increased further, the magnetization curve become less steep and its process become reversible once more. In the third section of magnetization curve, the displacement of domain walls have already been completed and the magnetization take place by rotation magnetization. This range is called rotation magnetization range. Beyond this range the magnetization gradually approaches to saturation magnetization. (Fig. 2.23 (b))

## References

[1] Goldman ,A., "Handbook of Modern Ferromagnetic Materials", Kluwer Academic Pub., Boston U.S.A, 1999.

[2] Valenzuela, R., "Magnetic Ceramics", Cambridge University Press, Cambridge, 1994.

[3] Haque ,M. M., "Influence of additives on the magnetic and electrical properties of iron-excess Mn-Zn ferrites," M. Phil. Thesis, BUET, Bangladesh, 2000.

[4] Jefferson, C. F. and West, R. G., "Ferrite system for application at lower microwave frequencies," Journal of Applied Physics, Vol- 32, pp 3905-3915, 1961.

[5] West, R. G. and Blankenship, A. C., "Magnetic properties of dense lithium ferrites," Journal of the American Ceramic Society, Vol- 50, pp. 343-349, 1967.

**pdfMachine**
**A pdf writer that produces quality PDF files with ease!**
Produce quality PDF files in seconds and preserve the integrity of your original documents. Compatible across nearly all Windows platforms, simply open the document you want to convert, click "print", select the "Broadgun pdfMachine printer" and that's it! Get yours now!

[6] Baba, P. D. and Banerjee, S. K., "Microwave ferrite program," Summary Technical Report, ESD-TR-68-251, 1968.

[7] Collins, T. and Brown , A. E., "Low-loss lithium ferrites for microwave latching applications, " Journal of Applied Physics, Vol- 42, pp 3451-3454, 1971.

[8] Pointon, A. J. and Saull, R. C., "Solid-state reactions in lithium ferrites," Journal of the American Ceramic Society, Vol-52, pp 157-160, 1969.

[9] Ridgley, D. H., Lessoff, H., and Childress, J. D., "Effects of lithium and oxygen losses on magnetic and crystallographic properties of spinel lithium ferrite," Journal of the American Ceramic Society, Vol-53, pp. 304 – 311, 1970.

[10] Argentina, G. M., and Baba, P.D., "Microwave Lithium Ferrites: An Overview", IEEE Transactions on Microwave Theory and Techniques, Vol. MTT-22, No. 6, pp 652-658, 1974.

[11] Bhatu, S S., Effect of nickel substitution on structural, infrared and elastic properties of lithium ferrite, Indian Journal of Pure & Applied Physics Vol- 45, pp 596-608, 2007.

[12] Soibam, Ibetombi, Phanjoubam, Sumitra, Prakash,, Chandra, "Mössbauer and magnetic studies of nickel substituted lithium zinc ferrites", Journal of Magnetism and Magnetic Materials, Vol. 321, pp. 2779-2782, 2009.

[13] Soibam, Ibetombi, Phanjoubam, Sumitra, Prakash, Chandra, "Mössbauer and magnetic studies of cobalt substituted lithium zinc ferrites prepared by citrate precursor method", Journal of Alloy and Compounds, Vol. 475, pp. 328–331, 2009.

[14] Widatallah, H. M., Johnson,C.,Gismelseed,A. M., Al-Omari, I.A.,Stewart S. J., Al-Harthi , S.H., Thomas, S. and Sitepu, H., "Structural and magnetic studies of nanocrystalline Mg-doped $Li_{0.5}Fe_{2.5}O_4$ particles prepared by mechanical milling" , Journal of Physics D: Applied Physics, Vol. 41, pp.165006(1) -165006(10), 2008.

[15] Tasaki, J. and Ito, T., "Effect of Sintering Atmosphere on the permeability of Sintered Ferrites.", Ferrites: proceedings of the International. Conference on Ferrites, Japan, pp.84-86, 1970.

[16] Nakamura,T., "Low-temperature sintering of Ni-Zn-Cu ferrite and its permeability spectra," Journal of Magnetism and Magnetic Materials,, Vol-168, pp.285-291, 1997.

[17] Roess, E., "Ferrites", University of Tokyo Press, Tokyo, p.187, 1971.

[18] Leung, L. K., Evans, B. J. and Morrish, A. H., "Low-temperature Mössbauer study of a nickel-zinc ferrite: $Zn_{1-x}Ni_xFe_2O_4$," Physics Review B, Vol-**8**, p.29-43,1973.

[19] Rezlescu,N., Rezlescu, E., Pasnicu, C. and Craus, M. L., "Effects of the rare-earth ions on some properties of a Nickel-Zinc ferrite," Journal of Physics: Condensed Matter, Vol-**6**,pp. 5707-5716,1994.

[20] E. Rezlescu, L. Sachelarie, P. D. Popa and N. Rezlescu, "Effect of substitution of diavalent ions on the electrical and magnetic properties of Ni-Zn-Me ferrites," IEEE Transactions on Magnetics, Vol- 36, pp. 3962-3967, 2000.

[21] Globus, A., "2nd EFS Conf. on Soft Magnetic Material.", Wolfson Center for Magnetic Technology, Cardiff, Wales, 1975.

**pdfMachine**
**A pdf writer that produces quality PDF files with ease!**
Produce quality PDF files in seconds and preserve the integrity of your original documents. Compatible across nearly all Windows platforms, simply open the document you want to convert, click "print", select the "Broadgun pdfMachine printer" and that's it! Get yours now!

[22] El-Shabasy,M., "DC electrical properties of Ni-Zn ferrites," Journal of Magnetism and Magnetic Materials,Vol-172, pp. 188-192, 1997.

[23] Wahab, M. A., "Solid State Physics-Structure and properties of materials", Narosa publishing house, New Delhi, 1999

[24] Chikazumi ,S., "Physics of Magnetism", John Wiley & Sons, Inc., New York, 1966.

[25] Brailsford,F., "Physical Principles of Magnetism", D. Van Nostrand Company Ltd., London, 1966.

[26] Dekker, A. J., "Solid State Physics", Macmillan India Ltd., New Delhi, 1998.

[27] Cullity, B. D., "Introduction to Magnetic Materials", Addison-Wiley Publishing Company, Inc., California, 1972.

[28] Goldman, Alex, "Modern Ferrite Technology", 2nd Ed, Springer Science-Business Media, Inc, Pittsburgh, PA, USA, 2006.

[29] Smit, J. and Wijn, H. P. J. , "Ferrites", John Wiley and Sons, New York, p. l49,1959.

[30] Kittel,C., "Introduction to Solid State Physics", 7th edition, John Wiley & Sons, Inc., Singapore, 1996.

[31] Jadhav , S.A., "Magnetic properties of Zn-substituted Li-Cu ferrites", Journal of Magnetism and Magnetic Materials, Vol-224, pp 167- 172, 2001.

[32] Hossain, A. K. M. A., Seki, M., Kawai, T. and Tabata, H., "Colossal magnetoresistance in spinel type $Zn_{1-x}Ni_xFe_2O_4$," Journal of Applied Physics, Vol.96, pp.1273-1275, 2004.

[33] Yafet, Y. and Kittel, C.," Antiferromagnetic arrangements in ferrites", Physical Review, Vol.87, pp. 290-294, 1952.

[34] Hadfield ,D., "Permanent Magnets and Magnetism", John Wiley & Sons, Inc., New York, 1962.

[35] Sikder, S. S., "Temperature dependence of magnetization and induced magnetic anisotropy of some Fe, Co and Ni-based amorphous ribbons," Ph. D. Thesis, BUET, Bangladesh, 1999.

[36] Snoek , J. L., Physica , "Dispersion and absorption in magnetic ferrites at frequencies above one Mc/s", Vol-14,pp 207-217, 1948.

[37] Irvine , J.T.S., West, A.R. , Amano , E., Huanosta , A. & Valenzuela. R., "Characterisation of magnetic materials by impedance spectroscopy", Solid State Ionics ,Vol.40-41, pp 220-223, 1990.

[38] Globus, A. &Duplex ,P., "Separation of susceptibility mechanisms for ferrites of low anisotropy", IEEE Transactions on Magnetics, Vol-2, pp 441-445, 1966.

[39] Chickazumi S. and Charap, S.H., "Physics of Magnetism", Krieger Pub. Co., p.248, 1978.

[40] Alan H, Morrish, "The Physical Properties of Magnetism", John Wiley and Sons , 1966.

[41] Yan , M. F. and Johnson, D. W., "Impurity induced exaggerated grain growth in Mn-Zn ferrites," Journal of the American Ceramic Society, Vol-61,pp 342-349, 1978.

**pdfMachine**
**A pdf writer that produces quality PDF files with ease!**
Produce quality PDF files in seconds and preserve the integrity of your original documents. Compatible across nearly all Windows platforms, simply open the document you want to convert, click "print", select the "Broadgun pdfMachine printer" and that's it! Get yours now!

[42] Hastings , J. M. and Corliss L. M , "Neutron Diffraction Studies of Zinc Ferrite and Nickel Ferrite," Reviews of .Modern. Physics, Vol- 25, pp 114-119, 1953.

[43] Chen, Qi, Rondinone, Adam J., Chakoumakos, Bryan C., and Zhang, Z. John, "Synthesis of superparamagnetic $MgFe_2O_4$ nanoparticles by coprecipitationa", Journal of Magnetism and Magnetic Materials, Vol-194, pp 1-7, 1999.

**pdfMachine**
**A pdf writer that produces quality PDF files with ease!**
Produce quality PDF files in seconds and preserve the integrity of your original documents. Compatible across nearly all Windows platforms, simply open the document you want to convert, click "print", select the "Broadgun pdfMachine printer" and that's it! Get yours now!

# CHAPTER 3

## SAMPLE FABRICATION, CHARACTERIZATION AND EXPERIMENTAL TECHNIQUES

### 3.1 Introduction

To achieve high permeability, high flux density, low loss and good homogenous product are apparently highly sensitive to the composition and manufacturing process. Many processing methods have been proposed but are mainly divided into two groups;

1. Conventional ceramic method, i.e., solid state reaction technique, involves milling of the reactants followed by heating at elevated temperatures range.
2. Non conventional method also called wet method. Among these methods, some are [1, 2]:
    - Sol-gel synthesis
    - Co-precipitation
    - Organic precursor method
    - Co-spray roasting
    - Freeze drying
    - Combustion synthesis
    - Glass Crystallization
    - Activated sintering
    - Fused salt synthesis

Presently, the conventional Ceramic process or Solid State Reaction technique is mostly preferred to produce ferrite powders. In this chapter, we describe the solid state reaction method that is used in this research work.

**pdfMachine**
**A pdf writer that produces quality PDF files with ease!**
Produce quality PDF files in seconds and preserve the integrity of your original documents. Compatible across nearly all Windows platforms, simply open the document you want to convert, click "print", select the "Broadgun pdfMachine printer" and that's it! Get yours now!

## 3.2 Conventional Solid State Reaction Method

In the solid state reaction method, the required composition is usually prepared from the appropriate amount of raw mineral oxides or carbonates by crushing, grinding and milling. The most common type of mill is the ball mill, which consists of a lined pot with hard spheres or rod inside. Milling can be carried out in a wet medium to increase the degree of mixing. This method depends on the solid state inter-diffusion between the raw materials. Solids do not usually react at room temperature over normal time scales. Thus it is necessary to heat them at higher temperatures for the diffusion length $(2Dt)^{1/2}$ to exceed the particle size, where $D$ is the diffusion constant for the fast-diffusing species, and t is the firing time. The ground powders are then calcined in air or oxygen at 600°C. For some time, this process is continued until the mixture is converted into the correct crystalline phase. The calcined powders are again crushed into fine powders. The pellets or toroid shaped samples are prepared from these calcined powders using die-punch assembly or hydrostatic or isostatic pressure. Sintering is carried out in the solid state, at temperature ranging 1100-1400°C, for times of typically 1-40 h and in various atmospheres (e.g. Air, $O_2$ and $N_2$) [3-6]. Fig. 3.1 shows, diagrammatically, the stages followed in ferrite preparation.

The general solid state reaction leading to a ferrite $MeFe_2O_4$ may be represented as

$$MeO + Fe_2O_3 \longrightarrow MeFe_2O_4$$

where *Me* is the divalent ions. There are basically four steps in the preparation of ferrite:

1) Preparation of materials to form an intimate mixture with the metal ions in the ratio which they will have in the final product,
2) Heating of this mixture to form the ferrite (often called calcining),
3) Grinding the calcined powders and pressing the fine powders into the required shape, and
4) Sintering to produce a highly densified product.

## 3.3 Details of Calcining, Pressing and Sintering

*Calcining* is defined as the process of obtaining a homogeneous and phase pure composition of mixed powders by heating them for a certain time at a high temperature

pdfMachine
A pdf writer that produces quality PDF files with ease!
Produce quality PDF files in seconds and preserve the integrity of your original documents. Compatible across nearly all Windows platforms, simply open the document you want to convert, click "print", select the "Broadgun pdfMachine printer" and that's it! Get yours now!

and then allowing it to cool slowly. During the calcining stage, the reaction of $Fe_2O_3$ with metal oxide (say, $MeO$ or $Me_2O_3$) takes place in the solid state to form spinel according to the reactions [7]:

$$MeO + Fe_2O_3 \longrightarrow MeFe_2O_4 \text{ (Spinel)}$$

$$2Me_2O_3 + 4Fe_2O_3 \longrightarrow 4MeFe_2O_4 \text{ (Spinel)} + O_2$$

The $NiO$, $MgO$ and $Li_2CO_3$ creeps into $Fe_2O_3$ as below, to form an intermediate phase

$$Fe_2O_3 + NiO \longrightarrow NiFe_2O_4$$

$$5Fe_2O_3 + Li_2CO_3 \longrightarrow 4\,Li_{0.5}Fe_{2.5}O_4 + CO_2$$

$$Fe_2O_3 + MgO \longrightarrow MgFe_2O_4$$

*And lastly*

$$(0.60\text{-}2x)\,NiFe_2O_4 + (0.40)MgFe_2O_4 + 2x\,Li_{0.5}Fe_{2.5}O_4 \longrightarrow Li_xMg_{0.4}Ni_{0.6-2x}Fe_{2+x}O_4.$$

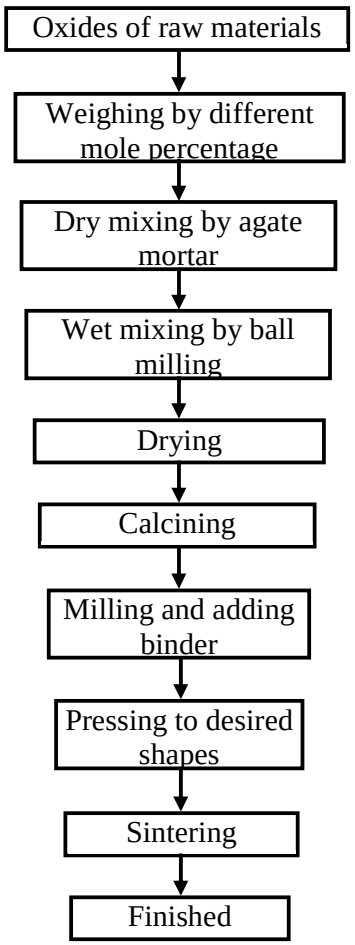


**Fig.3.1.** Flow chart of the stages in preparation of spinel ferrite.

**pdfMachine**
**A pdf writer that produces quality PDF files with ease!**
Produce quality PDF files in seconds and preserve the integrity of your original documents. Compatible across nearly all Windows platforms, simply open the document you want to convert, click "print", select the "Broadgun pdfMachine printer" and that's it! Get yours now!

The calcining process can be repeated several times to obtain a high degree of homogeneity. The calcined powders are crushed into fine powders. The ideal characteristics of fine powders are [2]:

1) small particle size (sub micron)
2) narrow distribution in particle size
3) dispersed particles
4) equiaxed shape of particles
5) high purity
6) homogeneous composition.

A small particle size of the reactant powders provides a high contact surface area for initiation of the solid state reaction; diffusion paths are shorted, leading to more efficient completion of the reaction. Porosity is easily eliminated if the initial pores are very small. A narrow size distribution of spherical particles as well as a dispersed state is important for compaction of the powder during green-body formation. Grain growth during sintering can be better controlled if the initial size is small and uniform.

A binder is usually added prior to compaction, at a concentration lower than 5wt % [2]. Binders are polymers or waxes; the most commonly used binder in ferrite is polyvinyl alcohol. The binder facilitates the particles flow during compacting and increases the bonding between the particles, presumably by forming bonds of the type *particle-binder-particle*. During sintering, binders decompose and are eliminated from the ferrite. Pressures are used for compacting very widely but are commonly several tons per square inch (i. e., up to $10^8$ N $m^{-2}$).

*Sintering* is defined as the process of obtaining a dense, tough body by heating a compacted powder for a certain time at a temperature high enough to significantly promote diffusion, but clearly lower than the melting point of the main component. The driving force for sintering is the reduction in surface free energy of the powder. Part of this energy is transferred into interfacial energy (grain boundaries) in the resulting polycrystalline body [2, 8]. The sintering time, temperature and the furnace atmosphere play very important role on the magnetic property of ferrite materials. The purposes of sintering process are:

1) to bind the particles together so as to impart sufficient strength to the product,
2) to densify the material by eliminating the pores and

pdfMachine
A pdf writer that produces quality PDF files with ease!
Produce quality PDF files in seconds and preserve the integrity of your original documents. Compatible across nearly all Windows platforms, simply open the document you want to convert, click “print”, select the “Broadgun pdfMachine printer” and that’s it! Get yours now!

3) to homogenize the materials by completing the reactions left unfinished in the calcining step.

Sintering of crystalline solids is dealt by Coble and Burke [9] who found the following empirical relationship regarding rate of grain growth:

$$\bar{d} = kt^n$$

where $\bar{d}$ is the mean grain diameter, $n$ is about 1/3, $t$ is sintering time and k is a temperature dependent parameter. Sintering is divided into three stages, Fig. 3.2 [2, 10].

Stage 1. Contact area between particles increases,

Stage 2. Porosity changes from open to closed porosity,

Stage 3. Pore volume decreases; grains grow.

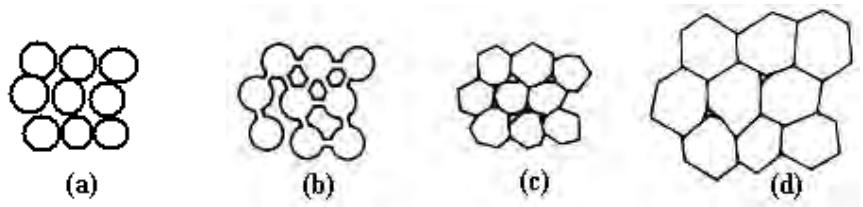


**Fig. 3.2.** Schematic representation of sintering stages: (a) greenbody, (b) initial stage, (c) intermediate stage, and (d) final stage.

In the initial stage, neighbouring particles form a neck by surface diffusion and presumably also at high temperatures by an evaporation-condensation mechanism. Grain growth begins during the intermediate stage of sintering. Since grain boundaries are the sinks for vacancies, grain growth tends to decrease the pore elimination rate due to the increase in distance between pores and grain boundaries, and by decreasing the total grain boundary surface area. In the final stage, the grain growth is considerably enhanced and the remaining pores may become isolated.

In *Li-Mg-Ni* ferrites, the presence of *Li* complicates the sintering process because high temperature coupled with low oxygen firing will cause *Li* loss. High density is important for high permeability, but so is *Li* conservation. Tasaki [1] described two alternative firings to achieve high density:

1) Low sintering temperature excluding $O_2$ (Vacuum, argon, nitrogen),
2) High temperature in pure oxygen to reduce *Li* loss.

**pdfMachine**
**A pdf writer that produces quality PDF files with ease!**
Produce quality PDF files in seconds and preserve the integrity of your original documents. Compatible across nearly all Windows platforms, simply open the document you want to convert, click "print", select the "Broadgun pdfMachine printer" and that's it! Get yours now!

Accordingly, other properties correlated along with density:

1) Lattice constant is greater for $O_2$, smaller for vacuum
2) Curie temperature is greater for vacuum, smaller for $O_2$
3) Resistivity is greater for $O_2$, smaller for vacuum.

## 3.4 Preparation of the Present Samples

The Polycrystalline ferrite with nominal chemical composition $Li_xMg_{0.4}Ni_{0.6-2x}Fe_{2+x}O_4$ (where x = 0.0 to 0.3 in steps of 0.05) were prepared by standard solid state reaction technique. Commercially available powders of *NiO* (99.9%), *MgO* (99.9%), $Li_2CO_3$ ($99^+$ %), $Fe_2O_3$ (99.9%), will be mixed thoroughly in an appropriate amount by ball milling. The mixed powders were calcined at 600˚C for 6 hours. The calcined powders were then pressed into disk- and toroid-shaped samples. The samples were sintered at 1050, 1100, 1150 and 1200˚C for 6 h in air. The heating and cooling rates for sintering were 5˚C/min.


**Fig. 3.3.** Sample (a) disk shaped, (b) Toroid shaped.

### 3.5 X-ray Diffraction

Bragg reflection is a coherent elastic scattering in which the energy of the X-ray is not changed on reflection. Let a beam of monochromatic radiation of wavelength λ is incident on a periodic crystal plane at an angle θ and is diffracted at the same angle as shown in Fig. 3.4.

When constructive interference occurs, from Fig 3.4 (a) it can be written as ,

$$n\lambda = AB + BC$$

As, $AB=BC$, $n\lambda = 2AB$

Again from Fig 3.4(b), $\sin\theta = AB/d$

So, $AB = d\sin\theta$

pdfMachine
A pdf writer that produces quality PDF files with ease!
Produce quality PDF files in seconds and preserve the integrity of your original documents. Compatible across nearly all Windows platforms, simply open the document you want to convert, click “print”, select the “Broadgun pdfMachine printer” and that’s it! Get yours now!

$$\text{i.e. } 2d\,Sin\theta = n\lambda \tag{3.1}$$

where $d$ is the distance between crystal planes and $n$ is the positive integer which represents the order of reflection. Equation (3.1) is known as Bragg law. This Bragg law suggests that the diffraction is only possible when $\lambda \leq 2d$ [11]. For this reason we cannot use the visible light to determine the crystal structure of a material. The X-ray diffraction (XRD) provides substantial information on the crystal structure.

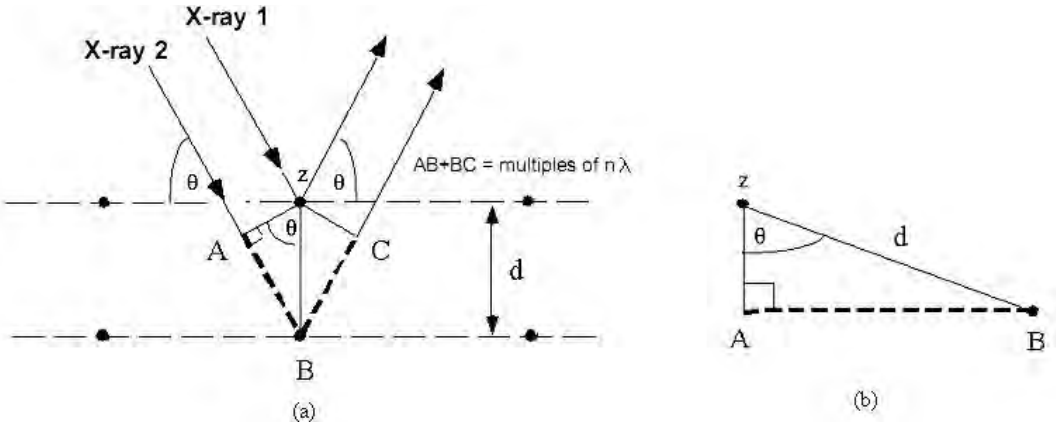


**Fig. 3.4.** Bragg law of diffraction.

X-ray diffraction was carried out using RIGAKU Smart-lab with rotating anode, Lyon Institute of Nanotechnology,France, using Cu-Kα Xray diffractometer (α = 1.540593 Å). Basic features of a XRD experiments is shown in Fig. 3.5 respectively.

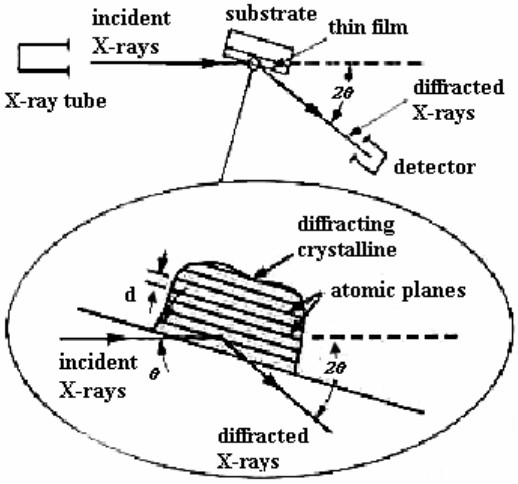


**Fig. 3.5.** Basic Features of Typical XRD Experiment

**pdfMachine**
**A pdf writer that produces quality PDF files with ease!**
Produce quality PDF files in seconds and preserve the integrity of your original documents. Compatible across nearly all Windows platforms, simply open the document you want to convert, click "print", select the "Broadgun pdfMachine printer" and that's it! Get yours now!

The lattice parameter for each peak of each sample was calculated by using the formula

$$a = d\sqrt{h^2 + k^2 + l^2} \tag{3.2}$$

where *h*, *k* and *l* are the indices of the crystal planes. To determine the precise lattice constant for each sample, Nelson-Riley method was used. The Nelson-Riley function $F(\theta)$ is given as

$$F(\theta) = \frac{1}{2}\left[\left(Cos^2\theta / Sin\theta\right) + \left(Cos^2\theta / \theta\right)\right] \tag{3.3}$$

The values of lattice parameter '*a*' of all the peaks for a sample are plotted against $F(\theta)$. Then using a least square fit method exact lattice constant '$a_o$' is determined. The point where the least square fit straight line cut the y-axis (i.e. at $F(\theta) = 0$) is the actual lattice constant of the sample. The theoretical density $\rho_{th}$ was calculated using following expression:

$$\rho_{th} = \frac{8M}{N_A a_o^3}\, g/cm^3 \tag{3.4}$$

where $N_A$ is Avogadro's number ($6.02 \times 10^{23}$ $mol^{-1}$), *M* is the molecular weight. The porosity was calculated from the relation $\{100(\rho_{th} - \rho_B)/ \rho_{th}\}\%$, where $\rho_B$ is the bulk density measured by the formula $\rho_B = M/V$ [12].

## 3.6 Microstructural Investigation

The microstructural study was performed in order to have an insight of the grain structures. The samples of different compositions and sintered at different temperatures were chosen for this purpose. The samples were visualized under a high-resolution optical microscope (Koehler Illuminator MA 1109, Swift Instruments, Inc.) and then photographed. Average grain sizes (grain diameter) of the samples were determined from optical micrographs by linear intercept technique [3]. To do this, several random horizontal and vertical lines were drawn on the micrographs. Therefore, we counted the number of grains intersected and measured the length of the grains along the line traversed. Finally the average grain size was calculated.

**pdfMachine**
**A pdf writer that produces quality PDF files with ease!**
Produce quality PDF files in seconds and preserve the integrity of your original documents. Compatible across nearly all Windows platforms, simply open the document you want to convert, click "print", select the "Broadgun pdfMachine printer" and that's it! Get yours now!

## 3.7. Complex Permeability Measurement

For high frequency application, the desirable property of a ferrite is high permeability with low loss. One of the most important goals of ferrite research is to fulfill this requirement. The techniques of permeability measurement and frequency characteristics of the present samples are described in sections 3.7.1 and 3.7.2.

### 3.7.1 Techniques for the Permeability Measurement

Measurements of permeability normally involve the measurements of the change in self-inductance of a coil in presence of the magnetic core. The behaviour of a self-inductance can now be described as follows. We assume an ideal loss less air coil of inductance $L_0$. On insertion of a magnetic core with permeability $\mu$, the inductance will be $\mu L_0$. The complex impedance $Z$ of this coil [1] can be expressed as follows:

$$Z = R + jX = j\omega L_0 \mu = j\omega L_0 (\mu' - j\mu'') \quad (4.5)$$

where the resistive part is $R = \omega L_0 \mu''$ (4.6)

and the reactive part is $X = \omega L_0 \mu'$ (4.7)

The RF permeability can be derived from the complex impedance of a coil, *Z*, given by equation (4.5). The core is taken as toroidal to avoid demagnetizing effects. The quantity $L_o$ is derived geometrically as shown in section 3.7.2.

### 3.7.2 Frequency Characteristics of the present samples

The frequency characteristics of the ferrite samples i.e. the initial permeability spectra were investigated using and Agilent Precision Impedance Analyzer (model no. 4294A). The complex permeability measurements on toroid shaped specimens were carried out at room temperature on all the samples in the frequency range 300 *kHz* - 110 *MHz*. The real part $(\mu_i')$ and imaginary part $(\mu_i'')$ of the complex permeability were calculated using the following relations [4]: $\mu_i' = L_s / L_0$ and $\mu_i'' = \mu_i' \tan\delta$, where $L_s$ is the self-inductance of the sample core and $L_0 = \mu_o N^2 S / \pi \bar{d}$ is derived geometrically. Here $L_o$ is the inductance of the winding coil without the sample core, *N* is the number

pdfMachine
A pdf writer that produces quality PDF files with ease!
Produce quality PDF files in seconds and preserve the integrity of your original documents. Compatible across nearly all Windows platforms, simply open the document you want to convert, click "print", select the "Broadgun pdfMachine printer" and that's it! Get yours now!

of turns of the coil ($N$ = 5), $S$ is the area of cross section of the toroidal sample as given below:

$$S = d \times h,$$

where $$d = \frac{d_2 - d_1}{2},$$

$d_1 =$ Inner diameter,
$d_2 =$ Outer diameter,
$h =$ Height

and $\bar{d}$ is the mean diameter of the toroidal sample as given below:

$$\bar{d} = \frac{d_1 + d_2}{2}$$

The relative quality factor is determined from the ratio $\frac{\mu_i'}{\tan\delta}$.

## 3.8 DC Magnetization measurement at room temperature

The DC magnetization ($M$) measurements were made using a VSM (Vibrating Sample magnetometer) at room temperature, made by the Department of Physics, Bangladesh University of Engineering Technology (BUET). Diameter of the sample was made as it fit to the sample rod finely. In VSM the sample is vibrated at 37 Hz frequency and magnetization strength is found from the magnitude of the emf induce in the sense coils placed in proximity with sample. The block diagram of the VSM is shown in Fig. 3.7. The pickup coils are mounted with axis perpendicular to magnetization field so as to minimize error signals arising from field fluctuations. The transmission of vibrations at a measured frequency must be carefully avoided, attaching a small permanent magnet to the remote part of the vibrating system. This moves its own pickup coils and provides a reference signal against which the signal produced by the sample can be measured accurately.

pdfMachine
A pdf writer that produces quality PDF files with ease!
Produce quality PDF files in seconds and preserve the integrity of your original documents. Compatible across nearly all Windows platforms, simply open the document you want to convert, click "print", select the "Broadgun pdfMachine printer" and that's it! Get yours now!

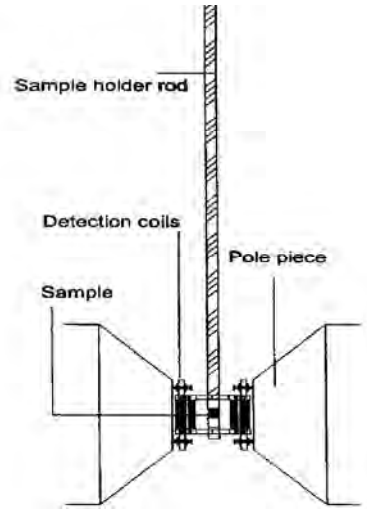


**Fig. 3.6.** Block diagram of vibrating sample magnetometer (VSM)

Magnetization values of all samples were recorded by setting up the magnet at a maximum applied field of 8 K Gauss. For the calculation of saturation magnetization, the values are obtained in milivolts (mV), these values are then calibrated in emu using nickel standard of value 1mv=0.279304 emu. The calculated values are then divided by mass of the respective sample to obtain the values in emu/g for each sample.

## References

[1] Goldman, A., Handbook of Modern Ferromagnetic Materials, Kulwer Acad. Pub, Boston, U.S.A, 1999.

[2] Valenzuela, R., Magnetic Ceramics, Cambridge University Press, Cambridge, 1994.

[3] Hossain, A. K. M. A., "Investigation of colossal magnetoresistance in bulk and thick film magnetites," Ph. D. Thesis, Imperial College, London, 1998.

[4] Cullity, B. D., "Introduction to Magnetic Materials", Addison-Wisley Publishing Company, Inc., California, 1972.

[5] Brook, R. J., "Sintering: An Overview", Concise Encyclopedia of Advanced Ceramic Materials, Pergamon Press, Oxford, p 438, 1991.

[6] Reijnen, P., Science of Ceramics, Academic Press, London, 1967.

**pdfMachine**
**A pdf writer that produces quality PDF files with ease!**
Produce quality PDF files in seconds and preserve the integrity of your original documents. Compatible across nearly all Windows platforms, simply open the document you want to convert, click "print", select the "Broadgun pdfMachine printer" and that's it! Get yours now!

[7] Slick , P. I., Ferrites for Non-microwave Applications, Vol. 2, North Holland Pub. Co. 1980.

[8] Kingery ,W. D., H. K. Bowen and D. R. Uhlman, Introduction to Ceramics, 2nd edition, Wiley Interscience, Newyork, pp 476, 1976.

[9] Coble, R. L. and Burke, J. E., 4th Int. Symp. On the Reactivity of Solids, Amsterdam, pp. 38-51, 1960.

[10] McColm, I. J. and Clark, N. J., Forming, Shaping and Working of high Performance Ceramics, Blackie, Glasgow, pp 1-338, 1988.

**pdfMachine**

**A pdf writer that produces quality PDF files with ease!**

Produce quality PDF files in seconds and preserve the integrity of your original documents. Compatible across nearly all Windows platforms, simply open the document you want to convert, click “print”, select the “Broadgun pdfMachine printer” and that’s it! Get yours now!

# CHAPTER 2

# LITERATURE REVIEW

## 2.1 Overview of the Materials

Ferrites commonly expressed by the general chemical formula $MeO.Fe_2O_3$, where *Me* represents divalent metals, first commanded the public attention when Hilpert (1909) focused on the usefulness of ferrites at high frequency [1]. A systematic investigation was launched by Snoek (1936) at Philips Research Laboratory [2]. At the same time Takai (1937) in Japan was seriously engaged in the research work on the same materials [1]. Snoek's extensive works on ferrites unveiled many mysteries regarding magnetic properties of ferrites. He was particularly looking for high permeability materials of cubic structure. This particular structure for symmetry reasons supports low crystalline anisotropy. He found suitable materials in the form of mixed spinels of the type $MeZnFe_2O_4$, where *Me* stands for metals like *Cu, Mg, Ni, Co* or *Mn*, for which permeability were found to be up to 4000 [1-2 ,3]. Here after starts the story of *Li*-ferrites. Lithium ferrites became commercially important as computer memory core materials in the early 1960's. The high Curie temperature, leading to unparalleled thermal stability, the excellent hysteresis loop properties, and the high saturation magnetization all prompted this commercial interest. For many of the same reasons there was considerable development effort aimed at providing micro-wave quality lithium ferrites [4-7]. The principal interest in microwave lithium ferrites is a low-cost replacement for the rare earth-iron garnets, offering competitive or improved temperature performance. Lithium ferrites with magnetizations comparable to the garnets are very refractory due to the high concentration and nature of the substituent elements, which requires relatively high sintering temperatures. This type of heat treatment causes the volatility of $Li_2O$ [8, 9] which results in some reduction of iron. For this reason lithium ferrites were considered difficult to prepare with low dielectric loss. In addition, these lower magnetization lithium ferrites were characterized by high porosities, and as a result, high coercive forces and broad resonance line-widths were experienced [10].

The structural and elastic properties of *Li-Ni* ferrite was studied by Bhatu *et al.* [11]. The observed increase in magnitude of elastic constants, elastic wave

**pdfMachine**
**A pdf writer that produces quality PDF files with ease!**
Produce quality PDF files in seconds and preserve the integrity of your original documents. Compatible across nearly all Windows platforms, simply open the document you want to convert, click "print", select the "Broadgun pdfMachine printer" and that's it! Get yours now!

velocities and infrared spectral analysis is found easier, valid and suitable for spinel ferrite.

The effect of magnetic properties of *Ni* concentration in *Li-Zn* ferrite was studied by I. Soibam *et al.*[12]. From their investigation of saturation magnetization, Curie temperature and Mossbaur studies, it has been observed that *Ni* substitution greatly affects the magnetic properties of the *Li-Zn* ferrite system. The value of saturation magnetization and Curie temperature was observed to decrease with increase in the *Ni* concentration in their system. Magnetic studies of cobalt substituted lithium zinc ferrites was also studied by I. Soibam. Magnetisation measurement indicated that cobalt shows anomalous behaviour when substituted in lithium ferrites in the presence of *Zn*.[13]

The structure and magnetic properties of spinel-related *Mg*-doped $Li_{0.5}Fe_{2.5}O_4$ nano-crystalline particles prepared by milling a pristine sample, $Li_{0.41}Fe_{2.41}Mg_{0.17}O_4$ for different times were investigated by H M Widatallah *et al* [14]. The saturation magnetization and Curie temperature were found to decrease and the material increasingly turned super-paramagnetic as milling proceeded. The coercivity and the magnetization increased initially and later decreased at higher milling times.

The sintering process is considered to be one of the most vital steps in ferrite preparation and often plays a dominant role in many magnetic properties. Tasaki *et al.* [15] studied the effect of sintering atmosphere on permeability of sintered ferrite. They found that high density is one of the factors, which contribute to greater permeability. However, permeability decreased in an atmosphere without $O_2$ at high sintering temperature where high density was expected. This decrease in permeability is attributed to the variation of chemical composition caused by volatilization of *Zn*. At low sintering temperature a high permeability is obtained in an atmosphere without $O_2$ because densification and stoichiometry plays a principal role in increasing permeability. At high sintering temperature the highest permeability is obtained in the presence of $O_2$ because the effect of decrease of *Zn* content can then be neglected.

Studying the electromagnetic properties of ferrites, Nakamura [16] suggested that both the sintering density and the average grain size increased with sintering temperature. These changes were responsible for variations in magnetization, initial permeability and electrical resistivity.

**pdfMachine**
**A pdf writer that produces quality PDF files with ease!**
Produce quality PDF files in seconds and preserve the integrity of your original documents. Compatible across nearly all Windows platforms, simply open the document you want to convert, click “print”, select the “Broadgun pdfMachine printer” and that’s it! Get yours now!

High permeability attainment is certainly affected by the microstructure of the ferrites. Roess showed that [17] the very high permeability is restricted to certain temperature ranges and the shapes of permeability versus temperature curves are strongly affected by any inhomogeneity in the ferrite structure.

Leung *et al.* [18] performed a Low-temperature Mössbauer study of a nickel-zinc ferrite: $Zn_{1-x}Ni_xFe_2O_4$. They found that for $x \leq 0.5$ the resultant *A*- and *B*- site *Fe*-spin moments have a collinear arrangement, whereas for $x > 0.5$ a non-collinear arrangement of *A*- and *B*-site *Fe*-spin moments exist. An explanation based on the relative strength of the exchange constant $J_{AB}$ and $J_{BB}$ is given to account for this difference.

Rezlescu *et al.* [19][1 reported that the sintering behaviour and microstructure of the ferrites samples largely affected by *PbO* addition. *PbO* significantly reduced the sintering temperatures, thus energy consumption is minimized and material loss by evaporation is minimized [20].

There are two mechanisms in the phenomenon of permeability; spin rotation in the magnetic domains and wall displacements. The uncertainty of contribution from each of the mechanisms makes the interpretation of the experimental results difficult. Globus [21] shows that the intrinsic rotational permeability $\mu_r$ and $180^0$ wall permeability $\mu_w$ may be written as: $\mu_r = 1 + 2\pi M_s^2 / K$ and $\mu_w = 1 + 3\pi M_s^2 D / 4\gamma$, where $M_s$ is the saturation magnetization, $K$ is the total anisotropy, $D$ is the grain diameter and $\gamma \equiv K\delta_w$ is the wall energy.

El-Shabasy [22] studied the DC electrical resistivity of $Zn_xNi_{1-x}Fe_2O_4$ ferrites. He shows that the ferrite samples have semiconductor behaviour where DC electrical resistivity decreases on increasing the temperature. $\rho(T)$ for all samples follows $\rho(T) = \rho_0 \exp(E/k_BT)$, where $E$ is the activation energy for electric conduction and $\rho_0$ is the pre-exponential constant or resistivity at infinitely high temperature. The DC resistivity, $\rho(T)$, decreases as the *Zn* ion substitution increases. It is reported that *Zn* ions prefer the occupation of tetrahedral (*A*) sites, *Ni* ions prefer the occupation of octahedral (*B*) sites while *Fe* ions partially occupy the *A* and *B* sites. On increasing *Zn* substitution (at *A* sites), the *Ni* ion concentration (at *B* sites) will decrease. This lead to the migration of some *Fe* ions from *A* sites to *B* sites to substitute the reduction in *Ni* ion concentration at *B* sites. As a result, the number of ferrous and ferric ions at *B* sites

**pdfMachine**
**A pdf writer that produces quality PDF files with ease!**
Produce quality PDF files in seconds and preserve the integrity of your original documents. Compatible across nearly all Windows platforms, simply open the document you want to convert, click “print”, select the “Broadgun pdfMachine printer” and that’s it! Get yours now!

(which is responsible for electric conduction in ferrites) increases. Consequently $\rho$ decreases on *Zn* substitution. Another reason for the decrease in $\rho$ on increasing *Zn* ion substitution is that, zinc is less resistive ($\rho = 5.92\ \mu\Omega cm$) than nickel ($\rho = 6.99\ \mu\Omega cm$). The main conductivity mechanism in ferrites is attributed to electron hopping between $Fe^{3+}$ and $Fe^{2+}$ in octahedral sites. Resistivity in spinels is very sensitive to stoichiometry; a small variation of *Fe* content in $Zn_{0.7}Ni_{0.3}Fe_{2+x}O_{4-y}$ results in resistivity variations of $\sim 10^7$. Excess *Fe* can easily dissolve in spinel phase by a partial reduction of *Fe* from $3Fe_2^{3+}O_3$ to $2Fe^{2+}Fe_2^{3+}O_4$ (and $1/2O_2 \uparrow$) [2].

## 2.2 Magnetic Ordering

The onset of magnetic order in solids has two basic requirements:

(i) Individual atoms should have magnetic moments (spins),

(ii) Exchange interactions should exist that couple them together.

Magnetic moments originate in solids as a consequence of overlapping of the electronic wave function with those of neighbouring atoms. This condition is best fulfilled by some transition metals and rare-earths. The exchange interactions depend sensitively upon the inter-atomic distance and the nature of the chemical bonds, particularly of nearest neighbour atoms. When the positive exchange dominates, which corresponds to parallel coupling of neighbouring atomic moments (spins), the magnetic system becomes ferromagnetic below a certain temperature $T_C$ called the Curie temperature. The common spin directions are determined by the minimum of magneto-crystalline anisotropy energy of the crystal. Therefore, ferromagnetic substances are characterized by spontaneous magnetization. But a ferromagnetic material in the demagnetized state displays no net magnetization in zero field because in the demagnetized state a ferromagnetic of macroscopic size is divided into a number of small regions called domains, spontaneously magnetized to saturation value and the directions of these spontaneous magnetization of the various domains are such that the net magnetization of the specimen is zero. The existence of domains is a consequence of energy minimization. The size and formation of these domains is in a complicated manner dependent on the shape of the specimen as well as its magnetic and thermal history. When negative exchange dominates, adjacent atomic moments (spins) align antiparallel

**pdfMachine**
**A pdf writer that produces quality PDF files with ease!**
Produce quality PDF files in seconds and preserve the integrity of your original documents. Compatible across nearly all Windows platforms, simply open the document you want to convert, click “print”, select the “Broadgun pdfMachine printer” and that’s it! Get yours now!

to each other, and the substance is said to be anti-ferromagnetic below a characteristic temperature, $T_N$, called the Néel temperature. In the simplest case, the lattice of an anti-ferromagnet is divided into two sublattices with the magnetic moments of these in anti-parallel alignment. This result is zero net magnetization. A special case of anti-ferromagnetism is ferrimagnetism. In ferrimagnetism, there are also two sublattices with magnetic moments in opposite directions, but the magnetization of the sublattices are of unequal strength resulting in a non-zero magnetization and therefore has net spontaneous magnetization. At the macroscopic level of domain structures, ferromagnetic and ferrimagnetic materials are therefore similar.

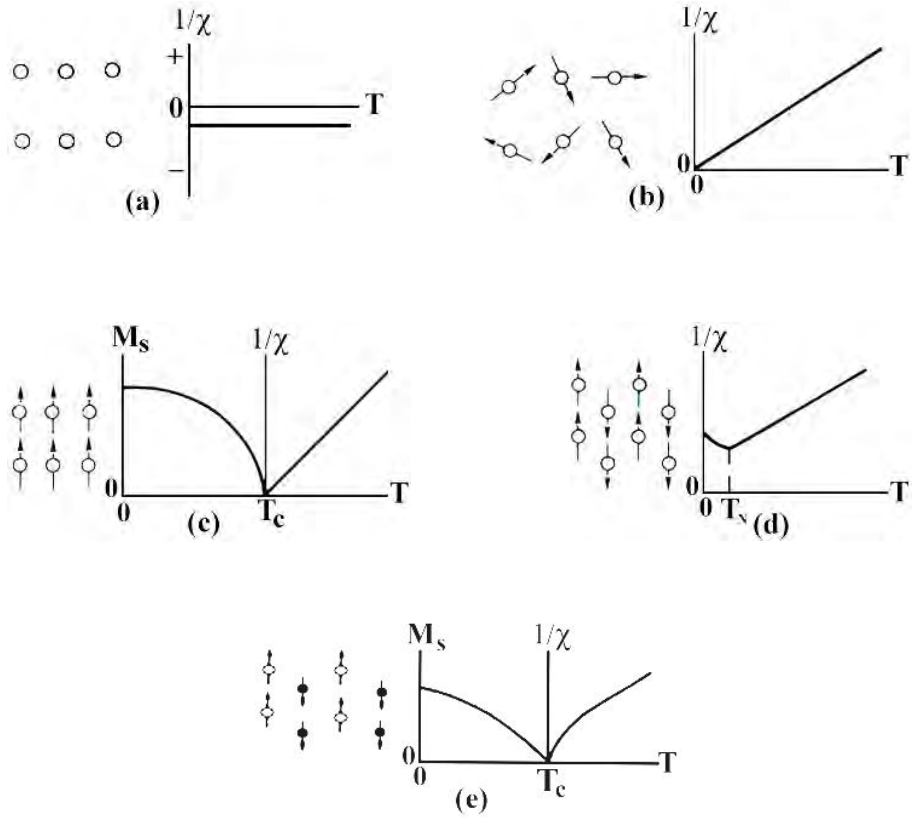


**Fig. 2.1.** Temperature dependence of the inverse susceptibility for: (a) a diamagnetic material; (b) a paramagnetic material, showing Curie's law behaviour; (c) a ferromagnetic material, showing a spontaneous magnetization for $T<T_C$ and Curie-Weiss behaviour for $T>T_C$; (d) an antiferromagnetic material; (e) a ferrimagnetic material, showing a net spontaneous magnetization for $T<T_C$ and non linear behaviour for $T>T_C$.

**pdfMachine**
**A pdf writer that produces quality PDF files with ease!**
Produce quality PDF files in seconds and preserve the integrity of your original documents. Compatible across nearly all Windows platforms, simply open the document you want to convert, click "print", select the "Broadgun pdfMachine printer" and that's it! Get yours now!

The Curie and Néel temperatures characterize a phase transition between the magnetically ordered and disordered (paramagnetic) states. From these simple cases of magnetic ordering various types of magnetic order exists, particularly in metallic substances. Because of long-range order and oscillatory nature of the exchange interaction, mediated by the conduction electrons, structures like helical, conical and modulated patterns might occur. *A* useful property for characterizing the magnetic materials is the magnetic susceptibility,$\chi$, defined as the magnetization, *M*, divided by the applied magnetic field, *H* i.e. $\chi = M / H$. The temperature dependence of susceptibility or, more accurately, inverse of susceptibility is a good characterization parameter for magnetic materials, Fig. 2.1. Fig. 2.1(e) shows that in the paramagnetic region, the variation of the inverse susceptibility with temperature of a ferrite material is decidedly non-linear. Thus the ferrite materials do not obey the Curie-Weiss law, $\chi = C/(T - T_C)$ [2, 27].

## 2.3 Crystal Structure of Spinel Ferrites

### 2.3.1 Ionic Charge Balance and Crystal Structure of Cubic Spinel Ferrite:

The spinel lattice is composed of a close-packed oxygen arrangement in which 32 oxygen ions form a unit cell that is the smallest repeating unit in the crystal network. Between the layers of oxygen ions, if we simply visualize them as spheres, there are interstices that may accommodate the metal ions. Now, the interstices are not all the same; some which are called *A* sites are surrounded by or coordinated with 4 nearest neighbouring oxygen ions whose lines connecting their centers form a tetrahedron. Thus, *A* sites are called tetrahedral sites (Fig. 2.2 (a)). The other type of site (*B* sites) is coordinated by 6 nearest neighbor oxygen ions whose center connecting lines describe an octahedron. The *B* sites are called octahedral sites (Fig. 2.2(b)). In the unit cell of 32 oxygen ions, there are 64 tetrahedral sites and 32 octahedral sites. If all of these were filled with metal ions, of either *+2* or +3 valence, the positive charge would be very much greater than the negative charge and so the structure would not be electrically neutral. It turns out that of the 64 tetrahedral sites, only 8 are occupied and out of 32 octahedral sites, only 16 are occupied. If, as in the mineral, spinel, the tetrahedral sites are occupied by divalent ions and the octahedral sites are occupied by the trivalent ions, the total positive charge would be 8x (+2) = +16 plus the 16x (+3) =+48 or a total of

**pdfMachine**
**A pdf writer that produces quality PDF files with ease!**
Produce quality PDF files in seconds and preserve the integrity of your original documents. Compatible across nearly all Windows platforms, simply open the document you want to convert, click “print”, select the “Broadgun pdfMachine printer” and that’s it! Get yours now!

+64 which is needed to balance the 32x (-2) = -64 for the oxygen ions. There would then be eight formula units of $MO.Fe_2O_3$ or $MFe_2O_4$ in a unit cell. *A* spinel unit cell contains two types of subcells . The two types of subcells alternate in a three- dimensional array so that each fully repeating unit cell requires eight subcells.

The crystallographic environments of the *A* and *B* sites are distinctly different. The unit cell contains so many ions that a two-dimensional drawing of the complete cell would not be very informative. Instead we can consider a unit cell of edge *a*, to be divided into eight octants, each of edge *a*/2, as shown in Fig. 2.2(c). The four shaded octants have identical contents, and so do the four unshaded octants. The contents of the two lower-left octants in Fig. 2.2(c) are shown in Fig. 2.2(d). One tetrahedral site occurs at the center of the right octant of Fig. 2.2(d), and other tetrahedral sites are at some but not all octant corners. Four octahedral sites occur in the left octant; one is connected by dashed lines to six oxygen ions, two of which, shown dotted, are in adjacent octants behind and below. The oxygen ions are arranged in the same way, in tetrahedra, in all octants. Not all of the available sites are actually occupied by metal ions. Only one-eighth of the *A* sites and one-half of the *B* sites are occupied, as shown in Table 2.1 [2]. In the mineral spinel, $MgO.Al_2O_3$, the $Mg^{2+}$ ions are in *A* sites and the $Al^{3+}$ ions are in *B* sites.

Some ferrites $MO.Fe_2O_3$ have exactly this structure, with $M^{2+}$ in *A* sites and $Fe^{3+}$ in *B* sites. This is called the normal spinel structure. If 8 divalent (*M*) ions occupy the *A*-site i.e., tetrahedral site and 16 tetravalent ions ($Fe^{3+}$) occupy the *B*-site i.e., octahedral site, the structure is said to be Normal spinel.

If *B*-site i.e., octahedral site is occupied half by divalent metal ion and half by trivalent iron ions, generally distributed in random and *A*-site i.e., tetrahedral site by trivalent iron ions, the structure is said to be Inverse spinel. Both zinc and cadmium ferrite have this structure and they are both nonmagnetic, i.e., paramagnetic. Many other ferrites, however, have the inverse spinel structure, in which the divalent ions are on *B* sites, and the trivalent ions are equally divided between *A* and B sites. The divalent and trivalent ions normally occupy the B sites in a random fashion, i.e., they are disordered. Iron, cobalt, and nickel ferrites have the inverse structure, and they are all ferrimagnetic.

The normal and inverse structures are to be regarded as extreme cases, because X-ray and neutron diffraction show that intermediate structures can exist. Thus

**pdfMachine**
**A pdf writer that produces quality PDF files with ease!**
Produce quality PDF files in seconds and preserve the integrity of your original documents. Compatible across nearly all Windows platforms, simply open the document you want to convert, click “print”, select the “Broadgun pdfMachine printer” and that’s it! Get yours now!

manganese ferrite is almost, but not perfectly, normal; instead of all the $Mn^{2+}$ ions being on *A* sites, a fraction 0.8 is on A sites and 0.2 on B sites. Similarly, magnesium ferrite is not quite inverse; a fraction 0.9 of the $Mg^{2+}$ ions is on B sites and 0.1 on A sites. The distribution of the divalent ions on A and B sites in some ferrites can be altered by heat treatment; it may depend, for example, on whether the material is quenched from a high temperature or slowly cooled.

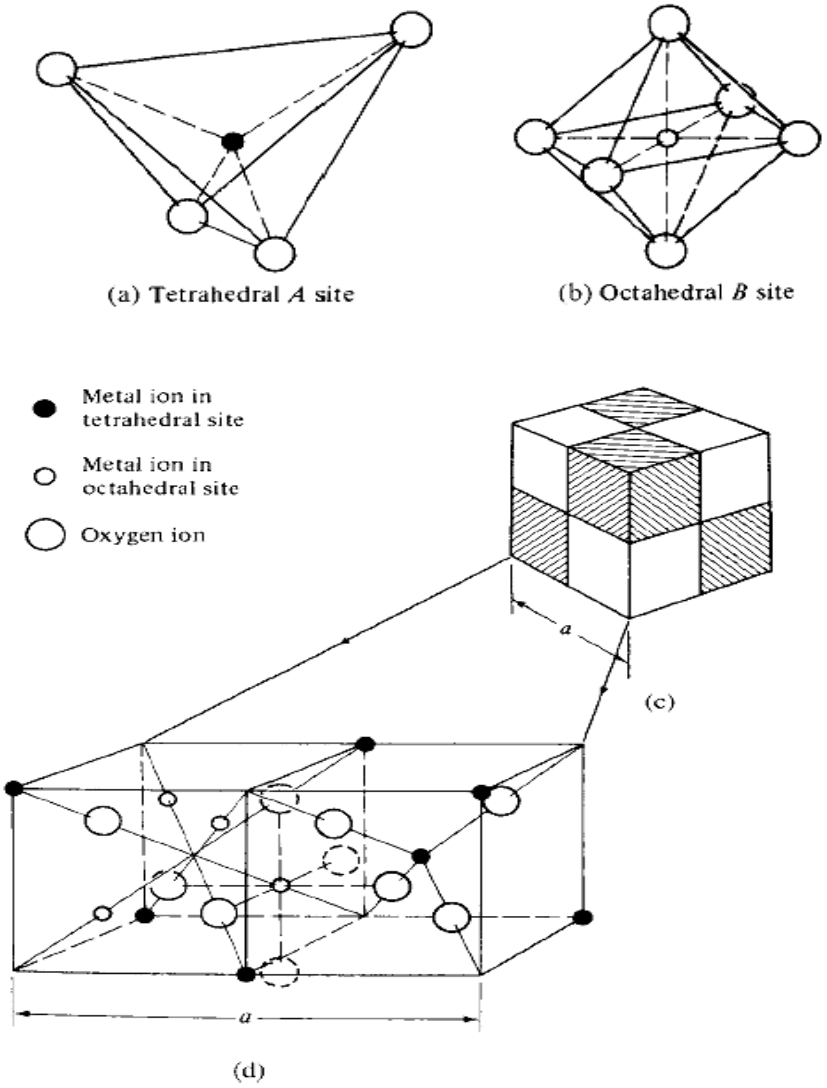


**Fig.2.2**. Crystal structure of a cubic ferrite [27].

**pdfMachine**
**A pdf writer that produces quality PDF files with ease!**
Produce quality PDF files in seconds and preserve the integrity of your original documents. Compatible across nearly all Windows platforms, simply open the document you want to convert, click "print", select the "Broadgun pdfMachine printer" and that's it! Get yours now!

**Table 2.1** Arrangements of Metal Ions in the Unit Cell of a Ferrite $MO.Fe_2O_3$ [27]

.

| Kind of Site | Number Available | Number Occupied | Occupants | |
|---|---|---|---|---|
| | | | Normal Spinel | Inverse Spinel |
| Tetrahedral (A) | 64 | 8 | $8M^{2+}$ | $8\ Fe^{3+}$ |
| Octahedral (B) | 32 | 16 | $16\ Fe^{3+}$ | $8\ Fe^{3+}$<br>$8\ M^{2+}$ |

The positions of the ions in the spinel lattice are not perfectly regular (as the packing of hard spheres) and some distortion does occur. The tetrahedral sites are often too small for the metal ions so that the oxygen ions move slightly to accommodate them. The oxygen ions connected with the octahedral sites move in such a way as to shrink the size the octahedral cell by the same amount as the tetrahedral site expands. The movement of the tetrahedral oxygen is reflected in a quantity called the oxygen parameter, which is the distance between the oxygen ion and the face of the cube edge along the cube diagonal of the spinel subcell. This distance is theoretically equal to $3/8a_o$ where $a_o$ is the lattice constant [1].

### 2.3.2 Site Preferences of the Ions

The preference of the individual ions for the two types of lattice sites is determined by;

1. The ionic radii of the specific ions
2. The size of the interstices
3. Temperature
4. The orbital preference for specific coordination

The most important consideration would appear to be the relative size of the ion compared to the size of the lattice site. The divalent ions are generally larger than the trivalent (because the larger charge produces greater electrostatic attraction and so pulls the outer orbits inward). The octahedral sites are also larger than the tetrahedral [28]. Therefore, it is reasonable that the trivalent ions such as $Fe^{3+}$ would go into the tetrahedral sites and the divalent ions would go into the octahedral. Two exceptions are found in $Zn^{2+}$ and $Cd^{2+}$ which prefer tetrahedral sites because the electronic

**pdfMachine**
**A pdf writer that produces quality PDF files with ease!**
Produce quality PDF files in seconds and preserve the integrity of your original documents. Compatible across nearly all Windows platforms, simply open the document you want to convert, click "print", select the "Broadgun pdfMachine printer" and that's it! Get yours now!

configuration is favorable for tetrahedral bonding to the oxygen ions. Thus *Zn* takes preference for tetrahedral sites over the $Fe^{3+}$ ions. $Zn^{2+}$ and $Co^{2+}$ have the same ionic radius but *Zn* prefers tetrahedral sites and $Co^{2+}$ prefers octahedral sites because of the configurationally exception. $Ni^{2+}$ and $Cr^{3+}$ have strong preferences for octahedral sites, while other ions have weaker preferences [28].

### 2.3.3 Unit Cell Dimensions

The dimensions of the unit cell are given in Angstrom Units which are equivalent to $10^{-8}$ cm. If we assume that the ions are perfect spheres and we pack them into a unit cell of measured (X-ray diffraction) dimensions we find certain discrepancies that show that the packing is not ideal. The positions of the ions in the spinel lattice are not perfectly regular (as the packing of hard spheres) and some distortion does occur. The tetrahedral sites are often too small for the metal ions so that the oxygen ions move slightly to accommodate them. The oxygen ions connected with the octahedral sites move in such a way as to shrink the size of the octahedral cell by the same amount as the tetrahedral site expands .The movement of the tetrahedral oxygen is reflected in a quantity called the oxygen parameter which is the distance between the oxygen ion and the face of the cube edge along the cube diagonal of the spinel subcell. This distance is theoretically equal to $3/8a_o$. The unit cell length of *Li*-Ferrite, *Ni* ferrite and *Mg* Ferrite are observed to be 8.33 Å, 8.3390 Å and 8.36 Å respectively [2].

## 2.4 Cation Distribution of Spinel Ferrites

In spinel structure the distribution of cations over the tetrahedral or *A* sites and octahedral or *B* sites can be present in a variety of ways. If all the $Me^{2+}$ ions in $Me^{2+}Me_2^{3+}O_4$ are in tetrahedral and all $Me^{3+}$ ions in octahedral positions, the spinel is then called normal spinel. Another cation distribution in spinel exists, where one half of the cations $Me^{3+}$ are in the *A* positions and the rest, together with the $Me^{2+}$ ions are randomly distributed among the *B* positions. The spinel having the latter kind of cation distribution is known as inverse spinel. The distribution of these spinels can be summarized as [2, 25-26]

1) Normal spinels, i.e. the divalent metal ions are on *A*-sites: $Me^{2+}[Me_2^{3+}]O_4$,
2) Inverse spinels, i.e. the divalent metal ions are on *B*-sites: $Me^{3+}[Me^{2+}Me_2^{3+}]O_4$.

**pdfMachine**
**A pdf writer that produces quality PDF files with ease!**
Produce quality PDF files in seconds and preserve the integrity of your original documents. Compatible across nearly all Windows platforms, simply open the document you want to convert, click “print”, select the “Broadgun pdfMachine printer” and that’s it! Get yours now!

A completely normal or inverse spinel represents the extreme cases. There are many spinel oxides which have cation distributions intermediate between these two extreme cases and are called mixed spinels.

The general cation distribution for the spinel can be indicated as:

$$(Me_x^{2+}Me_{1-x}^{3+})[Me_{1-x}^{2+}Me_{1+x}^{3+}]O_4$$

where the first and third brackets represent the A and B sites respectively. For normal spinel $x$=1, for inverse spinel $x$=0. The quantity x is a measure of the degree of inversion. In the case of some spinel oxides x depends upon the method of preparation.

The cation distributions of *Li*-Ferrite, *Mg*-Ferrite and *Ni*-Ferrite are shown below:

Li Ferrite : $(Fe^{3+})[Li_{0.5}Fe_{1.5}^{3+}]O_4$ [2,10]

Ni Ferrite : $(Fe^{3+})[Ni^{2+}Fe^{3+}]O_4$ [2, 42]

Mg Ferrite : $(Mg_{1-x}Fe^{3+})[Mg_xFe_{2-x}^{3+}]O_4$ [2, 43]

where x is the degree of inversion.

Both Li ferrite and Ni-Ferrite is a inverse spinel and Mg –Ferrite is a mixed ferrite.

The cation distribution of various $Li_xMg_{0.4}Ni_{0.6-2x}Fe_{2+x}O_4$ ferrite assumed as

$$(Fe_{0.9}^{3+})[Li_x^{1+}Mg_{0.4}^{2+}Ni_{0.6-2x}^{2+}Fe_{1.1+x}^{3+}] \quad [31]$$

The basic magnetic properties of the ferrites are very sensitive functions of their cation distributions. Mixed ferrites having interesting and useful magnetic properties are prepared by mixing two or more different types of metal ions

Spinel oxides are ionic compounds and hence the chemical bonding occurring in them can be taken as purely ionic to a good approximation. The total energy involved, however, consists of the Coulomb energy, the Born repulsive energy, the polarization and the magnetic interaction energy. The energy terms are all dependent on lattice constant, oxygen position parameter and the ionic distribution. In principle the equilibrium cation distribution can be calculated by minimizing the total energy with respect to these variables. But the only energy that can be written with any accuracy is the Coulomb energy. The individual preference of some ions for certain sites resulting from their electronic configuration also play an important role. The divalent ions are generally larger than the trivalent (because the larger charge produces greater electrostatic attraction and so pulls the outer orbits inward). The octahedral sites are also

**pdfMachine**
**A pdf writer that produces quality PDF files with ease!**
Produce quality PDF files in seconds and preserve the integrity of your original documents. Compatible across nearly all Windows platforms, simply open the document you want to convert, click “print”, select the “Broadgun pdfMachine printer” and that’s it! Get yours now!

larger than the tetrahedral. Therefore, it would be reasonable that the trivalent ions $Fe^{3+}$ (0.73Å) would go into the tetrahedral sites and the divalent ions $Fe^{2+}$ (0.86Å) go into the octahedral. Two exceptions are found in $Zn^{2+}$ and $Cd^{2+}$ which prefer tetrahedral sites because the electronic configuration is favourable for tetrahedral bonding to the oxygen ions. It is known that $Li^{1+}$(0.82Å), $Ni^{2+}$(0.73Å) and $Mg^{2+}$(0.80Å) ions occupy B sites [6]. Hence the factors influencing the distribution the cations among the two possible lattice sites are mainly their ionic radii of the specific ions, the size of the interstices, temperature, the matching of their electronic configuration to the surrounding anions and the electrostatic energy of the lattice, the so-called Madelung energy, which has the predominant contribution to the lattice energy under the constrain of overall energy minimization and charge neutrality.

## 2.5 Interaction Between Magnetic Moments on Lattice Sites

Spontaneous magnetization of spinels (at 0K) can be estimated on the basis of their composition, cation distribution, and the relative strength of the possible interaction. Since cation-cation distances are generally large, direct (ferromagnetic) interactions are negligible. Because of the geometry of orbital involved, the strongest superexchange interaction is expected to occur between octahedral and tetrahedral cations. The strength of interaction or exchange force between the moments of the two metal ions on different sites depends on the distances between these ions and the oxygen ion that links them and also on the angle between the three ions. The nearest neighbours of a tetrahedral, an octahedral and an anion site are shown in Fig. 2.3. The interaction is greatest for an angle of $180^0$ and also where the interionic distances are the shortest.

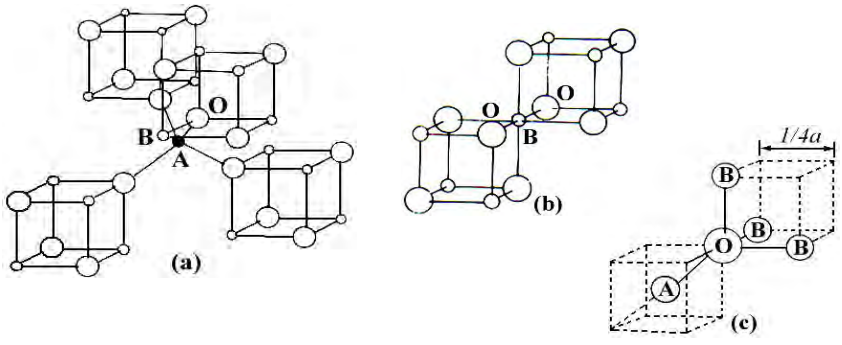


**Fig. 2.3.** Nearest neighbours of (a) a tetrahedral site, (b) an octahedral site and (c) an anion site.

**pdfMachine**
**A pdf writer that produces quality PDF files with ease!**
Produce quality PDF files in seconds and preserve the integrity of your original documents. Compatible across nearly all Windows platforms, simply open the document you want to convert, click "print", select the "Broadgun pdfMachine printer" and that's it! Get yours now!

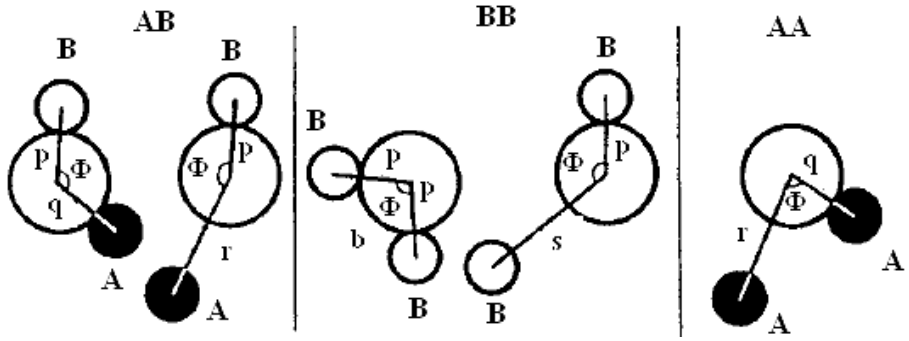


**Fig. 2.4.** Interionic distances and angles in the spinel structure for the different type of lattice site interactions [28, 29].

| **Distances M-O** | **Distances M-M** |
|---|---|
| $p = a(\frac{1}{2} - u)$ | $b = (a/4)\sqrt{2}$ |
| $q = a(u - \frac{1}{4})\sqrt{3}$ | $c = (a/8)\sqrt{11}$ |
| $r = a(1+u)\sqrt{11}$ | $d = (a/4)\sqrt{3}$ |
| $s = a(\frac{1}{3}u + 8)\sqrt{3}$ | $e = (3a/8)\sqrt{3}$ |
| | $f = (a/4)\sqrt{6}$ |

Fig. 2.4 shows the inter-atomic distances and the angles between the ions for the different types of interactions. In the A-A and B-B cases, the angles are too small or the distances between the metal ions and the oxygen ions are too large. The best combinations of distances and angles are found in the A-B interactions. For an undistorted spinel, the A-O-B angles are about 125˚ and 154˚ [1-2, 24]. The B-O-B angles are 90˚ and 125˚ but in the latter, one of the B-O distances is large. In the A-A case the angle is about 80˚. Therefore, the interaction between moments on the A and B sites is strongest. The B-B interaction is much weaker and the most unfavorable situation occurs in the A-A interaction. By examining the interactions involving the major contributor, or the A-B interaction which orients the unpaired spins of these ions antiparallel, Néel was able to explain the ferrimagnetism of ferrites The interaction between the tetrahedral and octahedral sites is shown in Fig. 2.4. An individual A site is interacted with a single B site, but each A site is linked to four such units and each B site is linked to six such units. Thus, to be consistent throughout the crystal, all A sites and all B sites act as unified blocks and are coupled antiparallel as blocks [28].

**pdfMachine**
**A pdf writer that produces quality PDF files with ease!**
Produce quality PDF files in seconds and preserve the integrity of your original documents. Compatible across nearly all Windows platforms, simply open the document you want to convert, click “print”, select the “Broadgun pdfMachine printer” and that’s it! Get yours now!

## 2.6 Magnetism in Spinel Ferrite

The magnetic moment of a free atom is associated with the orbital and spin motions of electrons in an incomplete sub-shell of the electronic structure of the atom. In crystals the orbital motions are quenched, that is the orbital planes may be considered to be fixed in space relative to the crystal lattice, and in such a way that in bulk the crystal has no resultant moment from this source. Moreover this orbital-lattice coupling is so strong that the application of a magnetic field has little effect upon it. The spin axes are not tightly bound to the lattice as are the orbital axes. The anions surrounding a magnetic cation subject it to a strong inhomogeneous electric field and influence the orbital angular momentum. However, the spin angular momentum remains unaffected. For the first transition group elements this crystal field effect is intense partly due to the large radius of the 3d shell and partly due to the lack of any outer electronic shell to screen the 3d shell whose unpaired electrons only contribute to the magnetic moment. We have originally defined the magnetic moment in connection with permanent magnets. The electron itself may well be called the smallest permanent magnet [1]. For an atom with a resultant spin quantum number *S*, the spin magnetic moment will be

$$\mu = g\sqrt{S(S+1)}\mu_B$$

Where $g$ is the Landé splitting factor and $\mu_B$, known as the Bohr magneton, is the fundamental unit of magnetic moment. The value of $g$ for pure spin moment is $2$ and the quantum number associated with each electron spin is $\pm 1/2$. The direction of the moment is comparable to the direction of the magnetization (from South to North poles) of a permanent magnet to which the electron is equivalent.

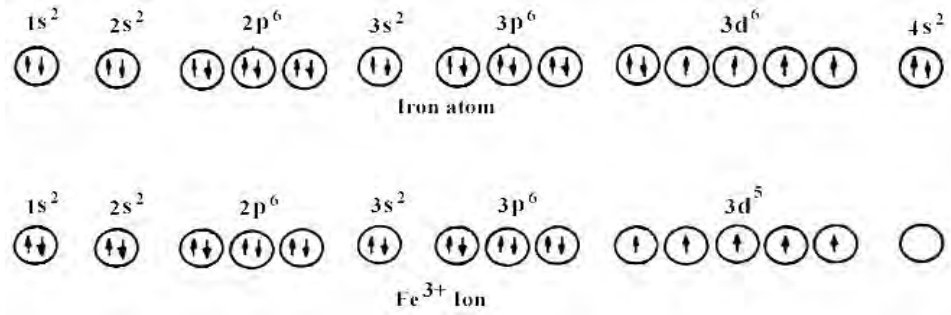


**Fig. 2.5.** Electronic configuration of atoms and ions [28].

**pdfMachine**
**A pdf writer that produces quality PDF files with ease!**
Produce quality PDF files in seconds and preserve the integrity of your original documents. Compatible across nearly all Windows platforms, simply open the document you want to convert, click "print", select the "Broadgun pdfMachine printer" and that's it! Get yours now!

Fig. 2.5 illustrates the electronic configuration of *Fe* atoms and $Fe^{3+}$ ions. *Fe* atom has four unpaired electrons and $Fe^{3+}$ ion has five unpaired electrons. Each unpaired electron spin produced 1 Bohr magneton. In compounds, ions and molecules, account must be taken of the electrons used for bonding or transferred in ionization. It is the number of unpaired electrons remaining after these processes occur that gives the net magnetic moment [1]. According to the Hund's rules the moment of *Fe* atom and $Fe^{3+}$ ion are $4\mu_B$ and $5\mu_B$ respectively. Similarly the moment of $Fe^{2+}$ and $Ni^{2+}$ ion are $4\mu_B$ and $\mu_B$ respectively.

### 2.6 .1 Magnetic Moments of Some Spinels Ferrites:

#### 2.6.1.1 Inverse Spinels

In the nickel ferrite it was observed that the moments of the eight $Ni^{2+}$ ions on the octahedral sites. The value of moment per $Ni^{2+}$ ion is $2\mu_B$ or $16\ \mu_B$ for a unit cell containing eight formula units. The magnetic moments of the other inverse spinels can be predicted in a similar manner. These predicted values are listed in Table 2.2 along with the measured values [28]. Because the effect of thermal agitation on the magnetic moments will lower the magnetic moment, the correlation of the moment to Bohr magnetons is always referred to the value at absolute zero or 0˚K. This is usually done by extrapolation of the values at very low temperatures. The deviations from the theoretical values can be attributed to several factors, namely:

- The ion distribution on the various sites may not be as perfect as predicted.
- The orbital magnetic contribution may not be zero as assumed.
- The directions of the spins may not be antiparallel in the interactions. In other words, they may be canted.

#### 2.6.1.2 Normal versus Inverse Spinels

Although some spinels are either normal or inverse, it is possible to get different mixtures of the two. Often, the ratio of the two will depend on the method of preparation. Some of the first ferrites studied by Neel (1948) were ones that contained *Mg* and *Cu* which by thermal treatment reduced the $Fe^{3+}$ on the tetrahedral A sites of the inverse spinel. As a result, there was an imbalance of the $Fe^{3+}$ ions on the two sites and

**pdfMachine**
**A pdf writer that produces quality PDF files with ease!**
Produce quality PDF files in seconds and preserve the integrity of your original documents. Compatible across nearly all Windows platforms, simply open the document you want to convert, click "print", select the "Broadgun pdfMachine printer" and that's it! Get yours now!

thus a magnetic moment. Even *Zn* ferrite, *Zn [Fe₂] O₄,* with a higher than 50 mole percentage of $Fe_2O_3$ and a special firing can have a small moment [28].

From the Table 2.2, it is observed that experimental magnetic moment of $Li_{0.5}Fe_{2.5}O_4$, $MgFe_2O_4$ and $NiFe_2O_4$ are 2.6, 1.1 and 2.3 respectively.

**Table 2.2**. Magnetic moment of Some Simple Ferrite [28].

| Ferrite | Magnetic Moment ($\mu_B$) | |
|---|---|---|
| | Experimental | Theoretical |
| $MnFe_2O_4$ | 4.6 | 5 |
| $FeFe_2O_4$ | 4.1 | 4 |
| $CoFe_2O_4$ | 3.7 | 3 |
| $NiFe_2O_4$ | 2.3 | 2 |
| $CuFe_2O_4$(Quenched) | 2.3 | 1 |
| $MgFe_2O_4$ | 1.1 | 0 |
| $Li_{0.5}Fe_{2.5}O_4$ | 2.6 | 2.5 |
| $\gamma$-$Fe_2O_3$ | 2.3 | 2.5 |

## 2.6.2 Exchange Interactions in Spinel

The intense short-range electrostatic field, which is responsible for the magnetic ordering, is the exchange force that is quantum mechanical in origin and is related to the overlapping of total wave functions of the neighbouring atoms. The total wave function consists of the orbital and spin motions. Usually the net quantum number is written as *S*, because the magnetic moments arise mostly due to the spin motion as described above. The exchange interactions coupling the spins of a pair of electrons are proportional to the scalar product of their spin vectors [23, 26, 30]

$$V_{ij} = -2J_{ij}\vec{S}_{i.}.\vec{S}_j \qquad (2.1)$$

where $J_{ij}$ is the exchange integral given in a self explanatory notation by

**pdfMachine**
**A pdf writer that produces quality PDF files with ease!**
Produce quality PDF files in seconds and preserve the integrity of your original documents. Compatible across nearly all Windows platforms, simply open the document you want to convert, click "print", select the "Broadgun pdfMachine printer" and that's it! Get yours now!

$$J_{ij} = \int \psi_i^*(1)\psi_j^*(2)\left[\frac{1}{r_{12}} + \frac{1}{r_{ij}} - \frac{1}{r_{i1}} - \frac{1}{r_{j2}}\right]\psi_i(2)\psi_j(2)dv_1 dv_2 \qquad (2.2)$$

In this expression $r$ 's are the distances, subscripts $i$ and $j$ refer to the atoms, 1 and 2 refers to the two electrons. If the $J$ in equation (2.1) is positive, we achieve ferromagnetism. A negative $J$ may give rise to anti-ferromagnetism or ferrimagnetism.

Magnetic interactions in spinel ferrites as well as in some ionic compounds are different from the one considered above because the cations are mutually separated by bigger anions (oxygen ions). These anions obscure the direct overlapping of the cation charge distributions, sometimes partially and sometimes completely making the direct exchange interaction very weak. Cations are too far apart in most oxides for a direct cation-cation interaction. Instead, super-exchange interactions appear, i.e., indirect exchange via anion *p*-orbitals that may be strong enough to order the magnetic moments. Apart from the electronic structure of cations this type of interactions strongly depends on the geometry of arrangement of the two interacting cations and the intervening anion. Both the distance and the angles are relevant. Usually only the interactions with in first coordination sphere (when both the cations are in contact with the anion) are important. In the Neél theory of ferrimagnetism the interactions taken as effective are inter- and intra-sublattice interactions *A-B*, *A-A* and *B-B*. The type of magnetic order depends on their relative strength.

The super-exchange mechanism between cations that operate via the intermediate anions was proposed by Kramer for such cases and was developed by Anderson and Van Vleck [23, 26]. A simple example of superexchange is provided by *MnO* which was chosen by Anderson. From the crystal structure of *MnO* it will be seen that the anti-parallel manganese ions are collinear with their neighbouring oxygen ions. The $O^{2-}$ ions each have six *2p* electrons in three anti-parallel pairs. The outer electrons of the $Mn^{2+}$ ions are in *3d* sub-shells which are half filled with five electrons in each. The phenomenon of super-exchange is considered to be due to an overlap between the manganese 3*d* orbits and the oxygen *2p* orbits with a continuous interchange of electrons between them. It appears that, for the overall energy of the system to be a minimum, the moments of the manganese ions on either side of the oxygen ion must be

**pdfMachine**
**A pdf writer that produces quality PDF files with ease!**
Produce quality PDF files in seconds and preserve the integrity of your original documents. Compatible across nearly all Windows platforms, simply open the document you want to convert, click "print", select the "Broadgun pdfMachine printer" and that's it! Get yours now!

anti-parallel. The manganese magnetic moments are thus, in effect, coupled through the intervening oxygen ion. The idea is illustrated in Fig. 2.6.

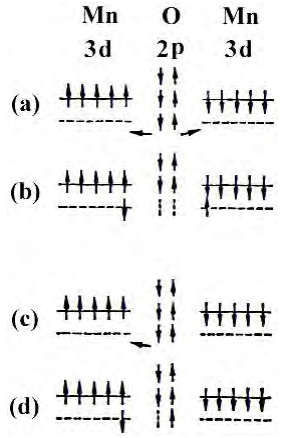


**Fig. 2.6.** Illustrating super-exchange in *MnO*.

In Fig. 2.6 (a) and Fig. 2.6 (c) the outer electrons in a pair of $Mn^{2+}$ ions, and in an intervening $O^{2-}$ ion in the unexcited state, are shown by the arrows. One suggested mode of coupling is indicated in Fig. 2.6 (b). The two electrons of a pair in the oxygen ion are simultaneously transferred, one to the left and the other to the right. If their directions of spin are unchanged then, by Hund's rules, the moments of the two manganese ions must be anti-parallel as shown. Another possibility is represented in Fig. 2.6(d). One electron only has been transferred to the manganese ion on the left. The oxygen ion now has a moment of $1\mu_B$ and if there is negative interaction between the oxygen ion and the right-hand manganese ion then again the moments of the manganese ions will be anti-parallel. If these ideas are accepted then the oxygen ions play an essential part in producing anti-ferromagnetism in the oxide. Moreover, because of the dumbbell shape of the *2p* orbits, the coupling mechanism should be most effective when the metal ions and the oxygen ions lie in one straight line, that is, the angle between the bonds is 180˚, and this is the case with *MnO*.

In the case of spinel ferrites the coupling is of the indirect type which involves overlapping of oxygen wave functions with those of the neighbouring cations. Consider two transition metal cations separated by an *O*, Fig. 2.7.

**pdfMachine**
**A pdf writer that produces quality PDF files with ease!**
Produce quality PDF files in seconds and preserve the integrity of your original documents. Compatible across nearly all Windows platforms, simply open the document you want to convert, click "print", select the "Broadgun pdfMachine printer" and that's it! Get yours now!

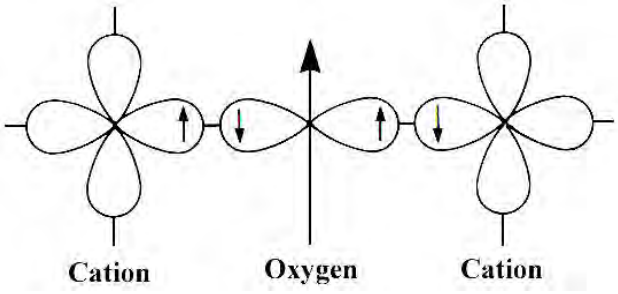


**Fig. 2.7.** Schematic representation of the superexchange interaction in the magnetic oxides. The *p* orbital of an anion (center) interact with the *d* orbitals of the transitional metal cations.

The $O^{2-}$ has no net magnetic moment since it has completely filled shells, with *p*-type outermost orbitals. Orbital $p_x$ has two electrons: one with spin up, and the other with spin down, consistent with pauli's exclusion principle. The essential point is that when an oxygen *p* orbital overlaps with a cation *d* orbital, one of the *p* electrons can be accepted by the cations. When one of the transition-metal cations is brought close the $O^{2-}$, partial electron overlap (between a *3d* electron from the cation and a *2p* electron form the $O^{2-}$) can occur only for anti-parallel spins, because electrons with the same spin are repelled. Empty *3d* states in the cation are available for partial occupation by the $O^{2-}$ electron, with an anti-parallel orientation. Electron overlap between the other cation and the $O^{2-}$ then occurs resulting in anti-parallel spins and therefore anti-parallel order between the cations. Since the *p* orbitals are linear, the strongest interaction is expected to take place for cation–$O^{2-}$–cation angles close to $180^{\circ}$ [2].

### 2.6.3 Néel Theory of Ferrimagnetism

If we consider the simplest case of a two-sublattice system having antiparallel and non-equal magnetic moments, the inequality may be due to:

1) different elements in different sites,
2) same element in different ionic states, and
3) different crystalline fields leading to different effective moments for ions having the same spin.

The spins on one sub-lattice are under the influence of exchange forces due to the spins on the second sub-lattice as well as due to other spins on the same sub-lattice. The molecular fields acting on the two sub-lattices A and B can be written as [2, 23-27]

**pdfMachine**
**A pdf writer that produces quality PDF files with ease!**
Produce quality PDF files in seconds and preserve the integrity of your original documents. Compatible across nearly all Windows platforms, simply open the document you want to convert, click "print", select the "Broadgun pdfMachine printer" and that's it! Get yours now!

$$\vec{H}_A = \lambda_{AA}\vec{M}_A + \lambda_{AB}\vec{M}_B,$$

$$\vec{H}_B = \lambda_{AB}\vec{M}_A + \lambda_{BB}\vec{M}_B$$

where $\vec{M}_A$ and $\vec{M}_B$ are the magnetizations of the two sub-lattices and $\lambda$'s are the Weiss constants. Since the interaction between the sub-lattices is anti-ferromagnetic, $\lambda_{AB}$ must be negative, but $\lambda_{AA}$ and $\lambda_{BB}$ may be negative or positive depending on the crystal structure and the nature of the interacting atoms. Probably, these interactions are also negative, though they are in general quite small.

Assuming all the exchange interactions to be negative the molecular fields will be then given by

$$\vec{H}_A = -\lambda_{AA}\vec{M}_A - \lambda_{AB}\vec{M}_B,$$

$$\vec{H}_B = -\lambda_{AB}\vec{M}_A - \lambda_{BB}\vec{M}_B$$

Since in general, $\lambda_{AA}$ and $\lambda_{BB}$ are small compared to $\lambda_{AB}$, it is convenient to express the strengths of these interactions relative to the dominant $\lambda_{AB}$ interaction.

Let $\lambda_{AA} = \alpha\lambda_{AB}$

and $\lambda_{BB} = \beta\lambda_{AB}$

In an external applied field $\vec{H}$, the fields acting on *A* and *B* sites are

$$\vec{H}_A = \vec{H} - \lambda_{AB}(\alpha\vec{M}_A - \vec{M}_B),$$

$$\vec{H}_B = \vec{H} - \lambda_{AB}(\vec{M}_A - \beta\vec{M}_B)$$

At temperatures higher than the transition temperature, $T_N$, $\vec{H}_A$, $\vec{M}_A$ and $\vec{M}_B$ are all parallel and we can write

$$\vec{M}_A = \frac{C_A}{T}[\vec{H} - \lambda_{AB}(\alpha\vec{M}_A - \vec{M}_B)], \qquad (2.3)$$

$$\vec{M}_B = \frac{C_B}{T}[\vec{H} - \lambda_{AB}(\vec{M}_A - \beta\vec{M}_B)] \qquad (2.4)$$

where $C_A$ and $C_B$ are the Curie constants for the two sublattices.

Here, $C_A = N_A g\mu_B^2 S_A(S_A+1)/3K$ and $C_B = N_B g\mu_B^2 S_B(S_B+1)/3K$

$N_A$ and $N_B$ denote the number of magnetic ions on *A* and *B* sites respectively and $S_A$ and $S_B$ are their spin quantum numbers. Solving for the susceptibility, $\chi$, one gets [2,27]

**pdfMachine**
**A pdf writer that produces quality PDF files with ease!**
Produce quality PDF files in seconds and preserve the integrity of your original documents. Compatible across nearly all Windows platforms, simply open the document you want to convert, click "print", select the "Broadgun pdfMachine printer" and that's it! Get yours now!

$$\frac{1}{\chi} = \frac{T}{C} - \frac{1}{\chi_0} - \frac{b}{T-\theta}$$

$$\frac{1}{\chi} = \frac{T + (C/\chi_0)}{C} - \frac{b}{T-\theta} \qquad (2.5)$$

Where $C$, $\chi_0$, $b$ and $\theta$ are constants for particular substance and are given by

$$C = C_A + C_B$$

$$\frac{1}{\chi_0} = -\frac{1}{C^2}[C_A^2\lambda_{AA} + C_B^2\lambda_{BB} + 2C_AC_B\lambda_{AB}]$$

$$b = \frac{C_AC_B}{C^3}[C_A^2(\lambda_{AA} - \lambda_{BB})^2 + C_B^2(\lambda_{BB} - \lambda_{AB})^2$$

$$- 2C_AC_B\{\lambda_{AB}^2 - (\lambda_{AA} + \lambda_{BB})\lambda_{AB} + \lambda_{AA}\lambda_{BB}\}]$$

$$\theta = -\frac{C_AC_B}{C}(\lambda_{AB} + \lambda_{BB}) - 2\lambda_{AB}$$

Equation (2.5) represents a hyperbola, and the physically meaning part of it is plotted in Fig. 2.9. This curvature of the plot of 1/χ versus $T$ is a characteristics feature of a ferrimagnet. It cuts the temperature axis at $T_C$, called the Ferrimagnetic Curie point. At high temperatures the last term of equation (2.5) become negligible, and reduces to a Curie-Weiss law:

$$\chi = \frac{C}{T + (C/\chi_0)}$$

This is the equation of straight line, shown dashed in Fig. 2.9, to which the 1/χ versus $T$ curve becomes asymptotic at high temperatures.

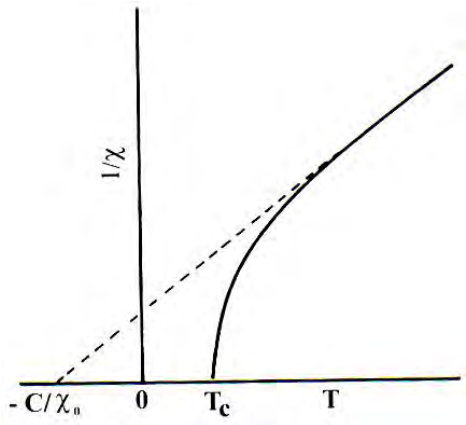


**Fig. 2.8.** The temperature dependence of the inverse susceptibility for ferrimagnets.

**pdfMachine**
**A pdf writer that produces quality PDF files with ease!**
Produce quality PDF files in seconds and preserve the integrity of your original documents. Compatible across nearly all Windows platforms, simply open the document you want to convert, click "print", select the "Broadgun pdfMachine printer" and that's it! Get yours now!

The Ferrimagnetic Curie temperature $T_C$ is obtained from equations (2.3) and (2.4) with $H = 0$ and setting the determinant of the coefficients of $M_i$ equal to zero. This gives

$$T_C = \frac{1}{2}[C_A\lambda_{AA} + C_B\lambda_{BB} + \{(C_A\lambda_{AA} - C_B\lambda_{BB})^2 + 4C_AC_B\lambda_{AB}^2\}^2] \qquad (2.6)$$

Equation (2.5) is in good agreement with the experiment, except near the Curie point. The experimental Curie temperature, the temperature at which the susceptibility becomes infinite and spontaneous magnetization appears, is lower than the theoretical Curie temperature [27]. This disagreement between theory and experiment in the region of Curie point is presumably due to the short-range spin order (spin clusters) at temperatures above experimental $T_C$ [2, 27].

The sub-lattice magnetizations will in general have different temperature dependences because the effective molecular fields acting on them are different. This suggests the possibility of having anomaly in the net magnetization versus temperature curves, Fig. 2.9. For most ferrimagnets the curve is similar to that of ferromagnets, but in a few cases there be a compensation point in the curve, Fig. 2.9(c) [1, 27]. At a point below the Curie temperature point, the two sub-lattice magnetizations are equal and thus appear to have no moment. This temperature is called the compensation point. Below this temperature one sub-lattice magnetization is larger and provides the net moment. Above this temperature the other magnetization does dominates and the net magnetization reverses direction.

The essential requisite for Néel configuration is a strong negative exchange interaction between *A* and *B* sub-lattices which results in their being magnetized in opposite directions below the transition point. But there may be cases where intra-sublattice interactions are comparable with inter-sublattice interaction. Neel's theory predicts paramagnetism for such substances at all temperatures. This is unreasonable since strong *AA* or *BB* interaction may lead to some kind of ordering especially at low temperature. In the cases of no *AB* interaction, antiferromagnetic ordering may be expected either in the *A* or in the *B* sub-lattice. Under certain conditions there may be non-collinear spin arrays of still lower energy.

**pdfMachine**
**A pdf writer that produces quality PDF files with ease!**
Produce quality PDF files in seconds and preserve the integrity of your original documents. Compatible across nearly all Windows platforms, simply open the document you want to convert, click “print”, select the “Broadgun pdfMachine printer” and that’s it! Get yours now!

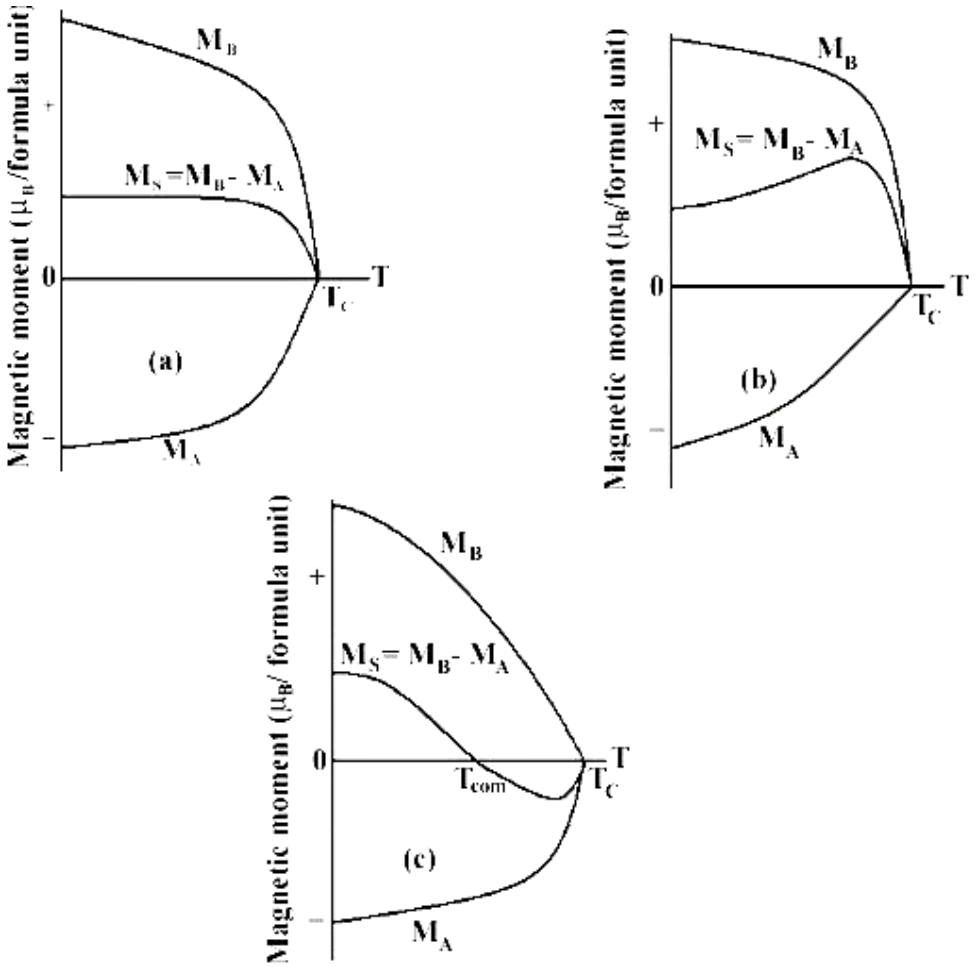


**Fig. 2.9.** Superposition of various combinations of two opposing sublattice magnetizations producing differing resultants including one with a compensation point (schematic).

### 2.6.4 Effect of Magnetic Moments in $Li_xMg_{0.4}Ni_{0.6-2x}Fe_{2+x}O_4$ Spinel Ferrites

$Fe_3O_4$ has ferromagnetic properties because of its inverse structure which leads to the formation of domains. A unit cell of $Fe_3O_4$ contains eight formula units each of which may be written in the form $Fe^{3+}[Fe^{2+}Fe^{3+}]O_4^{2-}$ [25]. Snoek and his co-workers found that oxides of inverse structure could be artificially produced in which the divalent ions of another element, for example *Mn*, *Ni*, *Co*, *Mg* or *Cu*, could be substituted for the divalent $Fe^{2+}$ ions in $Fe_3O_4$. An extensive range of ferrites could thus be made having the general formula $\vec{Fe}^{3+}[\overleftarrow{M}^{2+}\overleftarrow{Fe}^{3+}]O_4^{2-}$, where arrows indicate spin

**pdfMachine**
**A pdf writer that produces quality PDF files with ease!**
Produce quality PDF files in seconds and preserve the integrity of your original documents. Compatible across nearly all Windows platforms, simply open the document you want to convert, click "print", select the "Broadgun pdfMachine printer" and that's it! Get yours now!

ordering. Since the trivalent iron ions are equally distributed on *A* and *B* sites they cancel each other out magnetically, and the magnetic moment per formula unit is then theoretically the same as the magnetic moment of the divalent ion. The *Ni* ferrite has a moment of $2.3\mu_B$ compared with a theoretical value of $2\mu_B$ [1].

*Li* ferrite is a inverse spinel, with $Li^{1+}$ ions having no 3d shell's electron in *A* sites have zero magnetic moment; $Fe^{3+}$ ions in *B* sites have a magnetic moment $5\mu_B$. The cation distribution can be written as $\vec{Fe}^{3+}[\overleftarrow{Li}^{1+}\ \overleftarrow{Fe}^{3+}]O_4^{2-}$, where spin ordering is indicated by arrows. Again, *Ni* ferrites have inverse spinel structure and its formula may be written as $\vec{Fe}^{3+}[\overleftarrow{Ni}^{2+}\ \overleftarrow{Fe}^{3+}]O_4^{2-}$. On the other hand Mg ferrites have inverse spinel structure and its formula may be written as $Mg^{2+}{}_{1-x}\ \vec{Fe}^{3+}[Mg^{2+}{}_x\ \overleftarrow{Fe}^{3+}{}_{2-x}]O_4^{2-}$, where x is the degree of inversion.

The magnetic spins on each of the sites are antiparallel; so, the octahedral site is dominant. For reduction of magnetization a nonmagnetic ion (or magnetic ion having fewer spins than $Fe^{3+}$) is introduced on the octahedral sites as a replacement for $Fe^{3+}$.To increase the magnetization, a non magnetic ion is introduced on the tetrahedral site. In either case, the octahedral site normally remains dominant [10].

Theoretical aspect of magnetic moment in *Zn* substituted *Ni* Ferrite is explained by Velenzuala [2]. The zero magnetic moment of $Zn^{2+}$ ions leaves trivalent iron ions on *B* sites with a negative *BB* interaction between equal ions. Therefore *Zn* ferrite is not ferromagnetic. Zinc ferrite therefore be expected to be antiferromagnetic and thus to have a Néel point, though measurements show it to be paramagnetic only [1, 2, 25, 27]

Magnetic properties can be modified widely by cation substitution. In the present case An illustrative case is substituion of *Ni* by *Zn* in *Co* ferrite to form solid solutions $Ni_{1-x}Zn_xFe_2O_4$. The cation distribution can be written as $(Zn_x^{2+}Fe_{1-x}^{3+})[Ni_{1-x}^{2+}Fe_{1+x}^{3+}]O_4^{2-}$ [2]. $Zn^{2+}$ is diamagnetic and its main effect is to break linkages between magnetic cations. Another effect is to increase interaction distance by expanding the unit cell, since it has an ionic radious larger than the *Ni* and *Fe* radii. The most remarkable effect is that substitution of this diamagnetic cation (*Zn*) results in a significant increase in magnetic moment in a number of spinel solid solutions, Fig. 2.10.

**pdfMachine**
**A pdf writer that produces quality PDF files with ease!**
Produce quality PDF files in seconds and preserve the integrity of your original documents. Compatible across nearly all Windows platforms, simply open the document you want to convert, click "print", select the "Broadgun pdfMachine printer" and that's it! Get yours now!

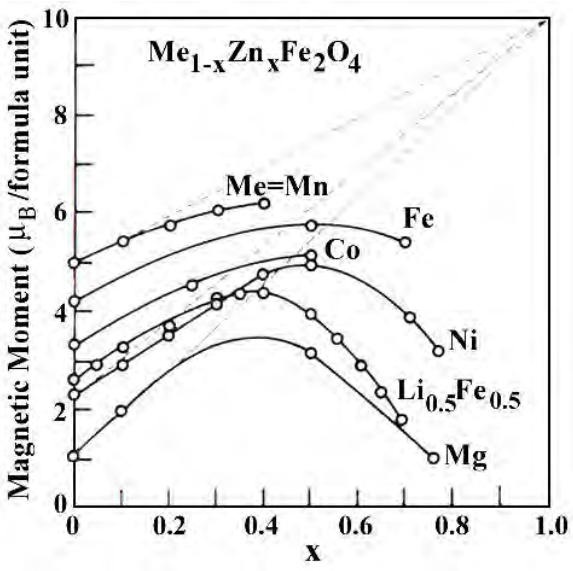


**Fig. 2.10.** Variation of Magnetic moment (in Bohr magnetons per formula unit) with increasing zinc substitution [1, 2].

Magnetic moment as a function of *Zn* content in *Li*-Ferrite, *Mg*-Ferrite and *Ni*-Ferrite shows an increase for small substitutions goes through a maximum for intermediate values, decreases and finally vanishes for high *Zn* contents. For *Zn* substituted *Li*-Ferrite it is observed that the magnetic moment increases up *Zn* content , $x$= 0.4 then it started to decrease. In *Zn* substituted *Ni* ferrite and *Mg* ferrite the magnetic moment increases up to *Zn* content , $x$= 0.5, then it decreases .

A simple analysis shows that this increase can be expected for an antiparallel alignment. As the *Zn* content increases, magnetic moments decreases in sublattice *A* and increase in sublattice *B*. If the magnetic moment of *Fe* and *Ni* are 5 and ~2.3 $\mu_B$/ion, respectively, then, per formula unit, the total moment in Bohr magnetons on *B* sublattice is $2.3(1-x)+5(1+x)$ and on *A* sublattice the total antiparallel moment is $5(1-x)$. If the resultant moment per formula unit is $M_S(0)$, then by taking the difference of *A* and *B* moments [26],

$$M_S(0) = 2.3(1-x)+5(1+x)-5(1-x)$$
$$= x(10-2.3)+2.3$$

A linear relationship is obtained with a slope of 7.7, predicting a moment value of $10\mu_B$ per formula unit for *Zn* substitution $x=1$, as shown by the broken lines in Fig. 2.10. This relationship is not followed over the entire composition range. However, as the *Zn* content increases, $A-O-B$ interactions become too weak and $B-O-B$ interactions

**pdfMachine**
**A pdf writer that produces quality PDF files with ease!**
Produce quality PDF files in seconds and preserve the integrity of your original documents. Compatible across nearly all Windows platforms, simply open the document you want to convert, click "print", select the "Broadgun pdfMachine printer" and that's it! Get yours now!

begin to dominate. That is, the average distance between the interacting spins gets larger. As a consequence, the system becomes frustrated causing a perturbation to the magnetically ordered spins as large number of *B* sites spins gets non-magnetic impurity atoms as their nearest neighbours.

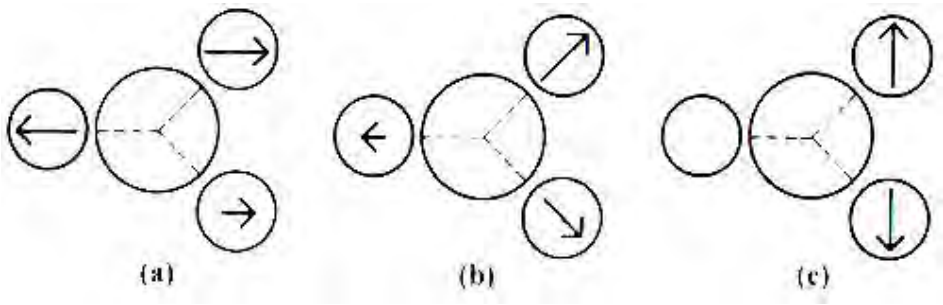


**Fig. 2.11.** Schematic representation of spin arrangements in $Ni_{1-x}Zn_xFe_2O_4$: (a) ferrimagnetic (for $x \leq 0.5$); (b) triangular or Yafet-Kittel (for $x > 0.5$); and (c) antiferromagnetic for $x \approx 1$.

The *B* spins are no longer held in place due to this weak anti-ferromagnetic *A*-*B* interaction leading to non-collinearity or canting among the *B* sublattice. Thus for $x > 0.5$ *Zn* content, instead of a collinear antiparallel alignment, canted structure appears, where spins in *B* sites are no longer parallel [2, 32], Fig. 2.11. Evidence of this triangular structure has been observed by neutron diffraction [22]; a theoretical analysis showed that departure from collinear order depends on the ratio of the $A-O-B$ to $B-O-B$ molecular field coefficients, $\lambda_{AB}/\lambda_{BB}$ [33]. For high *Zn* concentration, $B-O-B$ interactions dominant and the ferrite become antiferromagnetic for $x=1$ [2].

The theoretical aspect of the variation of magnetic moment in present ferrite system , $Li_xMg_{0.4}Ni_{0.6-2x}Fe_{2+x}O_4$ ferrite, increasing *Li* content can be explained as below from the cation distribution as stated in section

It is known that $Li^{1+}$, $Ni^{2+}$ and $Mg^{2+}$ ions occupy B sites, although Fe ions exist at both A and B sites [12]. The cation distribution of various $Li_xMg_{0.4}Ni_{0.6-2x}Fe_{2+x}O_4$ ferrite assumed as $(Fe^{3+}_{0.9})_A\,[Li^{1+}_xMg^{2+}_{0.4}Ni_{0.6-2x}\,Fe^{3+}_{1.1+x}]_B$ [31]

where the term within the square bracket indicates the octahedral (B) sites and the first term is tetrahedral (A) sites. When $Li^{1+}$ ions are introduced at the cost of $Ni^{2+}$ions, $Fe^{3+}$ ions concentration at B sites increases. As $Li^{1+}$ and $Mg^{2+}$ are non-magnetic, the magnetic moment of B site will depend on the $Ni^{2+}$ and $Fe^{3+}$ ion. Progressive substitution of $Li^+$ ion increases $Fe^{3+}$ ion and decreases $Ni^{2+}$ ion concentration at B sites.

**pdfMachine**
**A pdf writer that produces quality PDF files with ease!**
Produce quality PDF files in seconds and preserve the integrity of your original documents. Compatible across nearly all Windows platforms, simply open the document you want to convert, click "print", select the "Broadgun pdfMachine printer" and that's it! Get yours now!

The $Fe^{3+}$ content is increased by $2+x$ as the *Li* content increases As a result, the magnetic moments of B sublattice increases for small *Li* content.

## 2.7 Microstructure

A polycrystal is much more than many tiny crystals bonded together. The interfaces between the crystals, or the grain boundaries which separate and bond the grains, are complex and interactive interfaces. The whole set of a given material's properties (mechanical, chemical and especially electrical and magnetic) depend strongly on the nature of the microstructure.

In the simplest case, the grain boundary is the region, which accommodates the difference in crystallographic orientation between the neighbouring grains. For certain simple arrangements, the grain boundary is made of an array of dislocations whose number and spacing depends on the angular deviation between the grains. The ionic nature of ferrites leads to dislocation patterns considerably more complex than in metals, since electrostatic energy accounts for a significant fraction of the total boundary energy [2].

For low-loss ferrite, Ghate [1] states that the grain boundaries influence properties by

1) creating a high ressistivity intergranular layer,
2) acting as a sink for impurities which may act as a sintering aid and grain growth modifiers,
3) providing a path for oxygen diffusion, which may modify the oxidation state of cations near the boundaries.

In addition to grain boundaries, ceramic imperfections can impede domain wall motion and thus reduce the magnetic property. Among these are pores, cracks, inclusions, second phases, as well as residual strains. Imperfections also act as energy wells that pin the domain walls and require higher activation energy to detach. Stresses are microstructural imperfections that can result from impurities or processing problems such as too rapid a cool. They affect the domain dynamics and are responsible for a much greater share of the degradation of properties than would expect [1].

Grain growth kinetics depends strongly on the impurity content. A minor dopant can drastically change the nature and concentration of defects in the matrix, affecting

**pdfMachine**
**A pdf writer that produces quality PDF files with ease!**
Produce quality PDF files in seconds and preserve the integrity of your original documents. Compatible across nearly all Windows platforms, simply open the document you want to convert, click "print", select the "Broadgun pdfMachine printer" and that's it! Get yours now!

grain boundary motion, pore mobility and pore removal [2, 41]. The effect of a given dopant depends on its valence and solubility with respect to host material. If it is not soluble at the sintering temperature, the dopant becomes a second phase which usually segregates to the grain boundary.

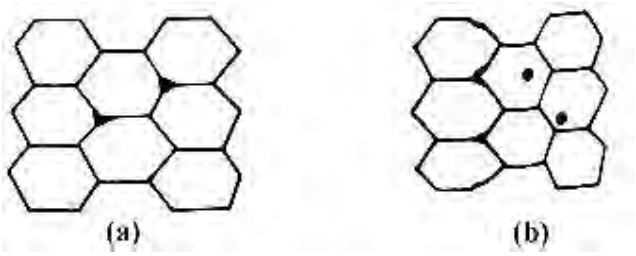


**Fig. 2.12.** Porosity character: (a) intergranular, (b) intragranular.

The porosity of ceramic samples results from two sources, intragranular porosity and intergranular porosity, Fig. 2.12. An undesirable effect in ceramic samples is the formation of exaggerated or discontinuous grain growth which is characterized by the excessive growth of some grains at the expense of small, neighbouring ones (Fig. 2.13). When this occurs, the large grain has a high defect concentration. Discontinuous growth is believed to result from one or several of the following: powder mixtures with impurities; a very large distribution of initial particle size; sintering at excessively high temperatures; in ferrites containing *Zn* and /or *Mn*, a low $O_2$ partial pressure in the sintering atmosphere. When a very large grain is surrounded by smaller ones, it is called 'duplex' microstructure.

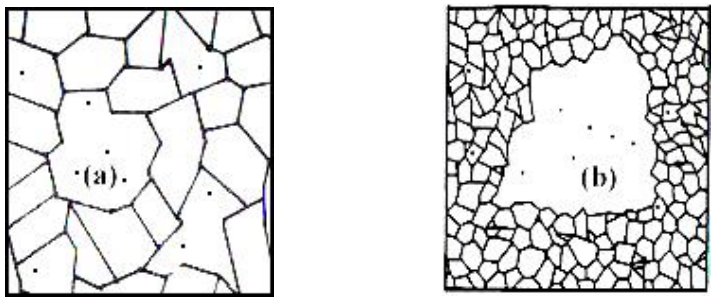


**Fig. 2.13.** Grain growth (a) discontinuous, (b) duplex (schematic).

**pdfMachine**
**A pdf writer that produces quality PDF files with ease!**
Produce quality PDF files in seconds and preserve the integrity of your original documents. Compatible across nearly all Windows platforms, simply open the document you want to convert, click "print", select the "Broadgun pdfMachine printer" and that's it! Get yours now!

## 2.8 Theories of Permeability

Permeability is defined as the proportionality constant between the magnetic field induction *B* and applied field intensity *H* [2, 24, 34]:

$$B = \mu H \tag{2.7}$$

If the applied field is very low, approaching zero, the ratio will be called the initial permeability, Fig. 2.15 and is given by

$$\mu_i = \frac{\Delta B}{\Delta H}_{(\Delta H \to 0)}$$

This simple definition needs further sophistications. A magnetic material subjected to an ac magnetic field can be written as

$$H = H_0 e^{i\omega t} \tag{2.8}$$

It is observed that the magnetic flux density *B* lag behind *H*. This is caused due to the presence of various losses and is thus expressed as

$$B = B_0 e^{i(\omega t-\delta)} \tag{2.9}$$

Here $\delta$ is the phase angle that marks the delay of *B* with respect to *H*. The permeability is then given by

$$\mu = \frac{B}{H} = \frac{B_0 e^{i(\omega t-\delta)}}{H_0 e^{i\omega t}} = \frac{B_0 e^{-i\delta}}{H_0} = \frac{B_0}{H_0}\cos\delta - i\frac{B_0}{H_0}\sin\delta = \mu^{/} - i\mu^{//} \tag{2.10}$$

where $$\mu^{/} = \frac{B_0}{H_0}\cos\delta \tag{2.11}$$

and $$\mu^{//} = \frac{B_0}{H_0}\sin\delta \tag{2.12}$$

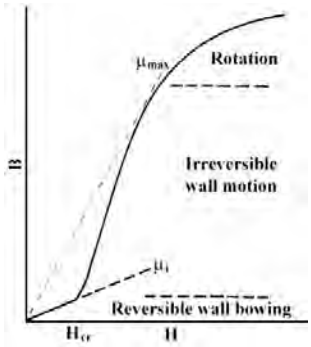


**Fig. 2.14.** Schematic magnetization curve showing the important parameter: initial permeability, $\mu_i$ (the slope of the curve at low fields) and the main magnetization mechanism in each magnetization range [2].

**pdfMachine**
**A pdf writer that produces quality PDF files with ease!**
Produce quality PDF files in seconds and preserve the integrity of your original documents. Compatible across nearly all Windows platforms, simply open the document you want to convert, click "print", select the "Broadgun pdfMachine printer" and that's it! Get yours now!

The real part ($\mu'$) of complex permeability ($\mu$), as expressed in equation (2.10) represents the component of *B* which is in phase with *H*, so it corresponds to the normal permeability. If there are no losses, we should have $\mu = \mu'$. The imaginary part $\mu''$ corresponds to that of *B*, which is delayed by phase angle 90° from *H* [23, 30]. The presence of such a component requires a supply of energy to maintain the alternating magnetization, regardless of the origin of delay. The ratio of $\mu''$ to $\mu'$, as is evident from equation (2.12) and (2.11) gives

$$\frac{\mu''}{\mu'} = \frac{\frac{B_0}{H_0}\sin\delta}{\frac{B_0}{H_0}\cos\delta} = \tan\delta \tag{2.13}$$

This $\tan\delta$ is called loss factor.

The quality factor is defined as the reciprocal of this loss factor, i.e.

$$\text{Quality factor} = \frac{1}{\tan\delta} \tag{2.14}$$

$$\text{And the relative quality factor, } Q = \frac{\mu'}{\tan\delta} \tag{2.15}$$

The curves that show the variation of both $\mu'$ and $\mu''$ with frequency are called the magnetic spectrum or permeability spectrum of the material [27]. The variation of permeability with frequency is referred to as dispersion. The measurement of complex permeability gives us valuable information about the nature of domain wall and their movements. In dynamic measurements the eddy current loss is very important. This occurs due to the irreversible domain wall movements. The permeability of a ferrimagnetic substance is the combined effect of the wall permeability and rotational permeability mechanisms.

### 2.8.1 Mechanisms of Permeability

The mechanisms can be explained as follows: A demagnetized magnetic material is divided into number of Weiss domains separated by Bloch walls. In each domain all the magnetic moments are oriented in parallel and the magnetization has its saturation value $M_s$. In the walls the magnetization direction changes gradually from the direction of magnetization in one domain to that in the next. The equilibrium positions

**pdfMachine**
**A pdf writer that produces quality PDF files with ease!**
Produce quality PDF files in seconds and preserve the integrity of your original documents. Compatible across nearly all Windows platforms, simply open the document you want to convert, click "print", select the "Broadgun pdfMachine printer" and that's it! Get yours now!

of the walls result from the interactions with the magnetization in neighbouring domains and from the influence of pores; crystal boundaries and chemical inhomogeneities which tend to favour certain wall positions.

### 2.8.1.1 Wall Permeability

The mechanism of wall permeability arises from the displacement of the domain walls in small fields. Lets us consider a piece of material in the demagnetized state, divided into Weiss domains with equal thickness $L$ by means of 180˚ Bloch walls (as in the Fig. 2.15).

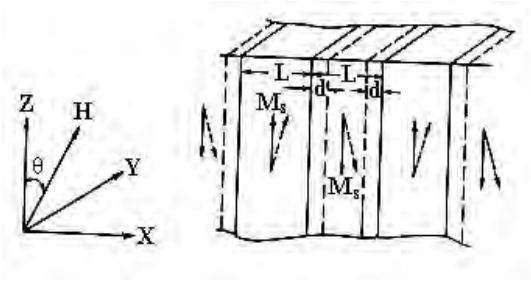


**Fig 2.15.** Magnetization by wall motion and spin rotation.

The walls are parallel to the $YZ$ plane. The magnetization $M_s$ in the domains is oriented alternately in the $+Z$ or $-Z$ direction. When a field $H$ with a component in the $+Z$ direction is applied, the magnetization in this direction will be favoured. A displacement $dx$ of the walls in the direction shown by the dotted lines will decrease the energy density by an amount [35, 36]:

$$\frac{2M_s H_z dx}{L}$$

This can be described as a pressure $M_s H_z$ exerted on each wall. The pressure will be counteracted by restoring forces which for small deviations may assume to be $kdx$ per unit wall surface. The new equilibrium position is then given by

$$d = \frac{M_s H_z dx}{L}$$

From the change in the magnetization

$$\Delta M = \frac{2M_s d}{L},$$

**pdfMachine**
**A pdf writer that produces quality PDF files with ease!**
Produce quality PDF files in seconds and preserve the integrity of your original documents. Compatible across nearly all Windows platforms, simply open the document you want to convert, click “print”, select the “Broadgun pdfMachine printer” and that’s it! Get yours now!

the wall susceptibility $\chi_w$ may be calculated. Let $H$ makes the angle $\theta$ with $Z$ direction. The magnetization in the $\theta$ direction becomes

$$(\Delta M)_\theta = \frac{2M_s d}{L}\cos\theta \text{, And with } H_z = H\cos\theta \text{ and } d = \frac{2M_s H_z}{K}$$

we obtain

$$\chi_w = \frac{(\Delta M)_\theta}{H} = \frac{4M_s^2\cos^2\theta}{KL} \tag{2.16}$$

### 2.8.1.2 Rotational Permeability

The rotational permeability mechanism arises from rotation of the magnetization in each domain. The direction of $M$ can be found by minimizing the magnetic energy $E$ as a function of the orientation. Major contribution to $E$ comes from the crystal anisotropy energy. Other contributions may be due to the stress and shape anisotropy. The stress may influence the magnetic energy via the magnetostriction. The shape anisotropy is caused by the boundaries of the sample as well as by pores, nonmagnetic inclusions and inhomogeneities. For small angular deviations, $\alpha_x$ and $\alpha_y$ may be written as

$$\alpha_x = \frac{M_x}{M_s} \text{ and } \alpha_y = \frac{M_y}{M_s}.$$

For equilibrium $Z$-direction, $E$ may be expressed as [36]

$$E = E_0 + \frac{1}{2}\alpha_x^2 E_{xx} + \frac{1}{2}\alpha_y^2 E_{yy}$$

where it is assumed that $x$ and $y$ are the principal axes of the energy minimum. Instead of $E_{xx}$ & $E_{yy}$, the anisotropy field $H_x^A$ and $H_y^A$ are often introduced. Their magnitude is given by

$$H_x^A = \frac{E_{xx}}{2M_s} \text{ and } H_y^A = \frac{E_{yy}}{2M_s},$$

$H_x^A$ & $H_y^A$ represent the stiffness with which the magnetization is bound to the equilibrium direction for deviations in $x$ and $y$ direction, respectively. The rotational susceptibilities $\chi_{r,x}$ and $\chi_{r,y}$ for fields applied along $x$ and $y$ directions, respectively are

pdfMachine
A pdf writer that produces quality PDF files with ease!
Produce quality PDF files in seconds and preserve the integrity of your original documents. Compatible across nearly all Windows platforms, simply open the document you want to convert, click "print", select the "Broadgun pdfMachine printer" and that's it! Get yours now!

$$\chi_{r,x} = \frac{M_s}{H_x^A} \text{ and } \chi_{r,y} = \frac{M_s}{H_y^A}.$$

For cubic materials it is often found that $H_x^A$ and $H_y^A$ are equal. For $H_x^A = H_y^A = H^A$ and a field $H$ which makes an angle $\theta$ with the $Z$ direction (as shown in Fig. 2.15) the rotational susceptibility, $\chi_{r,c}$ in one crystallite becomes

$$\chi_{r,c} = \frac{M_s}{H^A} \sin^2 \theta \tag{2.17}$$

A polycrystalline material consisting of a large number of randomly oriented grains of different shapes, with each grain divided into domains in a certain way. The rotational susceptibility $\chi_r$ of the material has to be obtained as a weighted average of $\chi_{r,c}$ of each crystallite, where the mutual influence of neighbouring crystallites has to be taken into account. If the crystal anisotropy dominates other anisotropies, then $H^A$ will be constant throughout the material, so only the factor $\sin^2 \theta$ (equation 2.17) has to be averaged. Snoek [36] assuming a linear averaging of $\chi_{r,c}$ and found

$$\chi_r = \frac{2M_s}{3H^A}$$

The total internal susceptibility

$$\chi = \chi_w + \chi_r = \frac{4M_s^2 \cos^2 \theta}{KL} + \frac{2M_s}{3H^A} \tag{2.18}$$

If the shape and stress anisotropies cannot be neglected, $H^A$ will be larger. Any estimate of $\chi_r$ will then be rather uncertain as long as the domain structure, and the pore distribution in the material are not known. A similar estimate of $\chi_w$ would require knowledge of the stiffness parameter $k$ and the domain width $L$. These parameters are influenced by such factors as imperfection, porosity and crystallite shape and distribution which are essentially unknown.

### 2.8.2 Frequency dependent Permeability Curve :

The techniques of impedance spectroscopy, widely used in dielectrics have been applied to magnetic materials [28]. In this method, impedance measurements as a function of frequency are modified by means of an equivalent circuit and its elements are associated with the physical parameters of the material. The complex permeability,

**pdfMachine**
**A pdf writer that produces quality PDF files with ease!**
Produce quality PDF files in seconds and preserve the integrity of your original documents. Compatible across nearly all Windows platforms, simply open the document you want to convert, click "print", select the "Broadgun pdfMachine printer" and that's it! Get yours now!

$\mu^*$, is determined from the complex impedance ,$Z^*$, by :

$$\mu^* = (jk/\omega)Z^* \qquad (2.19)$$

where $k$ is the geometric constant relating to inductance , $l$, to the permeability. The equivalent circuit for domain wall bowing (applied field lower than critical field) is a parallel *RL* arrangement; for wall displacement, additional Warbarg-type impedance element is required (Irvine *et al*.) [37].

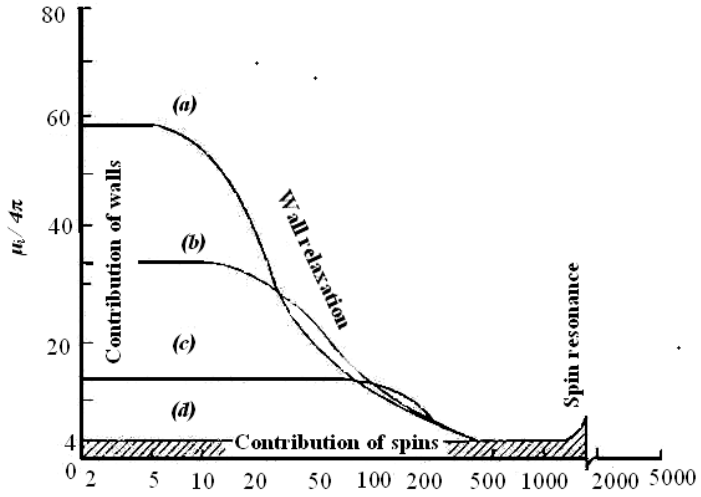


**Fig. 2.16.** Permeability spectra of $NiFe_2O_4$ samples with different grain size: (a)11µm;(b) 5µm;(c)2 µm (d)size <0.2 µm( single domain behaviour) [2]

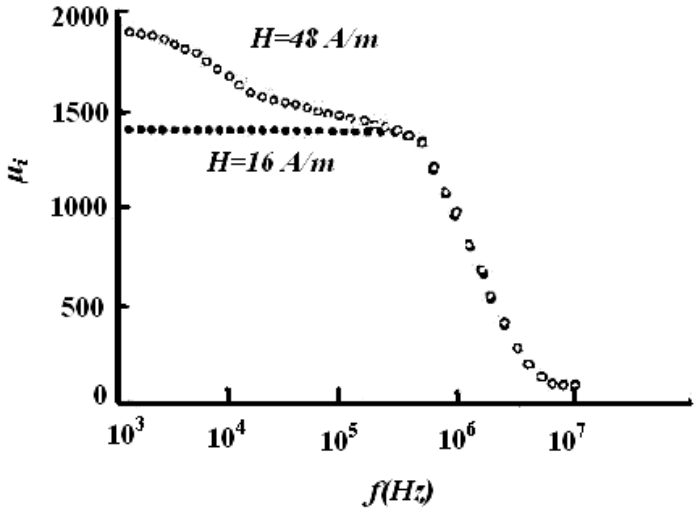


**Fig. 2.17.** Permeability spectrum of a *Ni-Zn* sample at fields above (open circles) and below (filled circles) the critical field [38].

**pdfMachine**
**A pdf writer that produces quality PDF files with ease!**
Produce quality PDF files in seconds and preserve the integrity of your original documents. Compatible across nearly all Windows platforms, simply open the document you want to convert, click "print", select the "Broadgun pdfMachine printer" and that's it! Get yours now!

Many of the specific applications of ferrites depend on their behaviour at high frequencies. When subjected to an ac field, ferrite permeability shows several dispersions; as the field frequency increases, the various magnetization mechanisms become unable to follow the field. The dispersion frequency for each mechanism is different time constants, Fig. 2.16. The low frequency dispersions are associated with domain wall dynamics and the high frequency dispersion, with spin resonance. The spin resonance phenomena occur usually in the GHz range. The two main magnetization mechanisms are wall bowing and wall displacement as discussed before in section 2.8. Any field results in a bowing of pinned walls, and if this field has higher value than the corresponding critical field, walls are unpinned and displaced. Otherwise, bowed walls remain pinned to material defects. Measurements at low fields therefore show only one wall dispersion. Measurements at high fields, several, complex dispersions are observed, such as those in Fig. 2.17. Wall displacement dispersion occurs at lower frequencies than wall bowing, since hysteresis is a more complex phenomenon of wall bowing, unpinning, displacement and pinning steps.

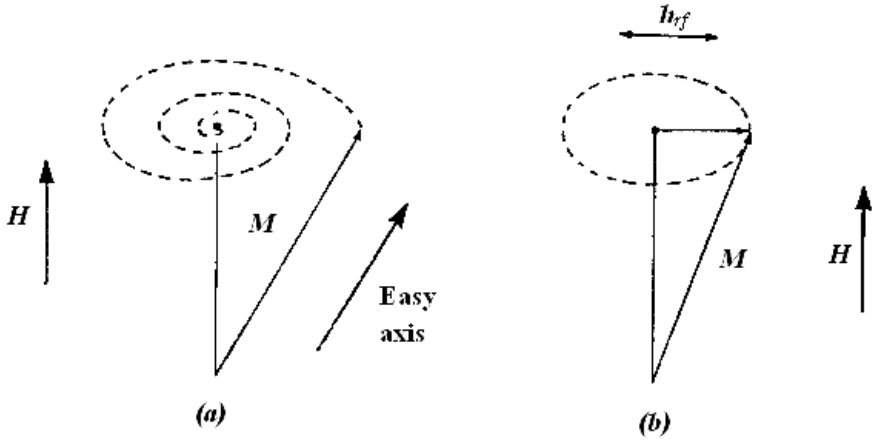


**Fig. 2. 18.** (a) Schematic representation of the spin deviation from an easy axis by precessional spiralling into the field direction, (b) Precession is maintained by a perpendicular rf field, $h_{rf}$ [2].

At very high frequencies, domain walls are unable to follow the field and the only remaining megnetisation mechanism is spin rotation within domains. This mechanism eventually also shows a dispersion, which always takes the form of a resonance. Spins are subjected to the anisotropy field, representing spin-lattice coupling; as an external field is applied (out of the spins' easy direction), spins experience a

**pdfMachine**
**A pdf writer that produces quality PDF files with ease!**
Produce quality PDF files in seconds and preserve the integrity of your original documents. Compatible across nearly all Windows platforms, simply open the document you want to convert, click "print", select the "Broadgun pdfMachine printer" and that's it! Get yours now!

torque. However, the response of spins is not instantaneous; spins precess around the field direction for a certain time (the relaxation time, $\tau$) before adopting the new orientation, Fig. 2.18.

The frequency of this precession is given by the Larmor frequency:

$$\omega_L = \gamma \mu_o H_T \qquad (2.20)$$

where $H_T$ is the total field acting on the spin.

$H_T = H_K + H + H_d + \ldots\ldots$, where $H_K$, $H$, $H_d$ are the anisotropy and the external and demagnetization fields, respectively. If an ac field of angular frequency $\omega_L$ is applied to the sample, a resonant absorption (ferromagnetic resonance) occurs. The Larmour frequency is independent of the precession amplitude.

## 2.9 Magnetization Mechanism

### 2.9.1 Concept of Magnetic Domain and Domain Wall (Weiss Domain Structure)

In 1907 Pierre Weiss in his paper "Hypothesis of the molecular field" [29, 39] postulated that a ferromagnetic material rather than be uniformly magnetized, is divided into a number of regions of domains, each of which is magnetized to saturation level but the direction of magnetization from domain to domain need not be parallel. The magnetization vectors are parallel to preferred direction such that the demagnetization field, and hence the demagnetization energy ($W_{dem.} = 1/8\pi\ H^2_D$) is as small as possible. The total magnetization is then given by the vector summation of individual magnetization over all domains. The demagnetized state of the magnet is from the view point of an observer outside the material. In ferromagnetic materials, the atomic magnetic moments aligned in parallel fashion, while in ferrite domain, the net moments of the anti ferromagnetic interaction are spontaneously oriented parallel to each other (even without applied magnetic field) [40]. The applied field serves as a control in changing the balance of potential energy within the, magnetic material. These uniformly magnetized domains are separated by a thin layer in which the magnetization gradually changes from one orientation to another. This transition boundary is called domain wall or Bloch wall.

The domain structure are found basically to reduce the magnetostatic energy i.e.,

**pdfMachine**
**A pdf writer that produces quality PDF files with ease!**
Produce quality PDF files in seconds and preserve the integrity of your original documents. Compatible across nearly all Windows platforms, simply open the document you want to convert, click "print", select the "Broadgun pdfMachine printer" and that's it! Get yours now!

the magnetic potential energy contained in the field lines (or flux lines) connecting north and south poles outside of the material. This concept can be understood by considering a simple case, as shown in Fig. 2.19, in which (a) to (e) represents a cross section of a ferromagnetic single crystal. In Fig. 2.19 (a) a single domain crystal is shown, the value of magnetostatic energy is high. The arrow indicates the direction of magnetization and hence the direction of spin alignment in the domain. If the crystal is divided into two domains (Fig. 2.19 (b), the magnetic energy will be reduced by roughly one half of the single domain case. This splitting process continues to lower the energy of the system until more energy is required to form the domain boundary. When a large domain is split into *n* domains, as shown in Fig. 2.19 (c) the magnetic energy will be reduced to approximately *1/n* of the magnetic energy of that of type (a). For the domain structure configuration in Fig. 2.19 (d) and (e), the magnetic energy is zero as the flux circuit is completed within a crystal, (i.e., flux path never leaves the boundary of the material). These triangular domains are callled closure domains. Therefore the magnetostatic energy is reduced. This type of structure may also be found at the surface of the material.

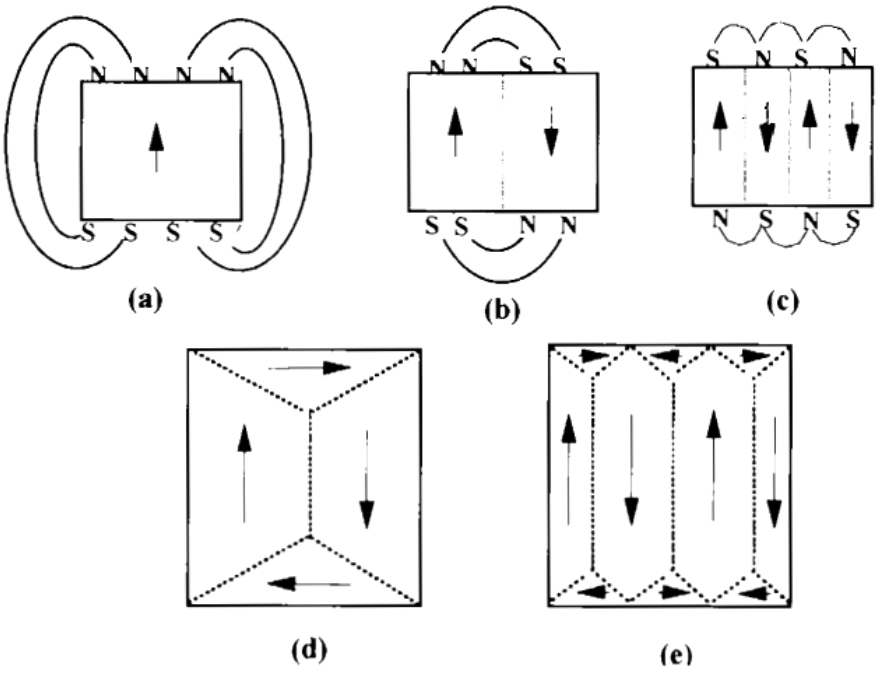


**Fig. 2.19.** Possible domain structures showing progressively low energy .Each part is representing a cross-section of a ferromagnetic single crystal [2, 28].

**pdfMachine**
**A pdf writer that produces quality PDF files with ease!**
Produce quality PDF files in seconds and preserve the integrity of your original documents. Compatible across nearly all Windows platforms, simply open the document you want to convert, click “print”, select the “Broadgun pdfMachine printer” and that’s it! Get yours now!

The boundaries between the domains, are not sharp on atomic scale but are spread over a finite thickness within which the direction of the spin changes gradually from one domain to the next [39]. The spin within a domain wall as shown in Fig. 2.20, are pointing in necessary directions, so that the crystal anisotropy energy within the wall is higher than it is in the adjacent domains. The exchange energy tries to align the spin in a direction parallel to the direction in the domain while the anisotropy energy tries to make the wall thin to minimize misalignment within the easy directions. The actual thickness of the domain wall is determined by the counterbalance of the exchange energy and anisotropy energy.

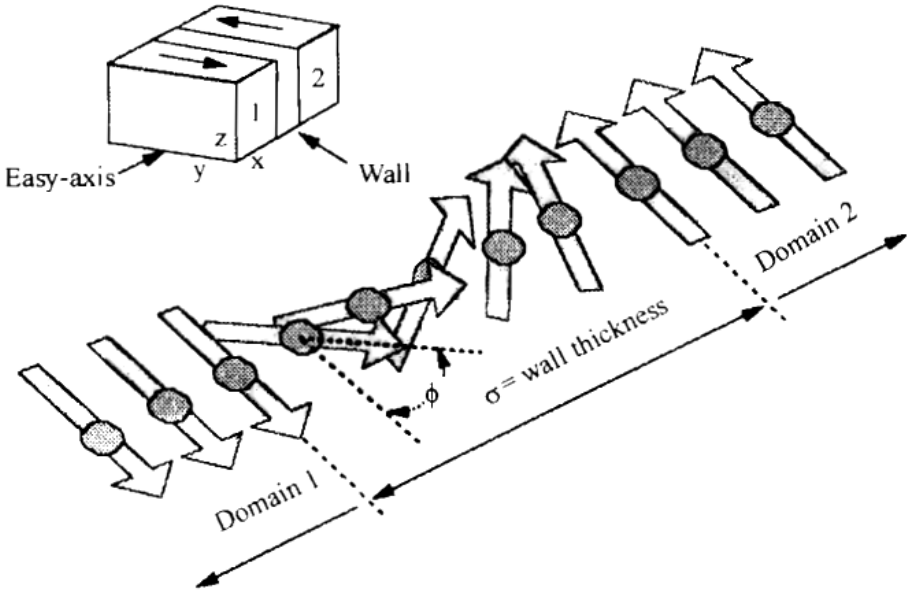


**Fig. 2.20.** Schematic representation of a domain wall. All spins, within the wall thickness are in non-easy direction [27].

### 2.9.2 The dynamic behaviour of Domains

Two general mechanisms are involved in changing the magnetization in a domain and, therefore, changing the magnetization in a sample. The first mechanism acts by rotating the magnetization towards the direction of the field. Since this may involve rotating the magnetization from an axis of easy magnetization in a crystal to one

**pdfMachine**
**A pdf writer that produces quality PDF files with ease!**
Produce quality PDF files in seconds and preserve the integrity of your original documents. Compatible across nearly all Windows platforms, simply open the document you want to convert, click “print”, select the “Broadgun pdfMachine printer” and that’s it! Get yours now!

of more difficult magnetization, a certain amount of anisotropy energy is required. The rotations can be small as indicated in Figure 2.21(a) or they can be almost the equivalent of a complete 180˚ reversal or flip if the crystal structure is uniaxial and if the magnetizing field is opposite to the original magnetization direction of the domain. The other mechanism for changing the domain magnetization is one in which the direction of magnetization remains the same, but the volumes occupied by the different domains may change. In this process, the domains whose magnetizations are in a direction closest to the field direction grow larger while those that are more unfavorably oriented shrink in size. Fig. 2.21(b) shows this process which is called domain wall motion.

The mechanism for domain wall motion starts in the domain wall. Present in the wall is a force (greatest with the moments in the walls that are at an angle of 90˚ to the applied field) that will tend to rotate those moments in line with the field. As a result, the center of the domain wall will move towards the domain opposed to the field. Thus, the area of the domain with favorable orientation will grow at the expense of its neighbour.

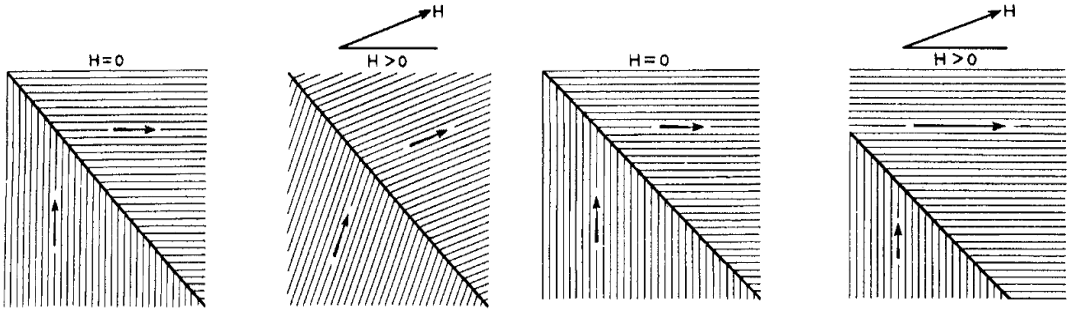


*(a)Volume constant , directions changed* *b)Volume changed , directions constant*

**Fig. 2.21.** (a) Change of domain magnetization by domain wall movement and (b) Change of domain magnetization by domain rotation [28].

### 2.9.3 Bulk Material Magnetization

Although domains are not physical entities such as atoms or crystal lattices and can only be visualized by special means, for the purpose of magnetic structure they are important in explaining the process of magnetization. A material that has strongly oriented moments in a domain often has no resultant bulk material magnetization. Non-magnetic material can be transformed into a strongly magnetic body by domain dynamics discussed above. If the material has been demagnetized, the domains point in

**pdfMachine**
**A pdf writer that produces quality PDF files with ease!**
Produce quality PDF files in seconds and preserve the integrity of your original documents. Compatible across nearly all Windows platforms, simply open the document you want to convert, click “print”, select the “Broadgun pdfMachine printer” and that’s it! Get yours now!

all random directions so that there is complete cancellation and the resultant magnetization is zero (Fig. 2.22). The possible steps to complete orientation of the domains or magnetization of the material are also shown in Fig. 2.22 [28].

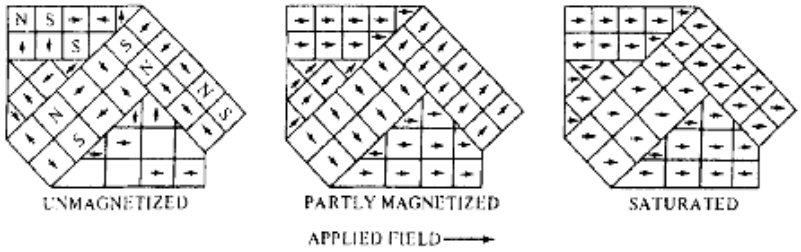


**Fig. 2.22.** Stages in Magnetization of a sample containing several crystals [28].

### 2.9.4 The Magnetization Curve

For unmagnetized bulk material, there is a zero net magnetic moment. It can be predicted that there will be an infinite number of degree of magnetization between the unmagnetized and saturation condition, when the material is subjected to an external magnetic field. These extreme situation correspond respectively, to random orientation of domains complete alignment in one direction with elimination of domain walls. It can be started with the a demagnetized specimen and increase the applied magnetic field and then the bulk material will be progressively magnetized by the domain dynamics. The magnetization of the sample will follow the course as shown in Fig. 2.23 (a) [28]. The slope from the origin to a point on the curve or the ratio *M/H* is defined as magnetic susceptibility. This curve is called Magnetization Curve. This curve is generally percieved as being made of three major portions.

The first, the lower section, is the initial susceptibility region and is characterized by reversible domain wall movements and rotations. By reversible means that after the magnetization slightly with an increase in field the original magnetization conditions can be reversed if the field is reduced to initial value. The contribution of the displacement walls to an initial permeability is entirely dependent on the sort of material studied.

In the second stage magnetization curve, if the field is increased, the intensity of the magnetization increases more drastically, is called the irreversible magnetization range. This range is obtained mainly by the irreversible domain wall motion from one stable state to another.

**pdfMachine**
**A pdf writer that produces quality PDF files with ease!**
Produce quality PDF files in seconds and preserve the integrity of your original documents. Compatible across nearly all Windows platforms, simply open the document you want to convert, click “print”, select the “Broadgun pdfMachine printer” and that’s it! Get yours now!

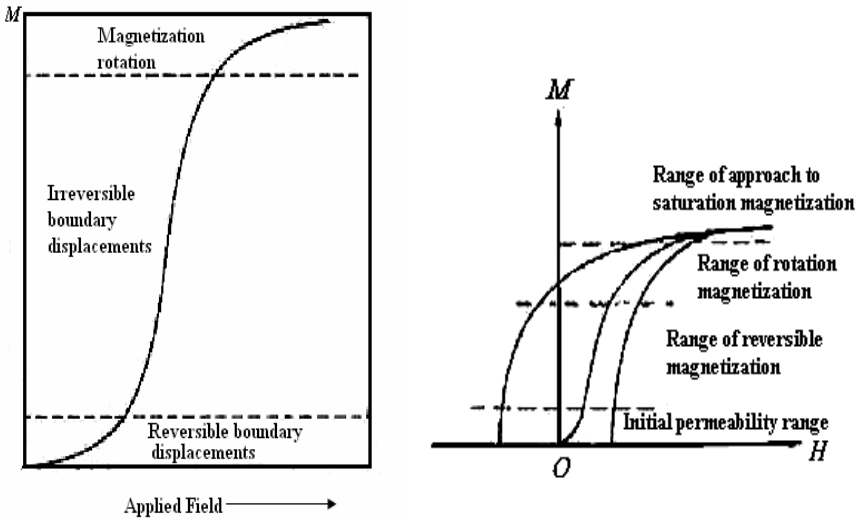


(a) (b)

**Fig. 2.23.** Domain dynamics during various parts of the magnetization curve [28].

If the field is increased further, the magnetization curve become less steep and its process become reversible once more. In the third section of magnetization curve, the displacement of domain walls have already been completed and the magnetization take place by rotation magnetization. This range is called rotation magnetization range. Beyond this range the magnetization gradually approaches to saturation magnetization. (Fig. 2.23 (b))

## References

[1] Goldman ,A., "Handbook of Modern Ferromagnetic Materials", Kluwer Academic Pub., Boston U.S.A, 1999.

[2] Valenzuela, R., "Magnetic Ceramics", Cambridge University Press, Cambridge, 1994.

[3] Haque ,M. M., "Influence of additives on the magnetic and electrical properties of iron-excess Mn-Zn ferrites," M. Phil. Thesis, BUET, Bangladesh, 2000.

[4] Jefferson, C. F. and West, R. G., "Ferrite system for application at lower microwave frequencies," Journal of Applied Physics, Vol- 32, pp 3905-3915, 1961.

[5] West, R. G. and Blankenship, A. C., "Magnetic properties of dense lithium ferrites," Journal of the American Ceramic Society, Vol- 50, pp. 343-349, 1967.

**pdfMachine**
**A pdf writer that produces quality PDF files with ease!**
Produce quality PDF files in seconds and preserve the integrity of your original documents. Compatible across nearly all Windows platforms, simply open the document you want to convert, click "print", select the "Broadgun pdfMachine printer" and that's it! Get yours now!

[6] Baba, P. D. and Banerjee, S. K., "Microwave ferrite program," Summary Technical Report, ESD-TR-68-251, 1968.

[7] Collins, T. and Brown , A. E., "Low-loss lithium ferrites for microwave latching applications, " Journal of Applied Physics, Vol- 42, pp 3451-3454, 1971.

[8] Pointon, A. J. and Saull, R. C., "Solid-state reactions in lithium ferrites," Journal of the American Ceramic Society, Vol-52, pp 157-160, 1969.

[9] Ridgley, D. H., Lessoff, H., and Childress, J. D., "Effects of lithium and oxygen losses on magnetic and crystallographic properties of spinel lithium ferrite," Journal of the American Ceramic Society, Vol-53, pp. 304 – 311, 1970.

[10] Argentina, G. M., and Baba, P.D., "Microwave Lithium Ferrites: An Overview", IEEE Transactions on Microwave Theory and Techniques, Vol. MTT-22, No. 6, pp 652-658, 1974.

[11] Bhatu, S S., Effect of nickel substitution on structural, infrared and elastic properties of lithium ferrite, Indian Journal of Pure & Applied Physics Vol- 45, pp 596-608, 2007.

[12] Soibam, Ibetombi, Phanjoubam, Sumitra, Prakash,, Chandra, "Mössbauer and magnetic studies of nickel substituted lithium zinc ferrites", Journal of Magnetism and Magnetic Materials, Vol. 321, pp. 2779-2782, 2009.

[13] Soibam, Ibetombi, Phanjoubam, Sumitra, Prakash, Chandra, "Mössbauer and magnetic studies of cobalt substituted lithium zinc ferrites prepared by citrate precursor method", Journal of Alloy and Compounds, Vol. 475, pp. 328–331, 2009.

[14] Widatallah, H. M., Johnson,C.,Gismelseed,A. M., Al-Omari, I.A.,Stewart S. J., Al-Harthi , S.H., Thomas, S. and Sitepu, H., "Structural and magnetic studies of nanocrystalline Mg-doped $Li_{0.5}Fe_{2.5}O_4$ particles prepared by mechanical milling" , Journal of Physics D: Applied Physics, Vol. 41, pp.165006(1) -165006(10), 2008.

[15] Tasaki, J. and Ito, T., "Effect of Sintering Atmosphere on the permeability of Sintered Ferrites.", Ferrites: proceedings of the International. Conference on Ferrites, Japan, pp.84-86, 1970.

[16] Nakamura,T., "Low-temperature sintering of Ni-Zn-Cu ferrite and its permeability spectra," Journal of Magnetism and Magnetic Materials,, Vol-168, pp.285-291, 1997.

[17] Roess, E., "Ferrites", University of Tokyo Press, Tokyo, p.187, 1971.

[18] Leung, L. K., Evans, B. J. and Morrish, A. H., "Low-temperature Mössbauer study of a nickel-zinc ferrite: $Zn_{1-x}Ni_xFe_2O_4$," Physics Review B, Vol-**8**, p.29-43,1973.

[19] Rezlescu,N., Rezlescu, E., Pasnicu, C. and Craus, M. L., "Effects of the rare-earth ions on some properties of a Nickel-Zinc ferrite," Journal of Physics: Condensed Matter, Vol-**6**,pp. 5707-5716,1994.

[20] E. Rezlescu, L. Sachelarie, P. D. Popa and N. Rezlescu, "Effect of substitution of diavalent ions on the electrical and magnetic properties of Ni-Zn-Me ferrites," IEEE Transactions on Magnetics, Vol- 36, pp. 3962-3967, 2000.

[21] Globus, A., "2nd EFS Conf. on Soft Magnetic Material.", Wolfson Center for Magnetic Technology, Cardiff, Wales, 1975.

**pdfMachine**
**A pdf writer that produces quality PDF files with ease!**
Produce quality PDF files in seconds and preserve the integrity of your original documents. Compatible across nearly all Windows platforms, simply open the document you want to convert, click "print", select the "Broadgun pdfMachine printer" and that's it! Get yours now!

[22] El-Shabasy,M., "DC electrical properties of Ni-Zn ferrites," Journal of Magnetism and Magnetic Materials,Vol-172, pp. 188-192, 1997.

[23] Wahab, M. A., "Solid State Physics-Structure and properties of materials", Narosa publishing house, New Delhi, 1999

[24] Chikazumi ,S., "Physics of Magnetism", John Wiley & Sons, Inc., New York, 1966.

[25] Brailsford,F., "Physical Principles of Magnetism", D. Van Nostrand Company Ltd., London, 1966.

[26] Dekker, A. J., "Solid State Physics", Macmillan India Ltd., New Delhi, 1998.

[27] Cullity, B. D., "Introduction to Magnetic Materials", Addison-Wiley Publishing Company, Inc., California, 1972.

[28] Goldman, Alex, "Modern Ferrite Technology", 2nd Ed, Springer Science-Business Media, Inc, Pittsburgh, PA, USA, 2006.

[29] Smit, J. and Wijn, H. P. J. , "Ferrites", John Wiley and Sons, New York, p. l49,1959.

[30] Kittel,C., "Introduction to Solid State Physics", 7th edition, John Wiley & Sons, Inc., Singapore, 1996.

[31] Jadhav , S.A., "Magnetic properties of Zn-substituted Li-Cu ferrites", Journal of Magnetism and Magnetic Materials, Vol-224, pp 167- 172, 2001.

[32] Hossain, A. K. M. A., Seki, M., Kawai, T. and Tabata, H., "Colossal magnetoresistance in spinel type $Zn_{1-x}Ni_xFe_2O_4$," Journal of Applied Physics, Vol.96, pp.1273-1275, 2004.

[33] Yafet, Y. and Kittel, C.," Antiferromagnetic arrangements in ferrites", Physical Review, Vol.87, pp. 290-294, 1952.

[34] Hadfield ,D., "Permanent Magnets and Magnetism", John Wiley & Sons, Inc., New York, 1962.

[35] Sikder, S. S., "Temperature dependence of magnetization and induced magnetic anisotropy of some Fe, Co and Ni-based amorphous ribbons," Ph. D. Thesis, BUET, Bangladesh, 1999.

[36] Snoek , J. L., Physica , "Dispersion and absorption in magnetic ferrites at frequencies above one Mc/s", Vol-14,pp 207-217, 1948.

[37] Irvine , J.T.S., West, A.R. , Amano , E., Huanosta , A. & Valenzuela. R., "Characterisation of magnetic materials by impedance spectroscopy", Solid State Ionics ,Vol.40-41, pp 220-223, 1990.

[38] Globus, A. &Duplex ,P., "Separation of susceptibility mechanisms for ferrites of low anisotropy", IEEE Transactions on Magnetics, Vol-2, pp 441-445, 1966.

[39] Chickazumi S. and Charap, S.H., "Physics of Magnetism", Krieger Pub. Co., p.248, 1978.

[40] Alan H, Morrish, "The Physical Properties of Magnetism", John Wiley and Sons , 1966.

[41] Yan , M. F. and Johnson, D. W., "Impurity induced exaggerated grain growth in Mn-Zn ferrites," Journal of the American Ceramic Society, Vol-61,pp 342-349, 1978.

**pdfMachine**
**A pdf writer that produces quality PDF files with ease!**
Produce quality PDF files in seconds and preserve the integrity of your original documents. Compatible across nearly all Windows platforms, simply open the document you want to convert, click "print", select the "Broadgun pdfMachine printer" and that's it! Get yours now!

[42] Hastings , J. M. and Corliss L. M , "Neutron Diffraction Studies of Zinc Ferrite and Nickel Ferrite," Reviews of .Modern. Physics, Vol- 25, pp 114-119, 1953.

[43] Chen, Qi, Rondinone, Adam J., Chakoumakos, Bryan C., and Zhang, Z. John, "Synthesis of superparamagnetic $MgFe_2O_4$ nanoparticles by coprecipitationa", Journal of Magnetism and Magnetic Materials, Vol-194, pp 1-7, 1999.

**pdfMachine**
**A pdf writer that produces quality PDF files with ease!**
Produce quality PDF files in seconds and preserve the integrity of your original documents. Compatible across nearly all Windows platforms, simply open the document you want to convert, click "print", select the "Broadgun pdfMachine printer" and that's it! Get yours now!

# CHAPTER 4

## RESULTS AND DISCUSSION

The polycrystalline $Li_xMg_{0.4}Ni_{0.6-2x}Fe_{2+x}O_4$ ($x$=0.00, 0.05, 0.10, 0.15, 0.20, 0.25 and 0.30) ferrites are studied. All ferrite samples are sintered at temperatures of 1050, 1100, 1150 and 1200˚C for six hours in air. Structural and surface morphology are studied by X-ray diffraction and optical microscopy respectively. The magnetic properties of the ferrites are characterized with high frequency (300 *KHz*-110 *MHz*) complex permeability. DC Magnetizations of all samples are also studied. The electrical properties of the samples are also studied. The effects of varying Li substitution and sintering temperature on the complex permeability of these ferrites are discussed.

### 4.1 XRD analysis of the polycrystalline $Li_xMg_{0.4}Ni_{0.6-2x}Fe_{2+x}O_4$

Fig. 4.1 illustrates the X-ray diffraction (XRD) patterns of various $Li_xMg_{0.4}Ni_{0.6-2x}Fe_{2+x}O_4$ ferrites sintered at 1200˚C in air. The XRD analysis confirms the $Li_xMg_{0.4}Ni_{0.6-2x}Fe_{2+x}O_4$ ferrite samples have the single phase cubic spinel structure having no impurity peak is formed as all the peaks in pattern match well with characteristic reflections reported earlier [1]. The XRD peaks are well indexed to the crystal plane of spinel ferrite (220), (311), (400), (422), (511) and (440), respectively.

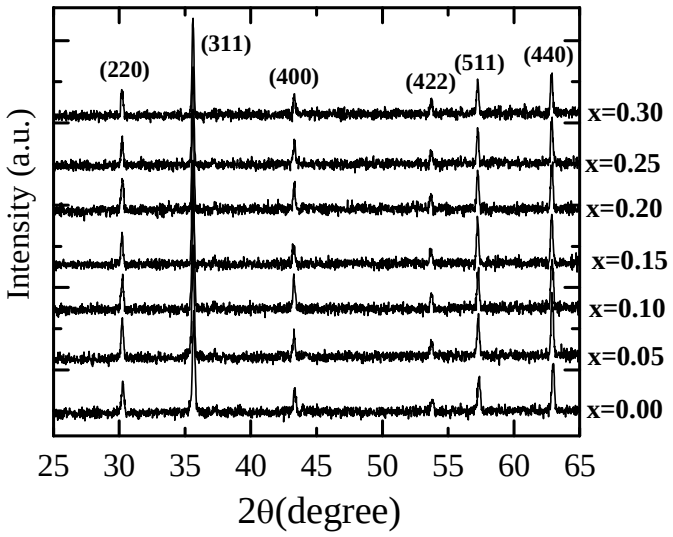


**Fig. 4.1.** The X-ray diffraction patterns $Li_xMg_{0.4}Ni_{0.6-2x}Fe_{2+x}O_4$ ferrites sintered at 1200˚C in air .


**pdfMachine**
**A pdf writer that produces quality PDF files with ease!**
Produce quality PDF files in seconds and preserve the integrity of your original documents. Compatible across nearly all Windows platforms, if you can print from a windows application you can use pdfMachine.
Get yours now!

## 4.2 Lattice Constants of the polycrystalline $Li_xMg_{0.4}Ni_{0.6-2x}Fe_{2+x}O_4$

The values of lattice parameters, *a*, obtained from each crystal plane are plotted against Nelson-Riley function F (θ) = ½ [$\cos^2\theta/\sin\theta + \cos^2\theta/\theta$] [2] where θ is the Bragg's angle and a straight line is obtained. The values of lattice parameters were estimated from the extrapolation of these lines to F(θ)=0 or (F(θ)=90˚C. From *a*-F(θ) curve, precise lattice constant, '$a_o$' is calculated for each sample. Fig. 4.2(a) shows *a*-F(θ) curve for $Li_{0.05}Mg_{0.40}Ni_{0.50}Fe_{2.05}O_4$ ferrite. Lattice constants of other samples are calculated in a similar way. The calculated lattice constants '$a_o$' of $Li_xMg_{0.4}Ni_{0.6-2x}Fe_{2+x}O_4$ ferrites are plotted as a function of *Li* content, as shown in Fig. 4.2(b). In the present case the lattice constant varies from 8.3549 Å for *Li*=0 to 8.3588 Å.

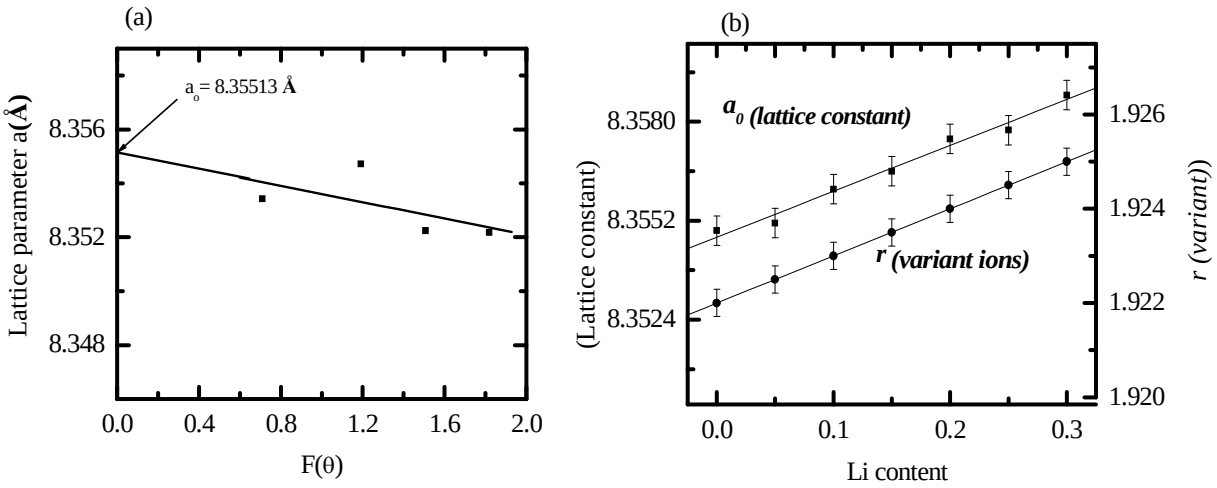


**Fig. 4.2.** (a) Variation of lattice parameter *a* with F(θ) and (b) Variation of the lattice constant $a_o$, and the mean ionic radius of the variant ion with the composition for $Li_xMg_{0.4}Ni_{0.6-2x}Fe_{2+x}O_4$ ferrites sintered at 1200˚C in air.

The lattice constant, density, porosity and average grain size for different samples sintered at different temperatures are given in Table 4.1.

It is clear from Fig. 4.2 (b) that the lattice constant of all the samples follows Vegard's law, as shown by solid line. This increase of lattice constant with *Li* contents can be explained on the basis of the ionic radii. The ionic radii of the cations used in $Li_xMg_{0.4}Ni_{0.6-2x}Fe_{2+x}O_4$ are 0.82Å ($Li^{1+}$), 0.77 Å ($Ni^{2+}$) and 0.73 Å ($Fe^{3+}$) [3]. Here $Ni^{2+}$ is substituting by the both $Li^{1+}$and $Fe^{3+}$ ion. So a small increase in lattice constant is expected, increasing *Li* content.

**pdfMachine**
**A pdf writer that produces quality PDF files with ease!**
Produce quality PDF files in seconds and preserve the integrity of your original documents. Compatible across nearly all Windows platforms, if you can print from a windows application you can use pdfMachine.
Get yours now!

**Table 4.1**. The lattice constant, density, porosity, grain size, natural resonance frequency, maximum Quality factor and initial permeability of the various $Li_xMg_{0.4}Ni_{0.6-2x}Fe_{2+x}O_4$ ferrites sintered at various temperatures with fixed dwell time 6h.

| $x$ | $T_s$ (°C) | $a_o$ (Å) | $\rho_{x\text{-}ray}$ ($g/cm^3$) | $\rho_B$ ($g/cm^3$) | $P$ (%) | Grain size ($\mu m$) | $f_r$ (MHz) | $Q_{max}$ | $\mu_i'$ (at 300 kHz) |
|---|---|---|---|---|---|---|---|---|---|
| 0 | 1050 | 8.3549 | 5.02 | 4.42 | 12.09 | □ | – | 1530 | 29.41 |
| | 1100 | | | 4.46 | 11.25 | 1.31 | □ | 1605 | 29.93 |
| | 1150 | | | 4.48 | 10.84 | 1.72 | 54.89 | 2442 | 46.10 |
| | 1200 | | | 4.49 | 10.64 | 2.5 | 54.87 | 2440 | 49.29 |
| 0.05 | 1050 | 8.35513 | 4.96 | 4.33 | 12.65 | □ | □ | 1872 | 36.80 |
| | 1100 | | | 4.37 | 11.91 | 1.67 | 58.82 | 2287 | 42.67 |
| | 1150 | | | 4.38 | 11.53 | 1.91 | 44.54 | 2591 | 48.40 |
| | 1200 | | | 4.39 | 11.02 | 2.63 | 27.37 | 2616 | 55.08 |
| 0.1 | 1050 | 8.3561 | 4.90 | 4.23 | 13.76 | □ | 54.86 | 2237 | 40.93 |
| | 1100 | | | 4.24 | 13.47 | 1.81 | 51.18 | 2652 | 51.08 |
| | 1150 | | | 4.22 | 13.84 | 3.44 | 36.15 | 2616 | 50.22 |
| | 1200 | | | 4.21 | 13.93 | 4.04 | 27.37 | 2644 | 59.62 |
| 0.15 | 1050 | 8.3566 | 4.86 | 4.18 | 13.95 | □ | 54.87 | 2350 | 43.81 |
| | 1100 | | | 4.18 | 13.95 | 2.76 | 38.14 | 3356 | 59.02 |
| | 1150 | | | 4.17 | 14.16 | 3.97 | 27.37 | 2731 | 52.29 |
| | 1200 | | | 4.16 | 14.36 | 6.56 | 20.72 | 2761 | 61.26 |
| 0.20 | 1050 | 8.3575 | 4.77 | 4.10 | 14.07 | □ | 47.74 | 3181 | 54.53 |
| | 1100 | | | 4.103 | 14.00 | 2.80 | 36.15 | 4222 | 64.12 |
| | 1150 | | | 4.08 | 14.49 | 5 | 25.53 | 2966 | 55.67 |
| | 1200 | | | 4.07 | 14.7 | 6.61 | 19.33 | 2998 | 62.82 |
| 0.25 | 1050 | 8.3577 | 4.71 | 4.03 | 14.41 | □ | 41.54 | 3559 | 58.23 |
| | 1100 | | | 4.04 | 14.205 | 2.82 | 29.34 | 4653 | 69.10 |
| | 1150 | | | 4.02 | 14.63 | 5.56 | 22.21 | 3083 | 57.43 |
| | 1200 | | | 4.01 | 14.82 | 7.56 | 14.64 | 3117 | 66.98 |
| 0.3 | 1050 | 8.3588 | 4.64 | 3.97 | 14.53 | □ | 41.54 | 2794 | 49.15 |
| | 1100 | | | 3.98 | 14.31 | 4.31 | 25.53 | 3535 | 62.21 |
| | 1150 | | | 3.95 | 14.96 | 6.46 | 20.72 | 2845 | 53.89 |
| | 1200 | | | 3.94 | 15.07 | 10.5 | 16.82 | 2881 | 61.87 |

**pdfMachine**
**A pdf writer that produces quality PDF files with ease!**
Produce quality PDF files in seconds and preserve the integrity of your original documents. Compatible across nearly all Windows platforms, if you can print from a windows application you can use pdfMachine.
Get yours now!

The samples under investigation have the chemical composition $Li_xMg_{0.4}Ni_{0.6-2x}Fe_{2+x}O_4$. Therefore, the mean ionic radius of the variant ions for composition $(Li_xMg_{0.4}Ni_{0.6-2x}Fe_{2+x}O_4)$ can be written as

$$r_{(variant)} = xr_{Li}+(0.6-2x)r_{Ni}+(2+x)r_{Fe} \quad (1)$$

where $r_{Li}$ is the radius of $Li^{1+}$ ion( = 0.82Å), $r_{Ni}$ is the ionic radius of $Ni^{2+}$ ion (=0.77 Å), and $r_{Fe}$ is the ionic radius of $Fe^{3+}$ ion (=0.73 Å). Data are from Whittaker and Muntus (1970) [3]. The variation of $r_{(variant)}$ with *Li* content is shown in Fig. 4.2 (b), where it increases with increasing *Li* content.

## 4.3 Density and porosity of the polycrystalline $Li_xMg_{0.4}Ni_{0.6-2x}Fe_{2+x}O_4$

Theoretical density, $\rho_{th}$, bulk density, $\rho_B$ and porosity of the various $Li_xMg_{0.4}Ni_{0.6-2x}Fe_{2+x}O_4$ ferrites are tabulated in the Table 4.1. Theoretical density, $\rho_{th}$ decreases with increasing $a_o$ in the *Li* substituted various $Li_xMg_{0.4}Ni_{0.6-2x}Fe_{2+x}O_4$ ferrites. It decreases because the molecular weight of the each sample decreases significantly with the addition $Li^+$ content. Both theoretical and bulk density decrease in a similar fashion with the increase of Li content in $Li_xMg_{0.4}Ni_{0.6-2x}Fe_{2+x}O_4$ ferrites for a fixed sintering temperature, as shown in Fig. 4.3.

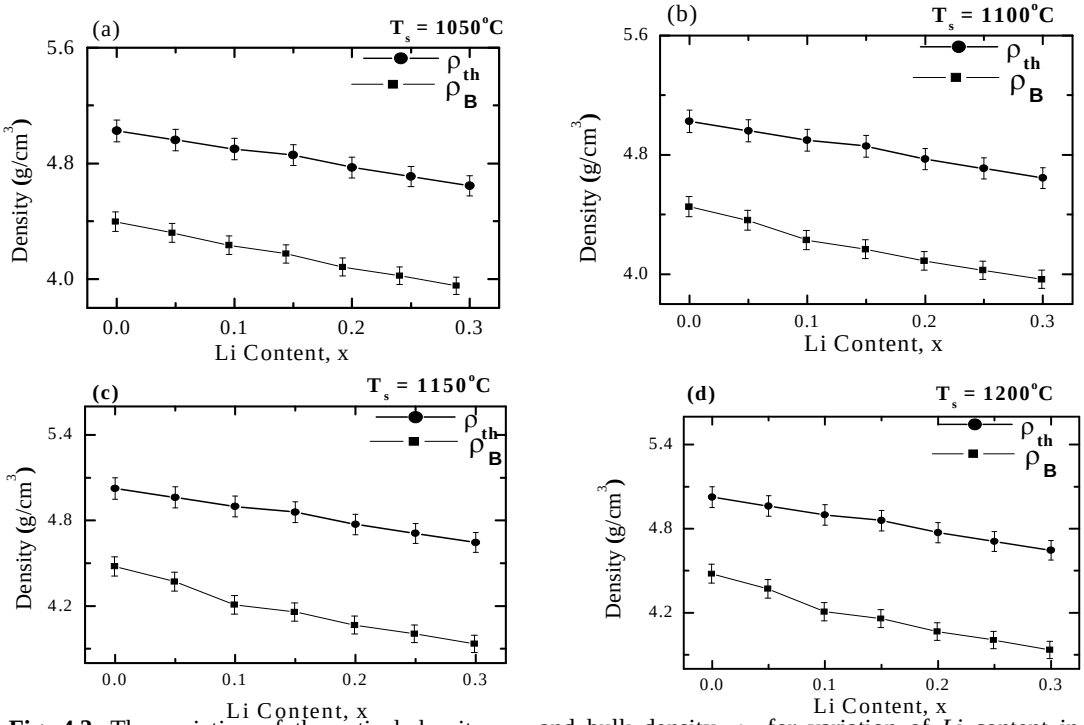


**Fig. 4.3.** The variation of theoretical density, $\rho_{th}$ and bulk density, $\rho_B$ for variation of *Li* content in $Li_xMg_{0.40}Ni_{0.6-2x}Fe_{2+x}O_4$ ferrites sintered at (a) 1050˚C, (b) 1100˚C, (c) 1150˚C, and (d) 1200˚C in air.

**pdfMachine**
**A pdf writer that produces quality PDF files with ease!**
Produce quality PDF files in seconds and preserve the integrity of your original documents. Compatible across nearly all Windows platforms, if you can print from a windows application you can use pdfMachine.
Get yours now!

Fig 4.4 indicates that as lithium content increases in $Li_xMg_{0.4}Ni_{0.6-2x}Fe_{2+x}O_4$ ferrites, density decreases and porosity increases. It is possible to explain this phenomenon in terms of the atomic weight. The atomic weight of *Ni* (58.6934 amu) is greater than atomic weight of the *Li* (6.941 amu) and *Fe* (55.845 amu) [4].

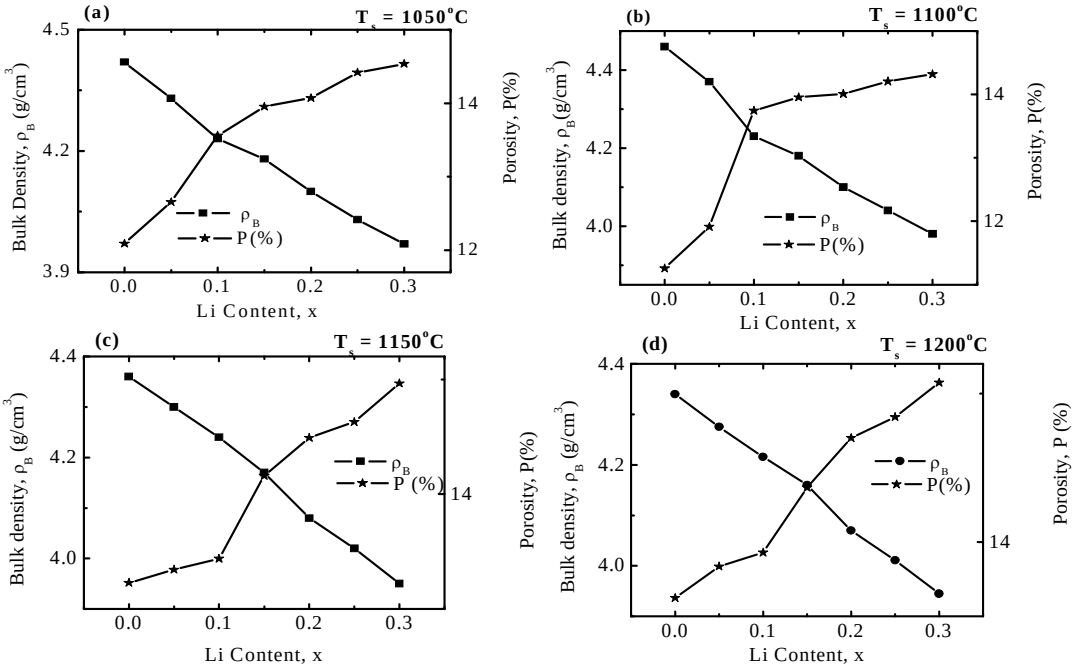


**Fig. 4.4.** The variation of density and porosity with *Li* content for $Li_xMg_{0.4}Ni_{0.6-2x}Fe_{2+x}O_4$sintered at (a) 1050˚C, (b) 1100˚C, (c) 1150˚C, and (d) 1200˚C in air

Fig.4.5 shows the variation of bulk density and porosity with the variation of sintering temperature for $Li_xMg_{0.4}Ni_{0.6-2x}Fe_{2+x}O_4$ ferrites. It is observed that the density increased with increasing sintering temperature for the contents x=0 and x=0.05 in. $Li_xMg_{0.4}Ni_{0.6-2x}Fe_{2+x}O_4$ ferrites On the other hand, porosity (P) of the sample decreased with increasing sintering temperature. During the sintering process, the thermal energy generates a force that drives the grain boundaries to grow over pores, thereby decreasing the pore volume and increasing the density of the materials. Beyond $x$=0.05 in $Li_xMg_{0.4}Ni_{0.6-2x}Fe_{2+x}O_4$ ferrites, it is found that density increases with increasing sintering temperature up to 1100˚C, then decreases. On the other hand, porosity (P) of the samples decreases with increasing sintering temperature up to 1100˚C and a increasing trend is shown beyond it.

**pdfMachine**
**A pdf writer that produces quality PDF files with ease!**
Produce quality PDF files in seconds and preserve the integrity of your original documents. Compatible across nearly all Windows platforms, if you can print from a windows application you can use pdfMachine.
Get yours now!

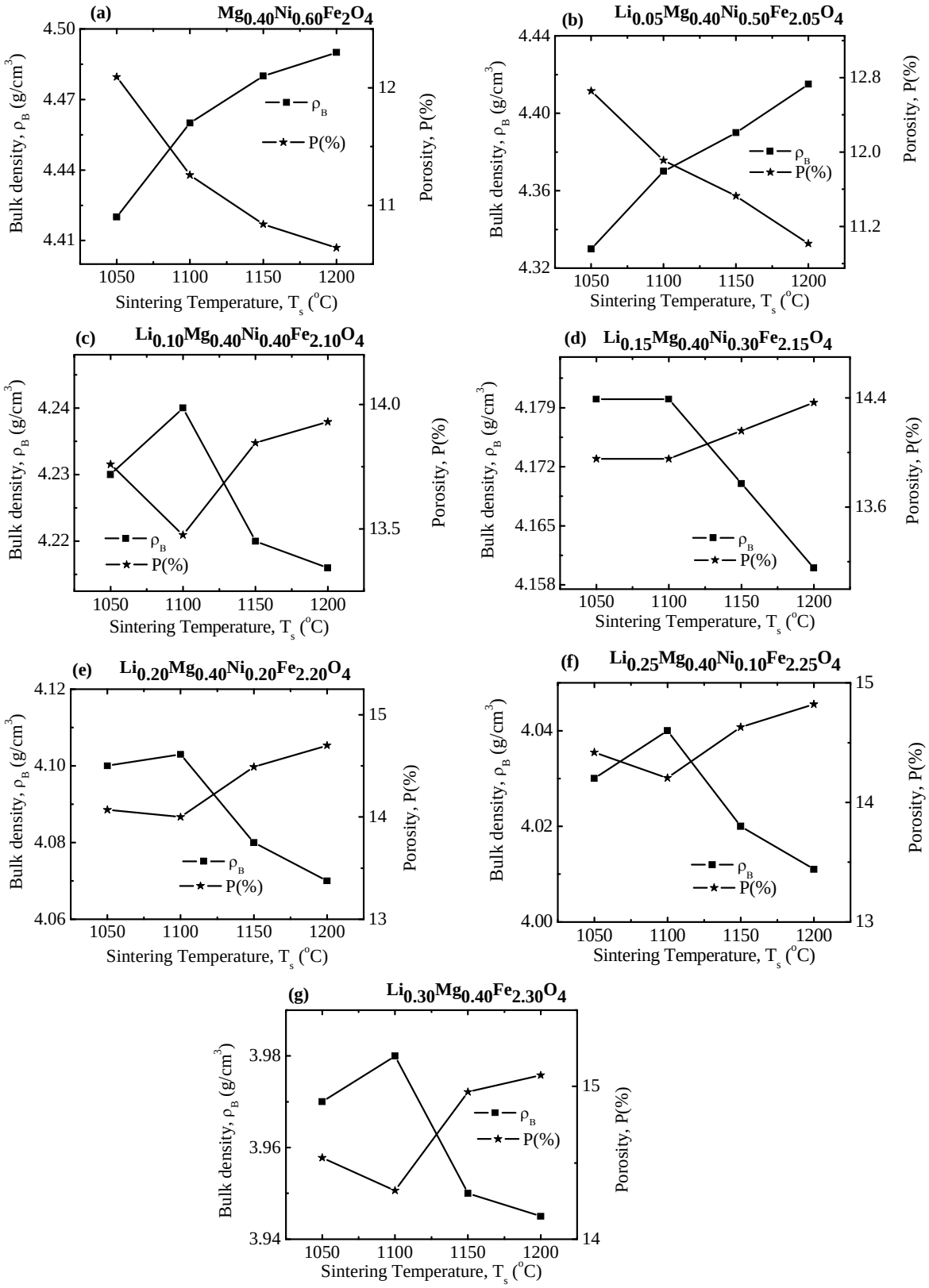


**Fig. 4.5.** The variation of density and porosity for (a) $Mg_{0.40}Ni_{0.60}Fe_2O_4$, (b) $Li_{0.05}Mg_{0.40}Ni_{0.50}Fe_{2.05}O_4$ (c) $Li_{0.10}Mg_{0.40}Ni_{0.40}Fe_{2.10}O_4$, (d) $Li_{0.15}Mg_{0.40}Ni_{0.30}Fe_{2.15}O_4$ (e) $Li_{0.20}Mg_{0.40}Ni_{0.20}Fe_{2.20}O_4$, (f) $Li_{0.25}Mg_{0.40}Ni_{0.10}Fe_{2.25}O_4$ *and* (g) $Li_{0.30}Mg_{0.40}Fe_{2.30}O_4$ ferrites

**pdfMachine**
**A pdf writer that produces quality PDF files with ease!**
Produce quality PDF files in seconds and preserve the integrity of your original documents. Compatible across nearly all Windows platforms, if you can print from a windows application you can use pdfMachine.
Get yours now!

At higher sintering temperature density is decreased because the intragranular porosity is increased because of discontinuous grain growth. It is known that the porosity of the ceramic samples results from two sources, intragranular porosity and intergranular porosity. When the grain growth rate is very high, pores may be left behind by rapidly moving grain boundaries, resulting in pores that are trapped inside the grains. This intragranular porosity leads to poor magnetic and mechanical properties. Thus the total porosity could be written as $P=P_{intra}+P_{inter}$. The intergranular porosity mainly depends on the grain size [5].

## 4.4 Microstructures of $Li_xMg_{0.4}Ni_{0.6-2x}Fe_{2+x}O_4$

The optical micrographs for the samples *Li*=0 to *Li*=0.3, in steps of 0.05 are shown in Fig.4.6. Strong dependence in average grain diameter varying *Li*-content is observed. The average grain size of various $Li_xMg_{0.4}Ni_{0.6-2x}Fe_{2+x}O_4$ ferrites with the variation of sintering temperatures 1100˚C, 1150˚C and 1200˚C, is listed in Table 4.1. No significant micrograph was observed for the samples sintered at 1050˚C. Variation of *Li* content shows a strong dependence in grain size. Fig.4.6(a), 4.6(b), 4.6(c) show the variation of average grain diameter with *Li* content sintered at 1100, 1150 and 1200˚C. It is clear from the Fig. 4.6 that average grain diameter goes on increasing with the *Li* content. This is probably due to the very lower melting temperature of *Li* (180.54˚C) compared to *Ni* (1453˚C), though *Fe* content (1535˚C) increases as *Li* content increases. It is also observed that average grain size of all samples increases with the increase of sintering temperature. Figure shows the influence of sintering temperature in $Li_{0.25}Mg_{0.40}Ni_{0.10}Fe_{2.25}O_4$ ferrite. Similar enlargement of grain size varying sintering temperature is observed for other samples. This complies with previously reported works [6].

**pdfMachine**
**A pdf writer that produces quality PDF files with ease!**
Produce quality PDF files in seconds and preserve the integrity of your original documents. Compatible across nearly all Windows platforms, if you can print from a windows application you can use pdfMachine.
Get yours now!

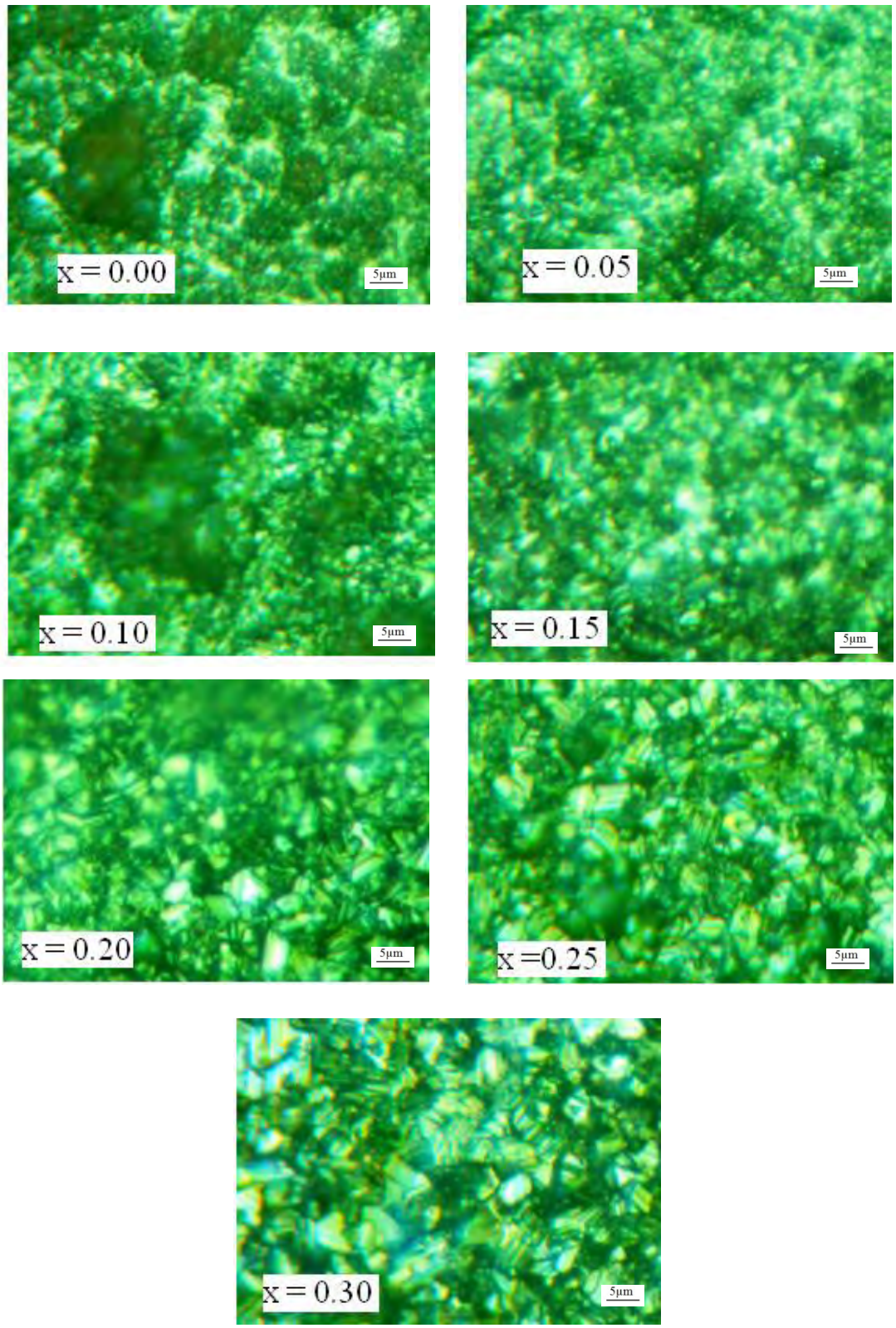


**Fig. 4.6. (a)** The optical micrographs for polycrystalline $Li_xMg_{0.4}Ni_{0.6-2x}Fe_{2+x}O_4$ ferrites sintered at 1100˚C in air.

**pdfMachine**
**A pdf writer that produces quality PDF files with ease!**
Produce quality PDF files in seconds and preserve the integrity of your original documents. Compatible across nearly all Windows platforms, if you can print from a windows application you can use pdfMachine.
Get yours now!

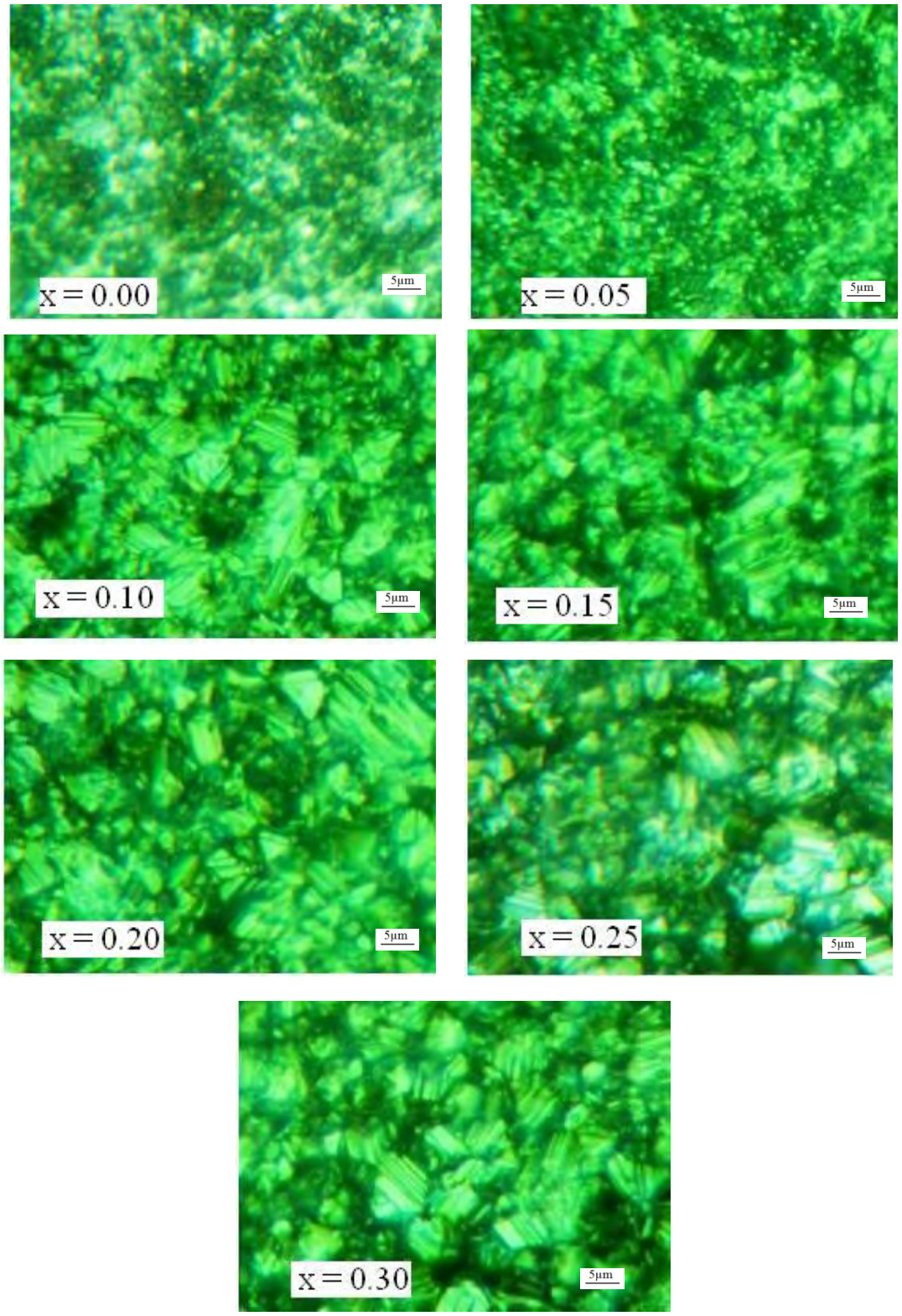


**Fig. 4.6. (b)** The optical micrographs for polycrystalline $Li_xMg_{0.4}Ni_{0.6-2x}Fe_{2+x}O_4$ ferrites sintered at 1150ºC in air.

**pdfMachine**
**A pdf writer that produces quality PDF files with ease!**
Produce quality PDF files in seconds and preserve the integrity of your original documents. Compatible across nearly all Windows platforms, if you can print from a windows application you can use pdfMachine.
Get yours now!

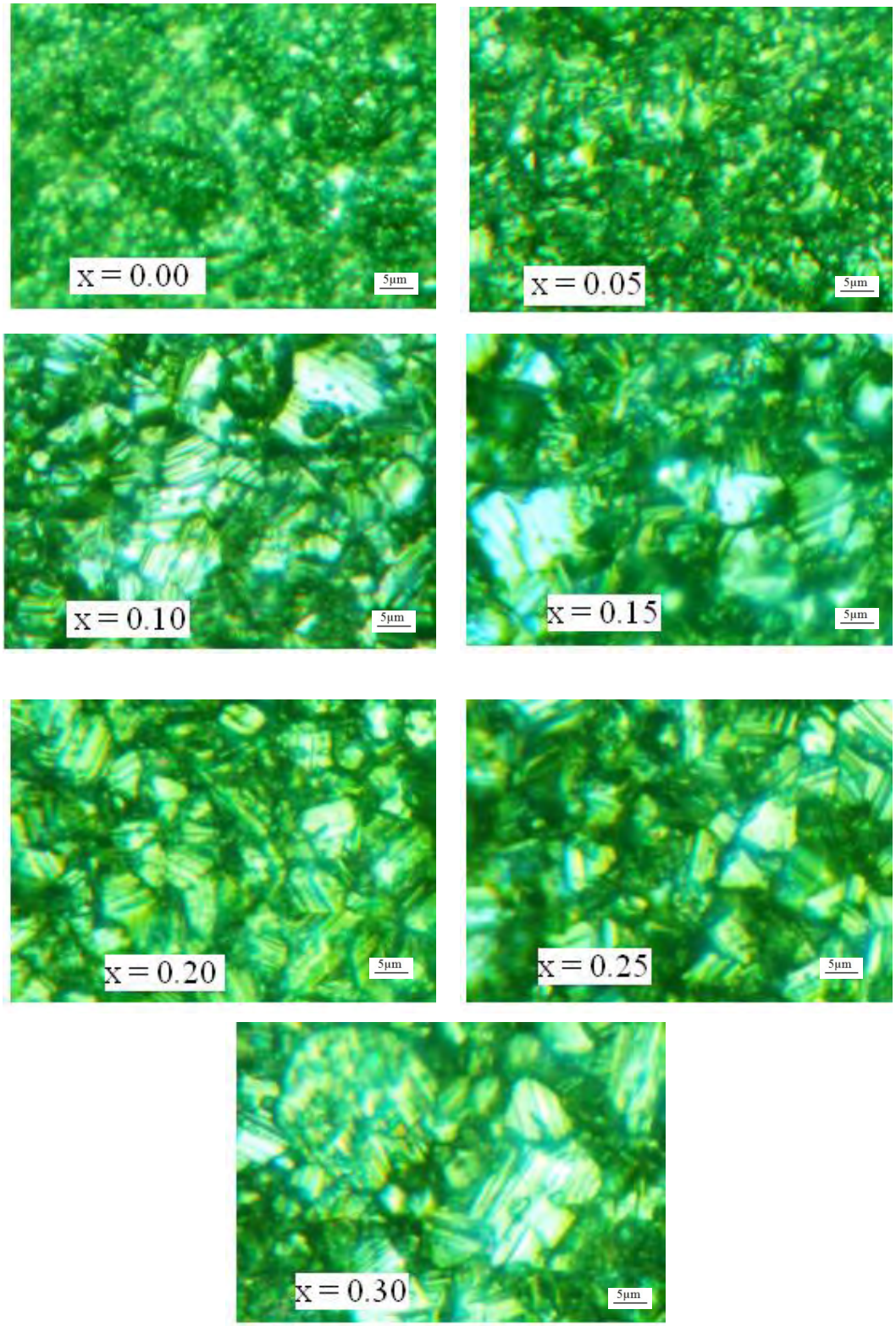


**Fig. 4.6. (c)** The optical micrographs for polycrystalline $Li_xMg_{0.4}Ni_{0.6-2x}Fe_{2+x}O_4$ ferrites sintered at 1200ºC in air.

**pdfMachine**
**A pdf writer that produces quality PDF files with ease!**
Produce quality PDF files in seconds and preserve the integrity of your original documents. Compatible across nearly all Windows platforms, if you can print from a windows application you can use pdfMachine.
Get yours now!

## 4.5 Complex permeability of the polycrystalline $Li_xMg_{0.4}Ni_{0.6-2x}Fe_{2+x}O_4$

The initial permeability ($\mu_i$) has been measured for all the ferrites in the frequency range of 300 *kHz*-110 *MHz*. Fig. 4.7 shows the complex permeability spectra for $Li_xMg_{0.4}Ni_{0.6-2x}Fe_{2+x}O_4$ ferrites sintered at 1050, 1100, 1150 and 1200˚C respectively.

The real ( $\mu_i^{/}$ ) and imaginary ( $\mu_i^{//}$ ) permeability increase with *Li* substitution up to *x*=0.25 in $Li_xMg_{0.4}Ni_{0.6-2x}Fe_{2+x}O_4$ ferrites and after that permeability decrease. The $\mu_i^{/}$ values increase with the increase of sintering temperature up to 1100˚C and above 1100˚C a decreasing trend is observed. In contrast resonance frequency is found to decrease with *Li* substitution. All samples show independence of frequency in their $\mu_i^{/}$ values up to the resonance frequency. Moreover, a sharp decrease in $\mu_i^{/}$ and increase in $\mu_i^{//}$ above the resonance frequency is noticed.

A variation of $\mu_i^{/}$ values the sintering temperatures for all compositions is observed. As $\mu_i^{/}$ increases, corresponding resonance frequency, $f_r$ decreases. For all compositions, $f_r$ value [7] shifted to a lower value as sintering temperature increases, which is found from Table-4.1. No resonance frequency is observed at 1050˚C and 1100˚C for $Mg_{0.40}Ni_{0.60}Fe_2O_4$ ferrite and at 1150˚C and 1200˚C $f_r$ values are 54.89 *MHz* and 54.87 *MHz* respectively. As sintering temperature increases from 1100˚C to 1200˚C, $f_r$ value for $Li_{0.05}Mg_{0.40}Ni_{0.50}Fe_{2.05}O_4$ ferrite decreases from 58.82 *MHz* to 27.37 *MHz* while no resonance frequency is observed at 1050˚C. Again $f_r$ value decreases from 54.86 *MHz* to 27.37 *MHz* for $Li_{0.10}Mg_{0.40}Ni_{0.40}Fe_{2.10}O_4$ ferrite, from 54.87 *MHz* to 20.72 *MHz* for $Li_{0.15}Mg_{0.40}Ni_{0.30}Fe_{2.15}O_4$ ferrite, from 47.74 *MHz* to 19.33 *MHz* for $Li_{0.20}Mg_{0.40}Ni_{0.20}Fe_{2.20}O_4$ ferrite, from 41.54 *MHz* to 14.64 *MHz* for $Li_{0.25}Mg_{0.40}Ni_{0.10}Fe_{2.25}O_4$ ferrite and from 41.54 *MHz* to 16.82 *MHz* for $Li_{0.30}Mg_{0.40}Fe_{2.30}O_4$ ferrite as sintering temperature increases from 1050˚C to 1200˚C. It is clearly noticeable that the maximum initial permeability $\mu_i^{/}$ of $Li_xMg_{0.4}Ni_{0.6-2x}Fe_{2+x}O_4$ ferrites are obtained at the 1100˚C and at higher sintering temperature a decreasing trend is observed.

**pdfMachine**
**A pdf writer that produces quality PDF files with ease!**
Produce quality PDF files in seconds and preserve the integrity of your original documents. Compatible across nearly all Windows platforms, if you can print from a windows application you can use pdfMachine.
Get yours now!

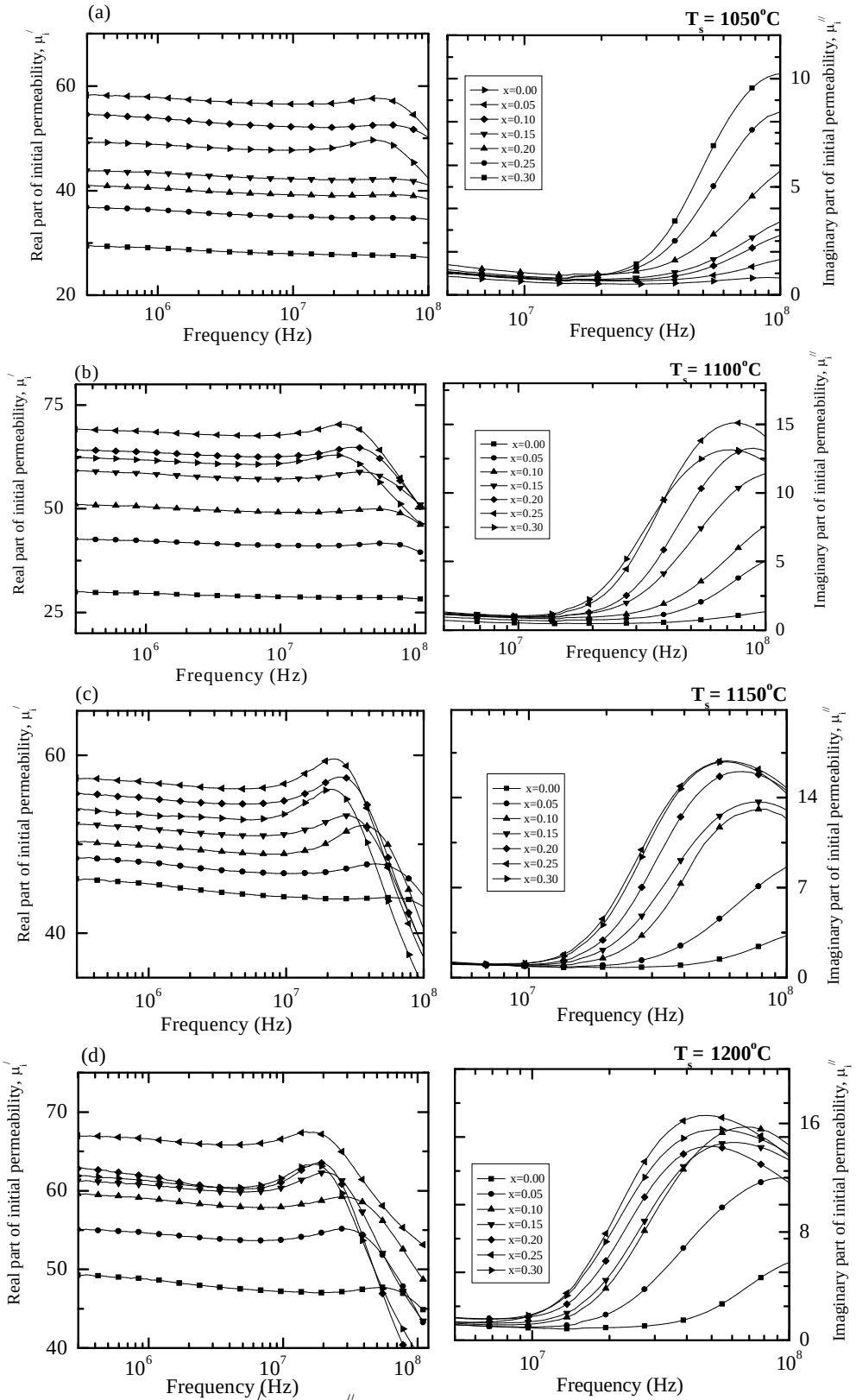


**Fig. 4.7.** The variation of $\mu_i^{/}$ and $\mu_i^{//}$ spectra for $Li_xMg_{0.4}Ni_{0.6-2x}Fe_{2+x}O_4$ sintered at (a) 1050˚C, (b)1100˚C, (c) 1150˚C and (d) 1200˚C in air.

**pdfMachine**
**A pdf writer that produces quality PDF files with ease!**
Produce quality PDF files in seconds and preserve the integrity of your original documents. Compatible across nearly all Windows platforms, if you can print from a windows application you can use pdfMachine.
Get yours now!

The resonance frequency and the room temperature $\mu_i'$ values measured at 300 *kHz* are listed in Table 4.1. Highest value of $\mu_i'$ ($\mu_i'$=69.10) is observed for $Li_{0.25}Mg_{0.40}Ni_{0.10}Fe_{2.25}O_4$ ferrite sintered at 1100˚C. On the other hand, maximum value of $f_r$ (58.82 *MHz*) is observed for $Li_{0.05}Mg_{0.40}Ni_{0.50}Fe_{2.05}O_4$ ferrite sintered at 1100˚C with the corresponding value of $\mu_i'$=42.67. Fig 4.8 shows the variation of $\mu_i'$ (at 300 *kHz*) and $f_r$ with *Li* content for $Li_xMg_{0.4}Ni_{0.6-2x}Fe_{2+x}O_4$ ferrites sintered at 1050, 1100, 1150 and 1200˚C in air. In this figure it is found that as $\mu_i'$ increases resonance frequency decreases with the function of sintering temperature. An inversely proportional relation of $\mu_i'$ and $f_r$ confirms the Snoek's limit [8].Similar trend is observed for all other sintering temperatures.

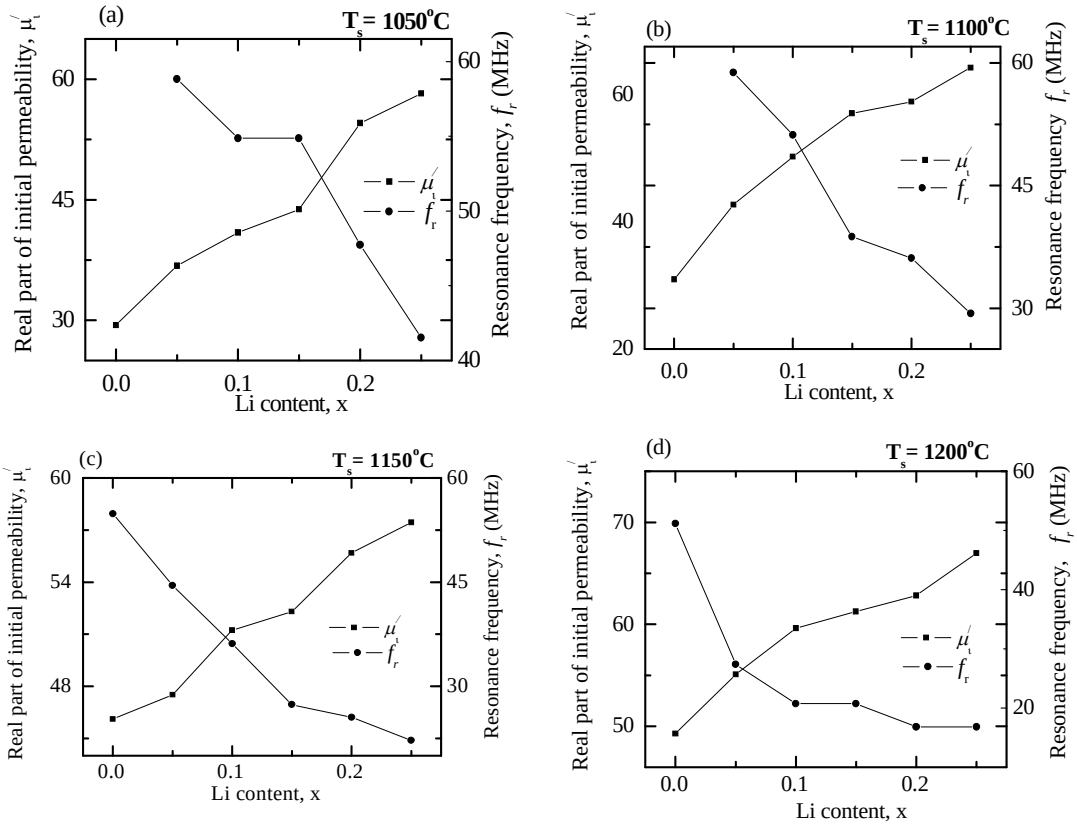


**Fig 4.8.** The variation of $\mu_i'$ (at 300kHz) and $f_r$ with Lithium content for $Li_xMg_{0.4}Ni_{0.6-2x}Fe_{2+x}O_4$ ferrites sintered at (a) 1050˚C,(b) 1100˚C, (c)1150˚C and (d) 1200˚C in air.

**pdfMachine**
**A pdf writer that produces quality PDF files with ease!**
Produce quality PDF files in seconds and preserve the integrity of your original documents. Compatible across nearly all Windows platforms, if you can print from a windows application you can use pdfMachine.
Get yours now!

The whole permeability phenomena can be explained as below .The permeability of polycrystalline ferrite is related to two different magnetizing mechanisms: spin rotation and domain wall motion [6, 9-10], which can be described as follows: $\mu_i=1+\chi_w+\chi_{spin}$ where $\chi_w$ is the domain wall susceptibility; $\chi_{spin}$ is intrinsic rotational susceptibility. $\chi_w$ and $\chi_{spin}$ may be written as : $\chi_w = 3\pi M_s^2 D/4\gamma$ and $\chi_{spin} = 2\pi M_s^2/K$ with $M_s$ saturation magnetization, $K$ the total anisotropy, D the average grain diameter, and γ the domain wall energy. In the present system room temperature *DC* magnetization value varying to *Li* content increases up to $x$= 0.25 and start to decrease at $x$=0.30. Since $\mu_i'$ is a function of magnetization therefore, $\mu_i'$ increases with the increase of *Li* content up to $x$=0.25 and beyond $x$=0.25, $\mu_i'$ decreases due to the non collinear spin arrangements [11]. Moreover, the magnetic properties of soft ferrite are strongly influenced by it□s composition, additives and microstructures of the material. Among all these factors, the microstructures have great influence on magnetic properties. It is generally believed that larger the grain sizes, the higher the saturation magnetization and initial permeability .In microstructure studies of the present ferrite system, is also observed that average grain diameter increases with the function of *Li* content up to the same optimum, $x$=0.25 and sudden decrease is observed beyond it. Therefore in the present case, variation of the initial permeability is strongly influenced by it□s grain size and *DC* magnetization property.

The increasing value of $\mu_i'$ with the increase of sintering temperature up to the 1100˚C is due to the lower porosity for samples sintered at higher sintering temperature. The porosity causes hindrance to the domain wall motion. As sintering temperature increases pores and voids are reduced with increasing sintering temperature. The value of $\mu_i'$ decreases above 1100˚C because the sample heated at higher sintering temperatures (above optimum $T_s$) contains increasing number of pores within the grains which results a decrease in permeability. Similar trend was observed by Guillaud [12]

The variation of initial permeability $\mu_i$, with frequency, shown in Fig. 4.7 can be explained on the basis of Globus model. According to this model, the relaxation character is

$$(\mu_i - 1)^2 f_r = \text{constant.} \qquad (2)$$

**pdfMachine**
**A pdf writer that produces quality PDF files with ease!**
Produce quality PDF files in seconds and preserve the integrity of your original documents. Compatible across nearly all Windows platforms, if you can print from a windows application you can use pdfMachine.
Get yours now!

Initial permeability in ferrites is due to domain wall displacement and remains constant with frequency as long as there is no phase lag between the applied field and the applied field and the domain wall displacement. In ferrites, two resonance peaks are normally observed: one at lower frequency (10-100*MHz*) which is due to the domain wall oscillations [13, 14] and the other at higher frequencies (~1*GHz*) due to Larmour precession of electron spins [15]. In the present case, the resonance frequency of domain wall oscillations is found in the range of 15*MHz*~60*MHz*.

The variation of loss factor, $tan\delta(=\mu_i^{//}/\mu_i^{/})$ with frequency for all samples has been studied. Fig.4.9 shows the variations of loss factors with frequency for $Li_xMg_{0.4}Ni_{0.6-2x}Fe_{2+x}O_4$ ferrites sintered at 1050, 1100, 1150 and 1200˚C.

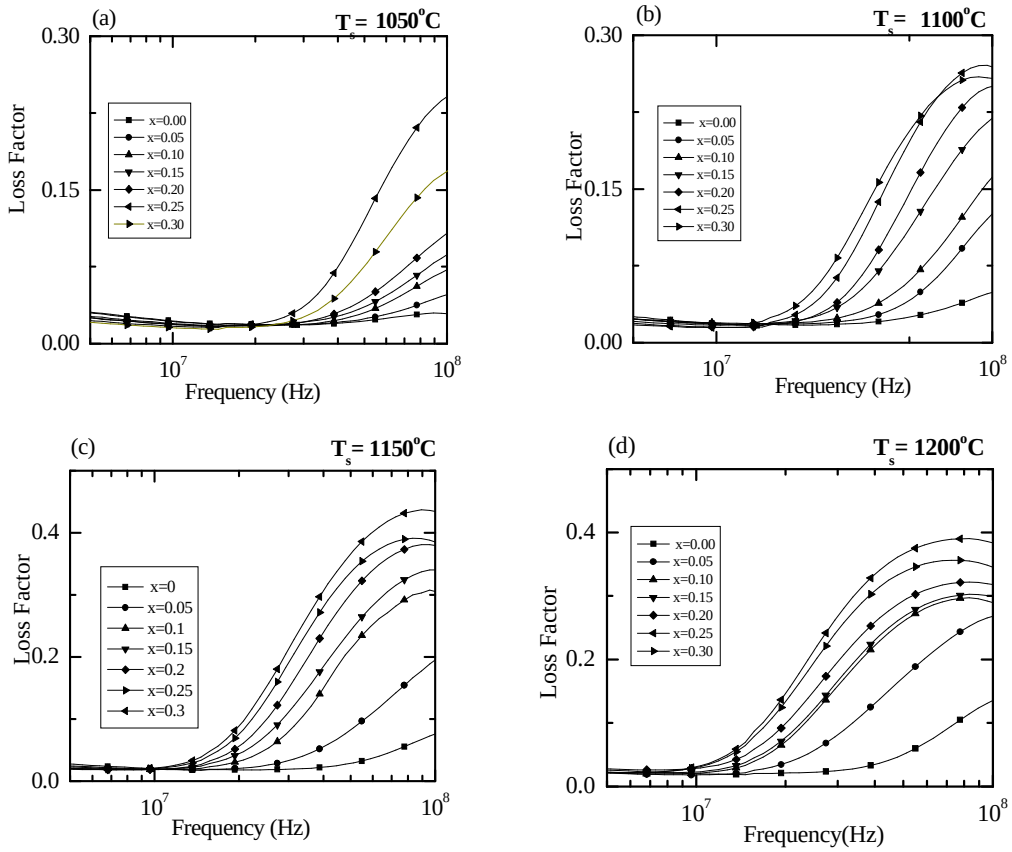


**Fig. 4.9.** The variations of Loss factor with frequency for $Li_xMg_{0.4}Ni_{0.6-2x}Fe_{2+x}O_4$ ferrites sintered at (a)1050˚C, (b)1100˚C,(c) 1150˚C and (d) 1200˚C in air.

The loss obtained in the present ferrite system is of the order of $10^{-2}$ □$10^{-3}$ in the frequency range of 300 *kHz* □110 *MHz* At lower frequencies a dispersion in magnetic

**pdfMachine**
**A pdf writer that produces quality PDF files with ease!**
Produce quality PDF files in seconds and preserve the integrity of your original documents. Compatible across nearly all Windows platforms, if you can print from a windows application you can use pdfMachine.
Get yours now!

loss is observed and remains constant up to certain a frequency, 13*MHz* □22 *MHz*; this frequency limit depends upon the sintering temperatures. The lag of domain wall motion with respect to the applied magnetic field is responsible for magnetic loss and this is accredited to lattice imperfections [15].

At higher frequencies, a rapid increase in loss factor is observed. A resonance loss peak is shown in this rapid increase of magnetic loss. At the resonance, maximum energy transfer occurs from the applied field to the lattice which results the rapid increases in loss factor. As it is observed that phase lag between domain rotation and applied field is greater than that between applied field and domain wall displacement, the magnetic losses due to domain rotation overrides those due to domain wall displacement [16].

The loss factor is also observed to increase with the increase of sintering temperature. The variation of initial loss with frequency for the sample $x$=0.25, i.e. $Li_{0.25}Mg_{0.4}Ni_{0.2}Fe_{2.25}O_4$ ferrite in the sintering temperature range 1050˚C □1200˚C is shown in Fig. 4.10. The increase in sintering temperature results in increased Li loss in the samples, thereby creating defects in the lattice, which gives rise to magnetic loss.

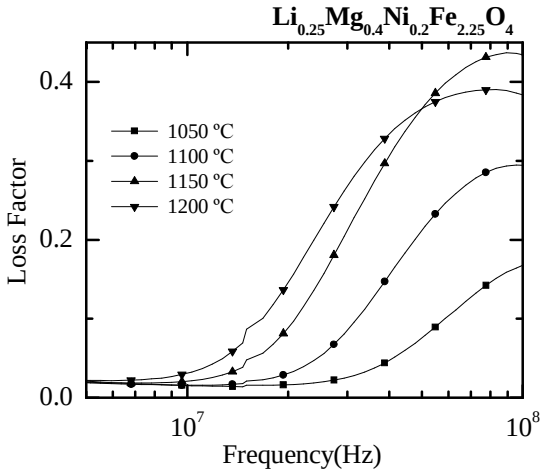


**Fig. 4.10.** The variations of Loss factor with frequency for $Li_{0.25}Mg_{0.4}Ni_{0.20}Fe_{2.25}O_4$ ferrite sintered at 1050, 1100, 1150 and 1200˚C in air.

From the loss factor, the relative quality factor (or *Q-factor*) is calculated. The relative quality factor (*Q-factor*) versus frequency plots of all the samples sintered at 1050, 1100, 1150 and 1200˚C are shown in Fig. 4.11. Calculated *Q-factor*s for various $Li_xMg_{0.4}Ni_{0.6-2x}Fe_{2+x}O_4$ ferrites sintered at various temperatures are listed in Table 4.1. It

**pdfMachine**
**A pdf writer that produces quality PDF files with ease!**
Produce quality PDF files in seconds and preserve the integrity of your original documents. Compatible across nearly all Windows platforms, if you can print from a windows application you can use pdfMachine.
Get yours now!

can be seen that the value of *Q*-factor increases with an increase of frequency and shows a peak around 10*MHz*. It is also observed from the Fig 4.12 (a) that the maximum value of *Q-factor*, $Q_{max}$ increases with increasing Li contents from $x$=0 to $x$=0.25 in $Li_xMg_{0.4}Ni_{0.6-2x}Fe_{2+x}O_4$, then it decreases at $x$=0.3, for the samples sintered at 1100˚C. Similar variation is observed for $Li_xMg_{0.4}Ni_{0.6-2x}Fe_{2+x}O_4$ ferrites sintered at other temperatures as well. It shows a similar trend of $\mu_i^{/}$ of the present system as it is proportional to the *Q*-factor from the relation: $Q = \mu_i^{/} / tan\delta$, as loss factor also shows an increasing trend with the increase of *Li* content. Among all the studied samples, highest value of *Q*-factor (=4653) is observed for $Li_{0.25}Mg_{0.40}Ni_{0.10}Fe_{2.25}O_4$ ferrite sintered at 1100˚C, similar to $\mu_i^{/}$. Fig 4.12 (b) shows the variation of *Q* value for $Li_{0.25}Mg_{0.40}Ni_{0.10}Fe_{2.25}O_4$ ferrite varying sintering temperature. Above 1100˚C, *Q-factor* is found to decrease because at higher sintering temperature, abnormal grain growth occurs which creates trapped pores inside the grain. This increasing amount of pores influences the loss factor and turns into higher value which results a lower value of *Q*-factor.

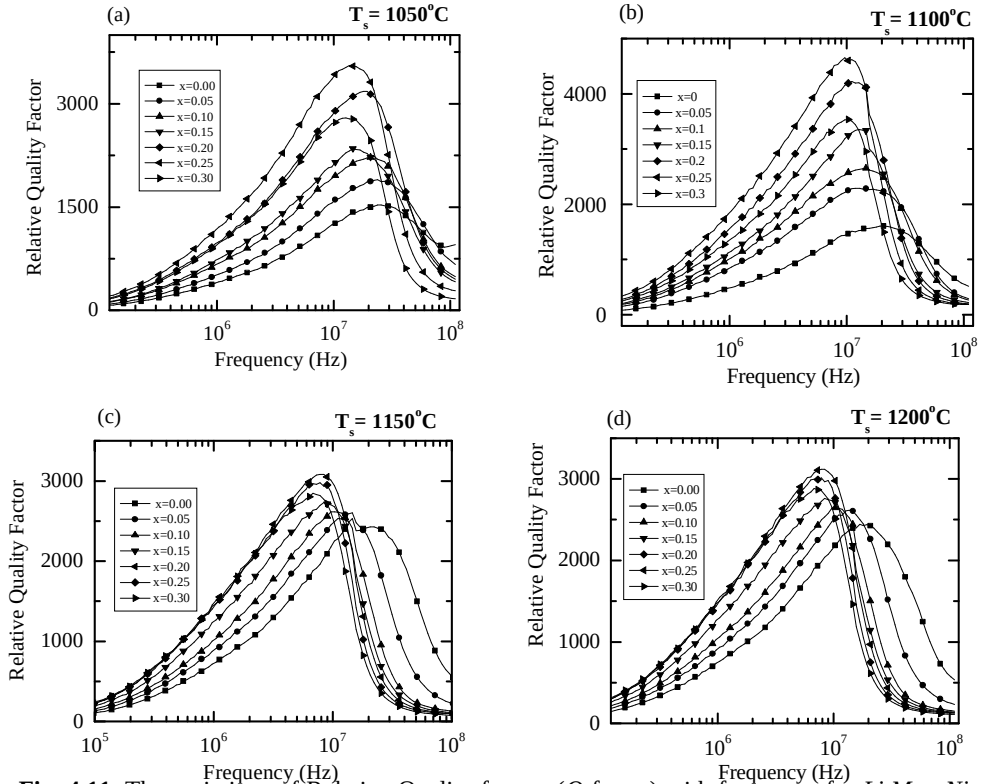


**Fig. 4.11.** The variations of Relative Quality factors (*Q*-factor) with frequency for $Li_xMg_{0.4}Ni_{0.6-2x}Fe_{2+x}O_4$ ferrites sintered at (a) 1050˚C, (b) 1100˚C (c) 1150˚C and (d) 1200˚C in air.

**pdfMachine**
**A pdf writer that produces quality PDF files with ease!**
Produce quality PDF files in seconds and preserve the integrity of your original documents. Compatible across nearly all Windows platforms, if you can print from a windows application you can use pdfMachine.
Get yours now!

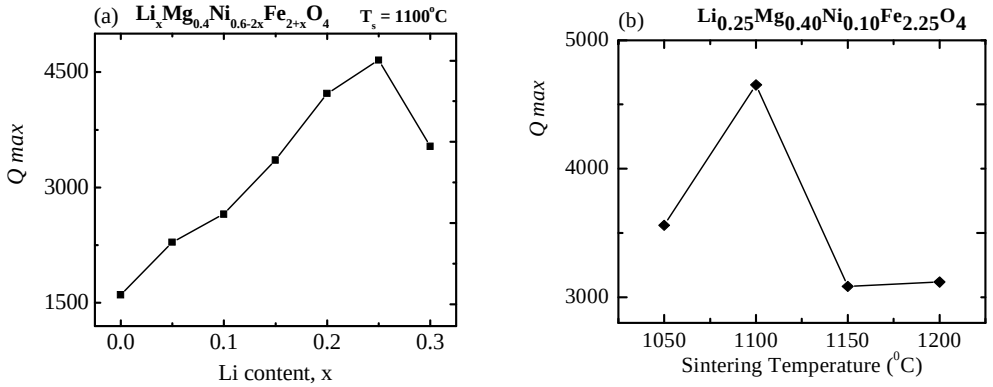


**Fig. 4.12.** (a) The variations of $Q_{max}$ with Li content for $Li_xMg_{0.4}Ni_{0.6-2x}Fe_{2+x}O_4$ ferrites sintered at 1100˚C and (b) the variations of $Q_{max}$ for $Li_{0.25}Mg_{0.40}Ni_{0.10}Fe_{2.25}O_4$ ferrite sintered at 1050, 1100, 1150 and 1200˚C.

## 4.6 *DC* Magnetization of $Li_xMg_{0.4}Ni_{0.6-2x}Fe_{2+x}O_4$

The magnetization as a function of applied magnetic field for various $Li_xMg_{0.4}Ni_{0.6-2x}Fe_{2+x}O_4$ samples at room temperature (300*K*) is shown in Fig. 4.13. The magnetization of all samples increases linearly with increasing the applied magnetic field up to 0.1T applied magnetic field (depending on compositions). Beyond 0.1T applied field magnetization increases slowly and then saturation occurs.

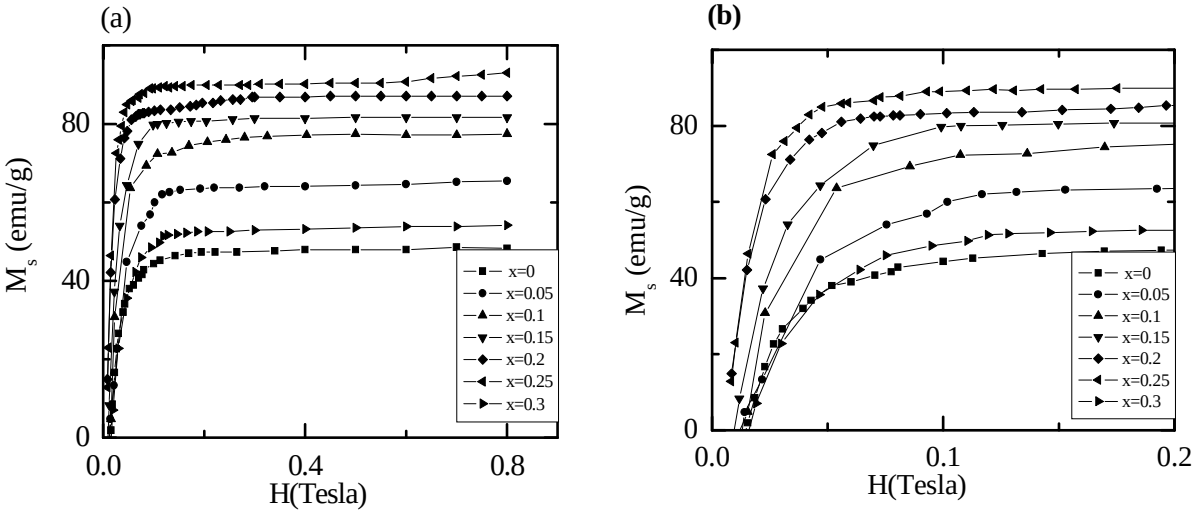


**Fig. 4.13.** The magnetization, *M* versus the applied magnetic field, *H* curves for $Li_xMg_{0.4}Ni_{0.6-2x}Fe_{2+x}O_4$ ferrites sintered at 1100˚C in air.

**pdfMachine**
**A pdf writer that produces quality PDF files with ease!**
Produce quality PDF files in seconds and preserve the integrity of your original documents. Compatible across nearly all Windows platforms, if you can print from a windows application you can use pdfMachine.
Get yours now!

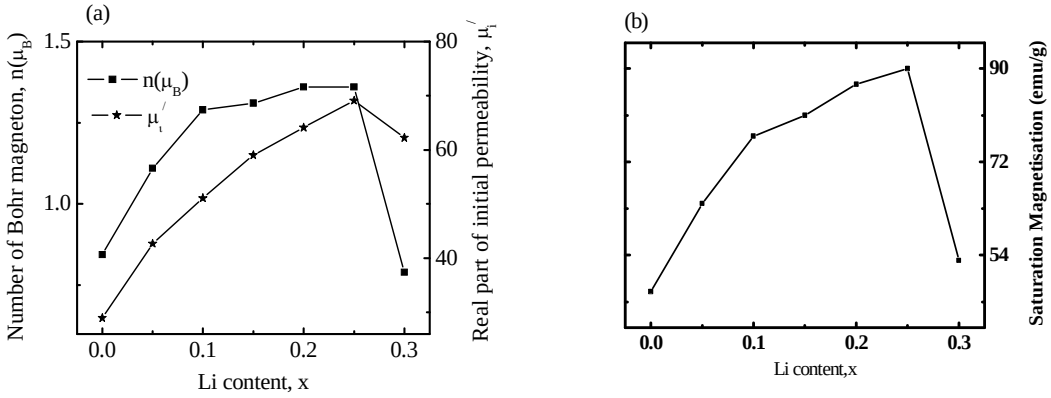


**Fig.4. 14.**(a) The variation of $n(\mu_B)$ and $\mu_i'$ (at 100*KHz*), and (b)The variation of $M_s$ with *Li* content, *x*, in $Li_xMg_{0.4}Ni_{0.6-2x}Fe_{2+x}O_4$ sintered at 1200˚C in air.

The $M_s$ for all the samples determined by the extrapolation of the magnetization (*M-H*) curve to $H_s$=0. Fig. 4.13 (b) shows the variation of saturation magnetization as a function of Lithium content. Using these values of $M_s$; the number of Bohr magneton, $n_B$, has been calculated by using the relation [17]

$$n_B = \frac{MM_s}{N_A\mu_B} \qquad (4)$$

where *M* is the molecular weight, $N_A$ is the Avogadro□s number and $\mu_B$ is the Bohr magneton. This formula is used to extract the microscopic magnetic information from the bulk magnetization measurements. The values of $n_B$ for each of the samples measured at room temperature (300*K*) are given in Table 4.2. The variation of $n_B$ with *Li* content is shown in Fig.4.14 (a). It is seen from Fig.4.14 (a) that the value of $n_B$ gradually increases with increasing $Li^{1+}$ concentration, becomes maximum at $x$ = 0.25 and then decreases with further increase in *Li* content. Similar trend is observed for the variation of $\mu_i'$ varying *Li* content, as indicated in Fig.4.14 (a)

The observed variation in $M_s$ can be explained on the basis of cations distribution and exchange interaction between A and B sites. It is known that $Li^{1+}$ [18] and $Ni^{2+}$[5] ions occupy B sites, although $Fe^{3+}$ions exist at both A and B sites[18] . The cation distribution of various $Li_xMg_{0.4}Ni_{0.6-2x}Fe_{2+x}O_4$ ferrite assumed as

$$(Fe^{3+}{}_{0.9})_A\,[Li^{1+}{}_xMg^{2+}{}_{0.4}Ni_{0.6-2x}\,Fe^{3+}{}_{1.1+x}]_B$$

**pdfMachine**
**A pdf writer that produces quality PDF files with ease!**
Produce quality PDF files in seconds and preserve the integrity of your original documents. Compatible across nearly all Windows platforms, if you can print from a windows application you can use pdfMachine.
Get yours now!

where the parentheses ( ) and the square brackets [ ] indicate ions distributed on tetrahedral A and octahedral B sites, respectively. In the above cationic distribution $Li^{1+}$ ions being non magnetic do not contribute to the magnetization of the sublattice and hence do not contribute to net magnetic moment. The net magnetic moment is therefore mainly due to the contributions from the $Fe^{3+}$ ions and $Ni^{2+}$ ions at B sites. As $Mg^{2+}$ ions are non-varying in respect to the *Li* content so it is expected that $Mg^{2+}$ ions will also occupy B sites [19]. Therefore $Mg^{2+}$ ions will not affect the magnetic properties of the present samples .At the B sites $Ni^{2+}$ ions (magnetic moment = $2\mu_B$) substitute non magnetic $Li^{1+}$ ions and $Fe^{3+}$ ions ( magnetic moment = 5 $\mu_B$ ). The environment of $Fe_B^{3+}$ is thus expected to be strictly more magnetic with the substitution.

As the net magnetization equals $M_B$–$M_A$ and increases with increasing Li concentration up to $x$ = 0.25, the phenomenon can be explained from the Neel□s two sublattice model. According to this model AB superexchange interaction is predominant over intrasublattice AA and BB interaction, and the saturation magnetization is given by the vector sum of the magnetic moments of the individual A and B sublattices i.e. $M_S = M_B - M_A$. As $Li^{1+}$ and $Mg^{2+}$ do not contribute to the magnetization because of being nonmagnetic, $Ni^{2+}$ ions and $Fe^{3+}$ ions having magnetic moment $2\mu_B$ and $5\mu_B$ respectively results the net magnetic moment which can be given by,

$M_B$-$M_A$=(6.7+$x$) $\mu_B$ □(0.9×5) $\mu_B$ =6.7 $\mu_B$ □4.5 $\mu_B$ +x $\mu_B$ = (2.2+$x$) $\mu_B$ .

Where, $M_B$=(0.6-2$x$)×2 $\mu_B$ +(1.1+$x$)×5 $\mu_B$ =(1.2-4$x$+5.5+5$x$) $\mu_B$ =(6.7+$x$) $\mu_B$

and $M_A$=0.9×5 $\mu_B$ =4.5 $\mu_B$.

Therefore saturation magnetization is expected to increase as *Li* content increases.

The fall in magnetization on addition of *Li* beyond $x$=0.25, is due to the occurrence of non-collinear spin structure, however, cannot be explained on the basis of the Neel□s two sublattice model, but instead on a three sublattice model suggested by Yafet and Kittel [20]. On addition of lithium, the A-B exchange interaction gets weakened while B-B sublattice interaction becomes strong, which in turn disturbs the parallel arrangement of spin magnetic moments on the B- site and hence canting of spin occurs. Thus decrease in the magnetic moment beyond $x$ = 0.25, indicates the possibility of a non-collinear spin arrangement [11, 20].

**pdfMachine**
**A pdf writer that produces quality PDF files with ease!**
Produce quality PDF files in seconds and preserve the integrity of your original documents. Compatible across nearly all Windows platforms, if you can print from a windows application you can use pdfMachine.
Get yours now!

**Table 4.2.** Saturation magnetizing field, Saturation magnetization and the number of Bohr magneton for polycrystalline $Li_xMg_{0.4}Ni_{0.6-2x}Fe_{2+x}O_4$ ferrites.

| *Composition* | $H_s$, ($T$) | $M_s$ (emu/g) | $n_B$ ($\mu_B$) |
|---|---|---|---|
| $Mg_{0.40}Ni_{0.60}Fe_2O_4$ | 0.1697 | 47 | 1.86 |
| $Li_{0.05}Mg_{0.40}Ni_{0.50}Fe_{2.05}O_4$ | 0.32 | 64 | 2.50 |
| $Li_{0.10}Mg_{0.40}Ni_{0.40}Fe_{2.10}O_4$ | 0.4032 | 77 | 2.97 |
| $Li_{0.15}Mg_{0.40}Ni_{0.30}Fe_{2.15}O_4$ | 0.2565 | 81 | 3.08 |
| $Li_{0.20}Mg_{0.40}Ni_{0.20}Fe_{2.20}O_4$ | 0.45 | 87 | 3.27 |
| $Li_{0.25}Mg_{0.40}Ni_{0.10}Fe_{2.25}O_4$ | 0.31 | 90 | 3.33 |
| $Li_{0.30}Mg_{0.40}Fe_{2.30}O_4$ | 0.4 | 53 | 1.97 |

## References:


[1] Hossain, A. K. M. A., Seki, M., Kawai, T. and Tabata, H., "Colossal magnetoresistance in spinel type $Zn_{1-x}Ni_xFe_2O_4$", Journal of Applied Physics, Vol-96, pp 1273-1275, 2004.

[2] Nelson, J. B.; Riley, D. P.; "An experimental investigation of extrapolation methods in the derivation of accurate unit-cell dimensions of crystals", *Proc. Phys. Soc. London*, Vol. 57, pp 160, 1945.

[3] Whittaker, E.J.W. and Muntus, R., "Ionic radii for use in geochemistry", Geochimica et Cosmochimica Acta, Vol-34, pp 945-956, 1970.

[4] Winter, M. J. ,www.webelements.com,©, University of Sheffield, UK, 1995-2006.

[5] Sattar, A. A., El-Sayed, H. M., El-Shokrofy, K. M. and El-Tabey, M. M., "Improvement of the magnetic properties of Mn-Ni-Zn ferrite by the non-magnetic $Al^{3+}$ ion substitution", Journal of Applied Science., Vol-5(1), pp 162-168, 2005.

[6] Mahmud, S.T., Hossain, A. K. M. A., Hakim, A. K. M. Abdul, Seki, M., Kawai T., Tabata, H., "Influence of microstructure on the complex permeability of spinel type Ni Zn ferrite", Journal of Magnetism and Magnetic Materials, Vol-305, pp 269 274, 2006.

[7] Valenzuela, R., Magnetic Ceramics, Cambridge University Press, Cambridge, 1994.

[8] Snoek, J.L., "Dispersion and absorption in magnetic ferrites at frequencies above one Mc/s", Physica, Vol-14, pp 207-217, 1948.

[9] Jun, Hu and Mi, Yan, "Preparation of high permeability Ni-Cu-Zn ferrite", Journal of Zhejiang University Science, Vol-6B (6), pp 580-583, 2005.


**pdfMachine**
**A pdf writer that produces quality PDF files with ease!**
Produce quality PDF files in seconds and preserve the integrity of your original documents. Compatible across nearly all Windows platforms, if you can print from a windows application you can use pdfMachine.
Get yours now!

[10] Tsutaoka, T, Ueshima, M., Tokunaga,T., Nakamura, T. and Hatakeyama, K., "Frequency dispersion and temperature variation of complex permeability of Ni-Zn ferrite composite materials", Journal of Applied Physics, Vol-78(6), pp 3983-3991, 1995.

[11] Hossain, A. K. M. A., Mahmud, S.T., Seki, M., Kawaia, T. and tabata ,H., "Structural, electrical transport, and magntic properties of $Ni_{1-x}Zn_xFe_2O_4$", Journal of Magnetism and Magnetic Materials.,Vol-312, pp 210-219, 2007.

[12] Guillaud ,C., "The properties of manganese-zinc ferrites and the physical processes governing them", Proceedings of the IEEE, Vol-104B, pp 165-173, 1957.

[13] Kang, S. H. and Yoo, H.I., "The effect of nonstoichiometry (δ) on the magnetic properties of $(Mg_{0.22}Mn_{0.07}Fe_{0.71})_{3-\delta}O_4$ ferrite", Journal of Applied Physics, Vol-88 , pp 4754-4757, 2000.

[14] Caltun, O. F. and Spinu, L., "Magnetic properties of high frequency NiZn ferrites doped with CuO", IEEE Transactions on Magnetics, Vol-37(4), pp 2353-2355, 2001.

[15] Rado ,G.T. , Wright ,R.W., Emerson, W. H. and Terris , A., "Ferromagnetism at Very High Frequencies. IV. Temperature Dependence of the Magnetic Spectrum of a Ferrite", Physical . Review., Vol-88, pp 909-915,1952.

[16] Chauhan, B. S., Kumar, R., Jadhav, K. M., Singh, M., "Magnetic study of substituted Mg-Mn ferrites Synthesized by citrate precursor method", Journal of Magnetism and Magnetic Materials, Vol-283, pp 71-81,2004.

[17] Smit, J., "Magnetic properties of materials", Mc-Graw Hill, NewYork, 1971.

[18] Jadhav, S.A., "Magnetic properties of Zn-substituted Li-Cu ferrites", Journal of Magnetism and Magnetic Materials, Vol-224, pp 167-172, 2001.

[19] Sheikh, A. M., Watae , S.C., Jadhav, S.A., Chougule, B.K., "Preparation and Characterization of Zn substituted Li-Mg ferrites", Materials Research Bulletin, Vol-37, pp 2547-2555,2002.

[20] Yafet, Y. and Kittel, C.,"Antiferromagnetic arrangements in ferrites", Physical review, Vol-87, pp 290-294, 1952.

**pdfMachine**
**A pdf writer that produces quality PDF files with ease!**
Produce quality PDF files in seconds and preserve the integrity of your original documents. Compatible across nearly all Windows platforms, if you can print from a windows application you can use pdfMachine.
Get yours now!

# CHAPTER 3

## SAMPLE FABRICATION, CHARACTERIZATION AND EXPERIMENTAL TECHNIQUES

### 3.1 Introduction

To achieve high permeability, high flux density, low loss and good homogenous product are apparently highly sensitive to the composition and manufacturing process. Many processing methods have been proposed but are mainly divided into two groups;

1. Conventional ceramic method, i.e., solid state reaction technique, involves milling of the reactants followed by heating at elevated temperatures range.
2. Non conventional method also called wet method. Among these methods, some are [1, 2]:
    - Sol-gel synthesis
    - Co-precipitation
    - Organic precursor method
    - Co-spray roasting
    - Freeze drying
    - Combustion synthesis
    - Glass Crystallization
    - Activated sintering
    - Fused salt synthesis

Presently, the conventional Ceramic process or Solid State Reaction technique is mostly preferred to produce ferrite powders. In this chapter, we describe the solid state reaction method that is used in this research work.

**pdfMachine**
**A pdf writer that produces quality PDF files with ease!**
Produce quality PDF files in seconds and preserve the integrity of your original documents. Compatible across nearly all Windows platforms, if you can print from a windows application you can use pdfMachine.
Get yours now!

## 3.2 Conventional Solid State Reaction Method

In the solid state reaction method, the required composition is usually prepared from the appropriate amount of raw mineral oxides or carbonates by crushing, grinding and milling. The most common type of mill is the ball mill, which consists of a lined pot with hard spheres or rod inside. Milling can be carried out in a wet medium to increase the degree of mixing. This method depends on the solid state inter-diffusion between the raw materials. Solids do not usually react at room temperature over normal time scales. Thus it is necessary to heat them at higher temperatures for the diffusion length $(2Dt)^{1/2}$ to exceed the particle size, where $D$ is the diffusion constant for the fast-diffusing species, and t is the firing time. The ground powders are then calcined in air or oxygen at 600°C. For some time, this process is continued until the mixture is converted into the correct crystalline phase. The calcined powders are again crushed into fine powders. The pellets or toroid shaped samples are prepared from these calcined powders using die-punch assembly or hydrostatic or isostatic pressure. Sintering is carried out in the solid state, at temperature ranging 1100-1400°C, for times of typically 1-40 h and in various atmospheres (e.g. Air, $O_2$ and $N_2$) [3-6]. Fig. 3.1 shows, diagrammatically, the stages followed in ferrite preparation.

The general solid state reaction leading to a ferrite $MeFe_2O_4$ may be represented as

$$MeO + Fe_2O_3 \longrightarrow MeFe_2O_4$$

where *Me* is the divalent ions. There are basically four steps in the preparation of ferrite:

1) Preparation of materials to form an intimate mixture with the metal ions in the ratio which they will have in the final product,
2) Heating of this mixture to form the ferrite (often called calcining),
3) Grinding the calcined powders and pressing the fine powders into the required shape, and
4) Sintering to produce a highly densified product.

## 3.3 Details of Calcining, Pressing and Sintering

*Calcining* is defined as the process of obtaining a homogeneous and phase pure composition of mixed powders by heating them for a certain time at a high temperature

pdfMachine
A pdf writer that produces quality PDF files with ease!
Produce quality PDF files in seconds and preserve the integrity of your original documents. Compatible across nearly all Windows platforms, if you can print from a windows application you can use pdfMachine.
Get yours now!

and then allowing it to cool slowly. During the calcining stage, the reaction of $Fe_2O_3$ with metal oxide (say, $MeO$ or $Me_2O_3$) takes place in the solid state to form spinel according to the reactions [7]:

$$MeO + Fe_2O_3 \longrightarrow MeFe_2O_4 \text{ (Spinel)}$$

$$2Me_2O_3 + 4Fe_2O_3 \longrightarrow 4MeFe_2O_4 \text{ (Spinel)} + O_2$$

The $NiO$, $MgO$ and $Li_2CO_3$ creeps into $Fe_2O_3$ as below, to form an intermediate phase

$$Fe_2O_3 + NiO \longrightarrow NiFe_2O_4$$

$$5Fe_2O_3 + Li_2CO_3 \longrightarrow 4\,Li_{0.5}Fe_{2.5}O_4 + CO_2$$

$$Fe_2O_3 + MgO \longrightarrow MgFe_2O_4$$

*And lastly*

$$(0.60\text{-}2x)\,NiFe_2O_4 + (0.40)MgFe_2O_4 + 2x\,Li_{0.5}Fe_{2.5}O_4 \longrightarrow Li_xMg_{0.4}Ni_{0.6-2x}Fe_{2+x}O_4.$$

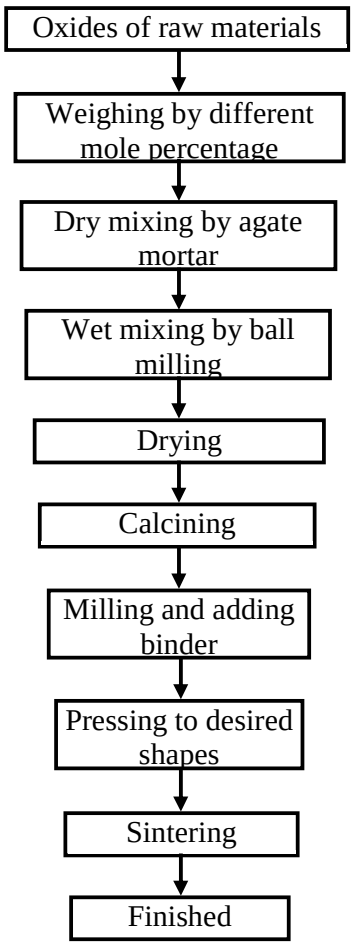


**Fig.3.1.** Flow chart of the stages in preparation of spinel ferrite.

**pdfMachine**
**A pdf writer that produces quality PDF files with ease!**
Produce quality PDF files in seconds and preserve the integrity of your original documents. Compatible across nearly all Windows platforms, if you can print from a windows application you can use pdfMachine.
Get yours now!

The calcining process can be repeated several times to obtain a high degree of homogeneity. The calcined powders are crushed into fine powders. The ideal characteristics of fine powders are [2]:

1) small particle size (sub micron)
2) narrow distribution in particle size
3) dispersed particles
4) equiaxed shape of particles
5) high purity
6) homogeneous composition.

A small particle size of the reactant powders provides a high contact surface area for initiation of the solid state reaction; diffusion paths are shorted, leading to more efficient completion of the reaction. Porosity is easily eliminated if the initial pores are very small. A narrow size distribution of spherical particles as well as a dispersed state is important for compaction of the powder during green-body formation. Grain growth during sintering can be better controlled if the initial size is small and uniform.

A binder is usually added prior to compaction, at a concentration lower than 5wt % [2]. Binders are polymers or waxes; the most commonly used binder in ferrite is polyvinyl alcohol. The binder facilitates the particles flow during compacting and increases the bonding between the particles, presumably by forming bonds of the type *particle-binder-particle*. During sintering, binders decompose and are eliminated from the ferrite. Pressures are used for compacting very widely but are commonly several tons per square inch (i. e., up to $10^8$ N $m^{-2}$).

*Sintering* is defined as the process of obtaining a dense, tough body by heating a compacted powder for a certain time at a temperature high enough to significantly promote diffusion, but clearly lower than the melting point of the main component. The driving force for sintering is the reduction in surface free energy of the powder. Part of this energy is transferred into interfacial energy (grain boundaries) in the resulting polycrystalline body [2, 8]. The sintering time, temperature and the furnace atmosphere play very important role on the magnetic property of ferrite materials. The purposes of sintering process are:

1) to bind the particles together so as to impart sufficient strength to the product,
2) to densify the material by eliminating the pores and

pdfMachine
A pdf writer that produces quality PDF files with ease!
Produce quality PDF files in seconds and preserve the integrity of your original documents. Compatible across nearly all Windows platforms, if you can print from a windows application you can use pdfMachine.
Get yours now!

3) to homogenize the materials by completing the reactions left unfinished in the calcining step.

Sintering of crystalline solids is dealt by Coble and Burke [9] who found the following empirical relationship regarding rate of grain growth:

$$\bar{d} = kt^n$$

where $\bar{d}$ is the mean grain diameter, $n$ is about 1/3, $t$ is sintering time and k is a temperature dependent parameter. Sintering is divided into three stages, Fig. 3.2 [2, 10].

Stage 1. Contact area between particles increases,

Stage 2. Porosity changes from open to closed porosity,

Stage 3. Pore volume decreases; grains grow.

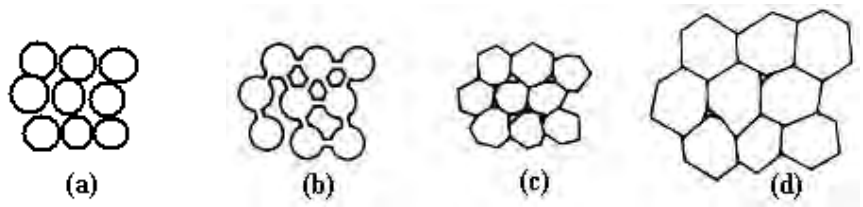


**Fig. 3.2.** Schematic representation of sintering stages: (a) greenbody, (b) initial stage, (c) intermediate stage, and (d) final stage.

In the initial stage, neighbouring particles form a neck by surface diffusion and presumably also at high temperatures by an evaporation-condensation mechanism. Grain growth begins during the intermediate stage of sintering. Since grain boundaries are the sinks for vacancies, grain growth tends to decrease the pore elimination rate due to the increase in distance between pores and grain boundaries, and by decreasing the total grain boundary surface area. In the final stage, the grain growth is considerably enhanced and the remaining pores may become isolated.

In *Li-Mg-Ni* ferrites, the presence of *Li* complicates the sintering process because high temperature coupled with low oxygen firing will cause *Li* loss. High density is important for high permeability, but so is *Li* conservation. Tasaki [1] described two alternative firings to achieve high density:

1) Low sintering temperature excluding $O_2$ (Vacuum, argon, nitrogen),
2) High temperature in pure oxygen to reduce *Li* loss.

**pdfMachine**
**A pdf writer that produces quality PDF files with ease!**
Produce quality PDF files in seconds and preserve the integrity of your original documents. Compatible across nearly all Windows platforms, if you can print from a windows application you can use pdfMachine.
Get yours now!

Accordingly, other properties correlated along with density:

1) Lattice constant is greater for $O_2$, smaller for vacuum
2) Curie temperature is greater for vacuum, smaller for $O_2$
3) Resistivity is greater for $O_2$, smaller for vacuum.

## 3.4 Preparation of the Present Samples

The Polycrystalline ferrite with nominal chemical composition $Li_xMg_{0.4}Ni_{0.6-2x}Fe_{2+x}O_4$ (where x = 0.0 to 0.3 in steps of 0.05) were prepared by standard solid state reaction technique. Commercially available powders of *NiO* (99.9%), *MgO* (99.9%), $Li_2CO_3$ ($99^+$ %), $Fe_2O_3$ (99.9%), will be mixed thoroughly in an appropriate amount by ball milling. The mixed powders were calcined at 600˚C for 6 hours. The calcined powders were then pressed into disk- and toroid-shaped samples. The samples were sintered at 1050, 1100, 1150 and 1200˚C for 6 h in air. The heating and cooling rates for sintering were 5˚C/min.


**Fig. 3.3.** Sample (a) disk shaped, (b) Toroid shaped.

### 3.5 X-ray Diffraction

Bragg reflection is a coherent elastic scattering in which the energy of the X-ray is not changed on reflection. Let a beam of monochromatic radiation of wavelength λ is incident on a periodic crystal plane at an angle θ and is diffracted at the same angle as shown in Fig. 3.4.

When constructive interference occurs, from Fig 3.4 (a) it can be written as ,

$$n\lambda = AB + BC$$

As, $AB=BC$, $n\lambda = 2AB$

Again from Fig 3.4(b), $\sin\theta = AB/d$

So, $AB = d\sin\theta$

pdfMachine
A pdf writer that produces quality PDF files with ease!
Produce quality PDF files in seconds and preserve the integrity of your original documents. Compatible across nearly all Windows platforms, if you can print from a windows application you can use pdfMachine.
Get yours now!

$$\text{i.e. } 2d\,Sin\theta = n\lambda \tag{3.1}$$

where $d$ is the distance between crystal planes and $n$ is the positive integer which represents the order of reflection. Equation (3.1) is known as Bragg law. This Bragg law suggests that the diffraction is only possible when $\lambda \leq 2d$ [11]. For this reason we cannot use the visible light to determine the crystal structure of a material. The X-ray diffraction (XRD) provides substantial information on the crystal structure.

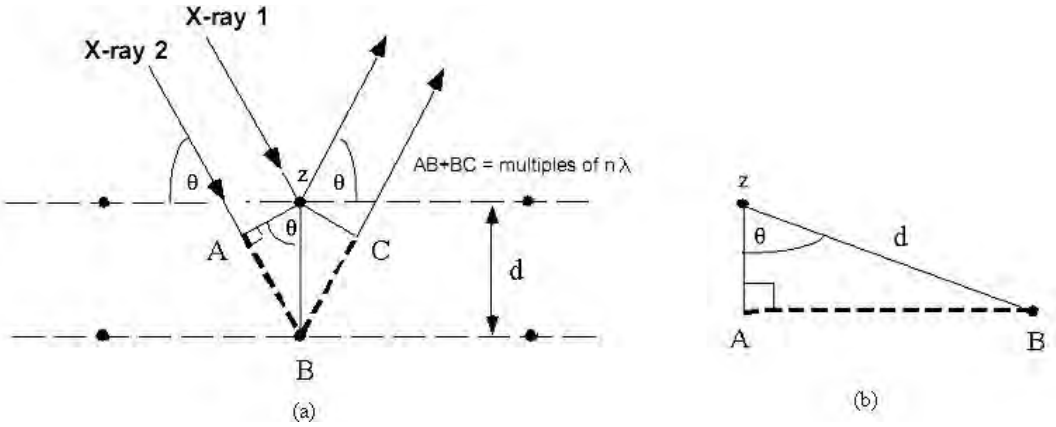


**Fig. 3.4.** Bragg law of diffraction.

X-ray diffraction was carried out using RIGAKU Smart-lab with rotating anode, Lyon Institute of Nanotechnology,France, using Cu-Kα Xray diffractometer (α = 1.540593 Å). Basic features of a XRD experiments is shown in Fig. 3.5 respectively.

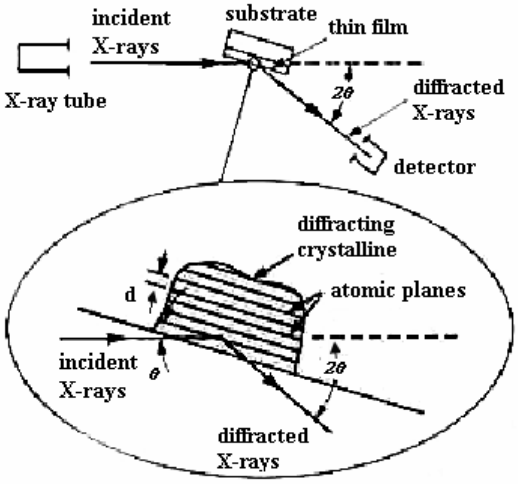


**Fig. 3.5.** Basic Features of Typical XRD Experiment

**pdfMachine**
**A pdf writer that produces quality PDF files with ease!**
Produce quality PDF files in seconds and preserve the integrity of your original documents. Compatible across nearly all Windows platforms, if you can print from a windows application you can use pdfMachine.
Get yours now!

The lattice parameter for each peak of each sample was calculated by using the formula

$$a = d\sqrt{h^2 + k^2 + l^2} \tag{3.2}$$

where *h*, *k* and *l* are the indices of the crystal planes. To determine the precise lattice constant for each sample, Nelson-Riley method was used. The Nelson-Riley function $F(\theta)$ is given as

$$F(\theta) = \frac{1}{2}\left[\left(Cos^2\theta / Sin\theta\right) + \left(Cos^2\theta / \theta\right)\right] \tag{3.3}$$

The values of lattice parameter '*a*' of all the peaks for a sample are plotted against $F(\theta)$. Then using a least square fit method exact lattice constant '$a_o$' is determined. The point where the least square fit straight line cut the y-axis (i.e. at $F(\theta) = 0$) is the actual lattice constant of the sample. The theoretical density $\rho_{th}$ was calculated using following expression:

$$\rho_{th} = \frac{8M}{N_A a_o^3}\, g/cm^3 \tag{3.4}$$

where $N_A$ is Avogadro's number ($6.02 \times 10^{23}$ $mol^{-1}$), *M* is the molecular weight. The porosity was calculated from the relation $\{100(\rho_{th} - \rho_B)/ \rho_{th}\}\%$, where $\rho_B$ is the bulk density measured by the formula $\rho_B = M/V$ [12].

## 3.6 Microstructural Investigation

The microstructural study was performed in order to have an insight of the grain structures. The samples of different compositions and sintered at different temperatures were chosen for this purpose. The samples were visualized under a high-resolution optical microscope (Koehler Illuminator MA 1109, Swift Instruments, Inc.) and then photographed. Average grain sizes (grain diameter) of the samples were determined from optical micrographs by linear intercept technique [3]. To do this, several random horizontal and vertical lines were drawn on the micrographs. Therefore, we counted the number of grains intersected and measured the length of the grains along the line traversed. Finally the average grain size was calculated.

**pdfMachine**
**A pdf writer that produces quality PDF files with ease!**
Produce quality PDF files in seconds and preserve the integrity of your original documents. Compatible across nearly all Windows platforms, if you can print from a windows application you can use pdfMachine.
Get yours now!

## 3.7. Complex Permeability Measurement

For high frequency application, the desirable property of a ferrite is high permeability with low loss. One of the most important goals of ferrite research is to fulfill this requirement. The techniques of permeability measurement and frequency characteristics of the present samples are described in sections 3.7.1 and 3.7.2.

### 3.7.1 Techniques for the Permeability Measurement

Measurements of permeability normally involve the measurements of the change in self-inductance of a coil in presence of the magnetic core. The behaviour of a self-inductance can now be described as follows. We assume an ideal loss less air coil of inductance $L_0$. On insertion of a magnetic core with permeability $\mu$, the inductance will be $\mu L_0$. The complex impedance $Z$ of this coil [1] can be expressed as follows:

$$Z = R + jX = j\omega L_0 \mu = j\omega L_0 (\mu' - j\mu'') \tag{4.5}$$

where the resistive part is $R = \omega L_0 \mu''$ (4.6)

and the reactive part is $X = \omega L_0 \mu'$ (4.7)

The RF permeability can be derived from the complex impedance of a coil, *Z*, given by equation (4.5). The core is taken as toroidal to avoid demagnetizing effects. The quantity $L_o$ is derived geometrically as shown in section 3.7.2.

### 3.7.2 Frequency Characteristics of the present samples

The frequency characteristics of the ferrite samples i.e. the initial permeability spectra were investigated using and Agilent Precision Impedance Analyzer (model no. 4294A). The complex permeability measurements on toroid shaped specimens were carried out at room temperature on all the samples in the frequency range 300 *kHz* - 110 *MHz*. The real part $(\mu_i')$ and imaginary part $(\mu_i'')$ of the complex permeability were calculated using the following relations [4]: $\mu_i' = L_s / L_0$ and $\mu_i'' = \mu_i' \tan\delta$, where $L_s$ is the self-inductance of the sample core and $L_0 = \mu_o N^2 S / \pi \bar{d}$ is derived geometrically. Here $L_o$ is the inductance of the winding coil without the sample core, *N* is the number

pdfMachine
A pdf writer that produces quality PDF files with ease!
Produce quality PDF files in seconds and preserve the integrity of your original documents. Compatible across nearly all Windows platforms, if you can print from a windows application you can use pdfMachine.
Get yours now!

of turns of the coil ($N$ = 5), $S$ is the area of cross section of the toroidal sample as given below:

$$S = d \times h,$$

where $$d = \frac{d_2 - d_1}{2},$$

$d_1 =$ Inner diameter,
$d_2 =$ Outer diameter,
$h =$ Height

and $\bar{d}$ is the mean diameter of the toroidal sample as given below:

$$\bar{d} = \frac{d_1 + d_2}{2}$$

The relative quality factor is determined from the ratio $\frac{\mu_i'}{\tan\delta}$.

## 3.8 DC Magnetization measurement at room temperature

The DC magnetization ($M$) measurements were made using a VSM (Vibrating Sample magnetometer) at room temperature, made by the Department of Physics, Bangladesh University of Engineering Technology (BUET). Diameter of the sample was made as it fit to the sample rod finely. In VSM the sample is vibrated at 37 Hz frequency and magnetization strength is found from the magnitude of the emf induce in the sense coils placed in proximity with sample. The block diagram of the VSM is shown in Fig. 3.7. The pickup coils are mounted with axis perpendicular to magnetization field so as to minimize error signals arising from field fluctuations. The transmission of vibrations at a measured frequency must be carefully avoided, attaching a small permanent magnet to the remote part of the vibrating system. This moves its own pickup coils and provides a reference signal against which the signal produced by the sample can be measured accurately.

pdfMachine
A pdf writer that produces quality PDF files with ease!
Produce quality PDF files in seconds and preserve the integrity of your original documents. Compatible across nearly all Windows platforms, if you can print from a windows application you can use pdfMachine.
Get yours now!

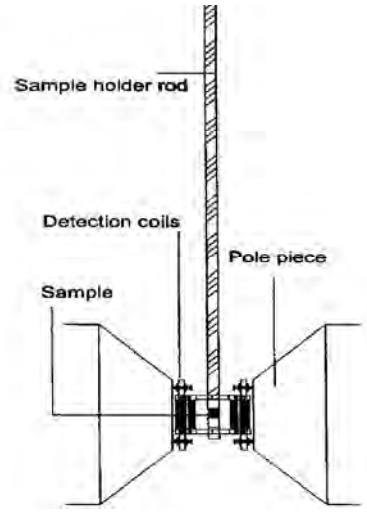


**Fig. 3.6.** Block diagram of vibrating sample magnetometer (VSM)

Magnetization values of all samples were recorded by setting up the magnet at a maximum applied field of 8 K Gauss. For the calculation of saturation magnetization, the values are obtained in milivolts (mV), these values are then calibrated in emu using nickel standard of value 1mv=0.279304 emu. The calculated values are then divided by mass of the respective sample to obtain the values in emu/g for each sample.

## References

[1] Goldman, A., Handbook of Modern Ferromagnetic Materials, Kulwer Acad. Pub, Boston, U.S.A, 1999.

[2] Valenzuela, R., Magnetic Ceramics, Cambridge University Press, Cambridge, 1994.

[3] Hossain, A. K. M. A., "Investigation of colossal magnetoresistance in bulk and thick film magnetites," Ph. D. Thesis, Imperial College, London, 1998.

[4] Cullity, B. D., "Introduction to Magnetic Materials", Addison-Wisley Publishing Company, Inc., California, 1972.

[5] Brook, R. J., "Sintering: An Overview", Concise Encyclopedia of Advanced Ceramic Materials, Pergamon Press, Oxford, p 438, 1991.

[6] Reijnen, P., Science of Ceramics, Academic Press, London, 1967.

**pdfMachine**
**A pdf writer that produces quality PDF files with ease!**
Produce quality PDF files in seconds and preserve the integrity of your original documents. Compatible across nearly all Windows platforms, if you can print from a windows application you can use pdfMachine.
Get yours now!

[7] Slick , P. I., Ferrites for Non-microwave Applications, Vol. 2, North Holland Pub. Co. 1980.

[8] Kingery ,W. D., H. K. Bowen and D. R. Uhlman, Introduction to Ceramics, 2nd edition, Wiley Interscience, Newyork, pp 476, 1976.

[9] Coble, R. L. and Burke, J. E., 4th Int. Symp. On the Reactivity of Solids, Amsterdam, pp. 38-51, 1960.

[10] McColm, I. J. and Clark, N. J., Forming, Shaping and Working of high Performance Ceramics, Blackie, Glasgow, pp 1-338, 1988.

**pdfMachine**

**A pdf writer that produces quality PDF files with ease!**

Produce quality PDF files in seconds and preserve the integrity of your original documents. Compatible across nearly all Windows platforms, if you can print from a windows application you can use pdfMachine.

Get yours now!

# CHAPTER 5

## CONCLUSIONS

### 5.1 Conclusions

The following conclusions have been drawn from the study of $Li_xMg_{0.4}Ni_{0.6-2x}Fe_{2+x}O_4$ ferrites.

- The XRD analysis of various $Li_xMg_{0.4}Ni_{0.6-2x}Fe_{2+x}O_4$ ferrites confirms that all the samples have single phase cubic spinel structure. No impurity peak is found in XRD pattern.

- The lattice constant slightly increases with the increasing of Li content in $Li_xMg_{0.4}Ni_{0.6-2x}Fe_{2+x}O_4$ ferrites. This phenomenon is explained on the basis of ionic radii. In the present case variant contents are *Li*, *Ni* and *Fe*, while *Ni* is substituted by both the *Li* and *Fe*. The variation of the lattice constant $a_o$, and the mean ionic radius of the variant ions show similar increasing trend for $Li_xMg_{0.4}Ni_{0.6-2x}Fe_{2+x}O_4$ ferrites.

- It is observed that the density of $Mg_{0.40}Ni_{0.60}Fe_2O_4$ and $Li_{0.05}Mg_{0.40}Ni_{0.50}Fe_{2.05}O_4$ ferrites increased with increasing sintering temperature. On the other hand, porosity (P) of the sample decreased with increasing sintering temperature. During the sintering process, the thermal energy generates a force that drives the grain boundaries to grow over pores, thereby decreasing the pore volume and increasing the density of the materials. It is observed that the density of $Li_{0.10}Mg_{0.40}Ni_{0.40}Fe_{2.10}O_4$, $Li_{0.15}Mg_{0.40}Ni_{0.30}Fe_{2.15}O_4$, $Li_{0.20}Mg_{0.40}Ni_{0.20}Fe_{2.20}O_4$, $Li_{0.25}Mg_{0.40}Ni_{0.10}Fe_{2.25}O_4$ and $Li_{0.30}Mg_{0.40}Fe_{2.30}O_4$ ferrites increases with increasing sintering temperature up to 1100˚C, then decreases. On the other hand, porosity *(P)* of the samples decreases with increasing sintering temperature up to 1100˚C and a increasing trend is shown beyond it. At higher sintering temperatures density decreases, because the intragranular porosity increases as a result of discontinuous grain growth that leads to decrease the sintered density.

**pdfMachine**
**A pdf writer that produces quality PDF files with ease!**
Produce quality PDF files in seconds and preserve the integrity of your original documents. Compatible across nearly all Windows platforms, if you can print from a windows application you can use pdfMachine.
Get yours now!

- As sintering temperature goes higher, enlargement of grain occurs in $Li_xMg_{0.4}Ni_{0.6-2x}Fe_{2+x}O_4$ ferrites. The thermal energy generates a force that drives the grain boundaries to grow over pores and reinforces to increase the grain diameter.

- The real ($\mu_i^{/}$) and imaginary ($\mu_i^{//}$) permeability increase with $Li^{1+}$ substitution up to $x$=0.25 in $Li_xMg_{0.4}Ni_{0.6-2x}Fe_{2+x}O_4$ ferrite and after that they decrease. With the increase of sintering temperature the real part of initial permeability $\mu_i^{/}$ increases up to 1100˚C and above 1100˚C a decreasing trend is observed. In contrast resonance frequency found to decrease with *Li* substitution. Larger grains tend to consist of a large number of domain walls. The initial permeability increases with grain size. *DC* magnetization value varying to *Li* content increases up to $x$= 0.25 and start to decrease at $x$=0.30.Since $\mu_i^{/}$ is a function of magnetization therefore, $\mu_i^{/}$ increases with the increase of *Li* content up to $x$= 0.25 and beyond $x$ = 0.25, $\mu_i^{/}$ decreases due to the non collinear spin arrangements.

- It is found that resonance frequency is shifted from higher value to lower value as sintering temperature increases for all samples. The maximum value of $f_r$ (58.82 MHz) is observed for $Li_{0.05}Mg_{0.40}Ni_{0.50}Fe_{2.05}O_4$ ferrite sintered at 1100˚C.

- The loss factor, tanδ is observed to increase with the increase of sintering temperature. The increase in sintering temperature results in increased *Li* loss in the samples, thereby creating defects in the lattice, which gives rise to magnetic loss. Highest value of *Q-factor* is observed for various $Li_xMg_{0.4}Ni_{0.6-2x}Fe_{2+x}O_4$ ferrites sintered at 1100˚C and among these, maximum *Q-factor* (*Q* value=4653) is found for $Li_{0.25}Mg_{0.40}Ni_{0.10}Fe_{2.25}O_4$ ferrite, similar to $\mu_i^{/}$. *Q-factor* is found to decrease for particular contents above 1100˚C because at higher sintering temperature abnormal grain growth occurs, which creates trapped pores inside the grain. This increasing amount of pores influences the loss factor and turns into higher value which results a lower value of *Q-factor*.

- From magnetization as a function of applied magnetic field, (*M-H)* curve, it is clear that at room temperature the polycrystalline $Li_xMg_{0.4}Ni_{0.6-2x}Fe_{2+x}O_4$ ferrites

**pdfMachine**
**A pdf writer that produces quality PDF files with ease!**
Produce quality PDF files in seconds and preserve the integrity of your original documents. Compatible across nearly all Windows platforms, if you can print from a windows application you can use pdfMachine.
Get yours now!

are in ferrimagnetic state. The saturation magnetization, $M_s$, as well as the number of Bohr magnetron, $\mu_B$ of $Li_xMg_{0.4}Ni_{0.6-2x}Fe_{2+x}O_4$ ferrites, increases linearly with increasing *Li* content. On the basis of cations distribution and exchange interaction between A and B sites this phenomenon is explained. The possible cations distribution in $Li_xMg_{0.4}Ni_{0.6-2x}Fe_{2+x}O_4$ ferrites is a mixed spinel type with a general formula $(Fe^{3+}{}_{0.9})_A\ [Li^{1+}{}_xMg^{2+}{}_{0.4}Ni_{0.6-2x}\ Fe^{3+}{}_{1.1+x}]_B$, where the parentheses ( ) and the square brackets [ ] indicate ions distributed on tetrahedral A and octahedral B sites, respectively. The saturation magnetization is given by the vector sum of the magnetic moments of the individual A and B sub-lattices i.e. $M_S = M_B - M_A$. As a result of substitution, it was observed that the saturation magnetization increases as the *Li* content increases Therefore, the $M_B$ will increase as a result of substitution. Hence the net magnetic moment is increased. On the other hand the saturation magnetization as well as the number of Bohr magnetron, $\mu_B$ increases with increasing of content for all the compositions. This result is expected because there is evidence from the grain size. The magnetization caused by domain wall movement requires less energy than that required by domain rotation. From the microstructures, it is observed that the average grain size increases with increasing Li contents. So the number of walls increases with increasing the grain sizes and this wall movement contributes to enhance the magnetization.

## 5.2 Suggestions for future work

It was found that among the $Li_xMg_{0.4}Ni_{0.6-2x}Fe_{2+x}O_4$ ferrites $Li_{0.25}Mg_{0.40}Ni_{0.10}Fe_{2.25}O_4$ had the maximum permeability $\mu_i'$ *and* maximum *Q*-factor. So *Zn* and other Metals which prefers A sublattice to occupy, can be substituted in $Li_{0.25}Mg_{0.40}Ni_{0.10}Fe_{2.25}O_4$ ferrite to enhance the permeability value. Sintering additives like $Bi_2O_3$ and $V_2O_5$ can be mixed to promote densification and getting better result in lower sintering temperatures to magnetic materials.

**pdfMachine**
**A pdf writer that produces quality PDF files with ease!**
Produce quality PDF files in seconds and preserve the integrity of your original documents. Compatible across nearly all Windows platforms, if you can print from a windows application you can use pdfMachine.
Get yours now!

# ABSTRACT

A series of polycrystalline spinel type ferrites with the nominal composition $Li_xMg_{0.4}Ni_{0.6-2x}Fe_{2+x}O_4$, where $x$ = 0.0 to 0.3 in steps of 0.05, has been investigated thoroughly. The samples are fabricated using conventional solid state reaction technique. Pellet and toroid shaped samples are prepared from each composition and sintered at temperatures of 1050, 1100,1150 and 1200˚C in air for 6 hours. Structural and surface morphology are studied by x-ray diffraction technique and high resolution optical microscopy, respectively. The *AC* magnetic properties of these ferrites are characterized by high frequency (300 *kHz*-110 *MHz*) complex permeability measurements. *DC* magnetizations of all samples are measured by Vibrating Sample Magnetometer (VSM). The influence of microstructure, various cation substitution and sintering temperatures on the complex permeability of above mentioned ferrites are discussed. A possible correlation among sintering temperature, average grain size and density is also discussed.

It is noticeable that X-ray diffraction patterns of all samples show the formation of spinel crystal structure. Lattice parameters are calculated using the Nelson Riley function. The lattice constants increase linearly with the increase of Li content, obeying Vegard's law. This result is explained with the help of ionic radii of substituted cations. The microstructural study shows that both sintering temperatures and cations substitutions have great influence on the average grain size. In $Li_xMg_{0.4}Ni_{0.6-2x}Fe_{2+x}O_4$ ferrites the real part of initial permeability, $\mu_i'$ and saturation magnetization, $M_s$, increase with the increase of *Li* content up to $x$= 0.25 and beyond $x$= 0.25, both $\mu_i'$ and $M_s$ decrease. The decrease of $\mu_i'$ and $M_s$ beyond x= 0.25 indicate the possibility of noncollinear spin canting effect. It is also found that $\mu_i'$ increases with increasing average grain size of the samples. It is also observed that $\mu_i'$ increases with sintering temperatures for all ferrites because high sintering temperature performs uniform grain growth. Highest value of $\mu_i'$ and *Q-factor* is observed for various $Li_xMg_{0.4}Ni_{0.6-2x}Fe_{2+x}O_4$ ferrites sintered at 1100˚C and among these, highest $\mu_i'$ ($\mu_i'$=66 ) and maximum *Q-factor* (*Q* value=4653) is found for $Li_{0.25}Mg_{0.40}Ni_{0.10}Fe_{2.25}O_4$, ferrite. From DC magnetization data it is found that $Li_{0.25}Mg_{0.40}Ni_{0.10}Fe_{2.25}O_4$ ferrite has maximum saturation magnetization value among $Li_xMg_{0.4}Ni_{0.6-2x}Fe_{2+x}O_4$ ferrites.

**pdfMachine - is a pdf writer that produces quality PDF files with ease!**
**Get yours now!**
"Thank you very much! I can use Acrobat Distiller or the Acrobat PDFWriter but I consider your product a lot easier to use and much preferable to Adobe's" A.Sarras - USA

## CANDIDATE'S DECLARATION

*It is hereby declared that this thesis or any part of it has not been submitted elsewhere for the award of any degree or diploma.*

MD. ABDUR RAHMAN

**pdfMachine - is a pdf writer that produces quality PDF files with ease!**
**Get yours now!**
"Thank you very much! I can use Acrobat Distiller or the Acrobat PDFWriter but I consider your product a lot easier to use and much preferable to Adobe's" A.Sarras - USA

**BANGLADESH UNIVERSITY OF ENGINEERING & TECHNOLOGY**
**DEPARTMENT OF PHYSICS, DHAKA 1000, BANGLADESH**

# CERTIFICATION OF THESIS

The thesis titled "Study of magnetic properties of $Li_xMg_{0.4}Ni_{0.6-2x}Fe_{2+x}O_4$ ferrites" submitted by **Md. Abdur Rahman**, Roll No.: 040814004F, Session: April 2008, has been accepted as satisfactory in partial fulfillment of the requirement for the degree of **Master of Philosophy** in Physics on November 29, 2010.

## BOARD OF EXAMINERS

| | | |
|---|---|---|
| 1. | (_____)<br>Dr. A. K. M. Akther Hossain (Supervisor)<br>Professor, Department of Physics,<br>BUET, Dhaka-1000,Bangladesh. | Chairman |
| 2. | (_____)<br>Head, Department of Physics,<br>BUET, Dhaka-1000, Bangladesh. | Member |
| 3. | (_____)<br>Dr. Md. Mostak Hossain,<br>Professor, Department of Physics,<br>BUET, Dhaka-1000, Bangladesh. | Member |
| 4. | (_____)<br>Dr. Md. Rafi Uddin,<br>Assistant Professor, Department of Physics,<br>BUET, Dhaka-1000, Bangladesh. | Member |
| 5. | (_____)<br>Dr. Md. Tofazzal Hossain<br>Director, Planning and Development<br>BCSIR, Dhaka-1205, Bangladesh. | Member<br>(External) |

**pdfMachine - is a pdf writer that produces quality PDF files with ease!**
**Get yours now!**
"Thank you very much! I can use Acrobat Distiller or the Acrobat PDFWriter but I consider your product a lot easier to use and much preferable to Adobe's" A.Sarras - USA

*DEDICATED TO*

*MY*

*BELOVED PARENTS*

**pdfMachine**

**A pdf writer that produces quality PDF files with ease!**

Produce quality PDF files in seconds and preserve the integrity of your original documents. Compatible across nearly all Windows platforms, simply open the document you want to convert, click “print”, select the “Broadgun pdfMachine printer” and that’s it! Get yours now!

# CONTENTS




**pdfMachine**

**Is a pdf writer that produces quality PDF files with ease!**

Produce quality PDF files in seconds and preserve the integrity of your original documents. Compatible across nearly all Windows platforms, if you can print from a windows application you can use pdfMachine.

Get yours now!

# CHAPTER 3

## SAMPLE FABRICATION, CHARACTERIZATION AND EXPERIMENTAL TECHNIQUES 48-59



**pdfMachine**
**Is a pdf writer that produces quality PDF files with ease!**
Produce quality PDF files in seconds and preserve the integrity of your original documents. Compatible across nearly all Windows platforms, if you can print from a windows application you can use pdfMachine.
Get yours now!

**pdfMachine**

**Is a pdf writer that produces quality PDF files with ease!**

Produce quality PDF files in seconds and preserve the integrity of your original documents. Compatible across nearly all Windows platforms, if you can print from a windows application you can use pdfMachine.

Get yours now!

# LIST OF FIGURES




**pdfMachine**

**A pdf writer that produces quality PDF files with ease!**

Produce quality PDF files in seconds and preserve the integrity of your original documents. Compatible across nearly all Windows platforms, simply open the document you want to convert, click "print", select the "Broadgun pdfMachine printer" and that's it! Get yours now!

**pdfMachine**

**A pdf writer that produces quality PDF files with ease!**

Produce quality PDF files in seconds and preserve the integrity of your original documents. Compatible across nearly all Windows platforms, simply open the document you want to convert, click “print”, select the “Broadgun pdfMachine printer” and that’s it! Get yours now!

**pdfMachine**
**A pdf writer that produces quality PDF files with ease!**
Produce quality PDF files in seconds and preserve the integrity of your original documents. Compatible across nearly all Windows platforms, simply open the document you want to convert, click "print", select the "Broadgun pdfMachine printer" and that's it! Get yours now!

**pdfMachine**
**A pdf writer that produces quality PDF files with ease!**
Produce quality PDF files in seconds and preserve the integrity of your original documents. Compatible across nearly all Windows platforms, simply open the document you want to convert, click “print”, select the “Broadgun pdfMachine printer” and that’s it! Get yours now!

# LIST OF SYMBOLS AND ABBREVIATIONS

| | |
|---|---|
| $AC$ | Alternating current |
| $B$ | Magnetic induction |
| $CMR$ | Colossal magnetoresistance |
| $F(\theta)$ | Nelson-Riley function |
| $f_r$ | Resonance frequency |
| $g$ | Landé splitting factor |
| $H_{cr}$ | Critical field |
| $J$ | Exchange integral |
| $K$ | Total anisotropy |
| $K_1$ | Magnetocrystalline anisotropy constant |
| $L_s$ | Self-inductance of the sample core |
| $L_o$ | Inductance of the winding coil without sample |
| $M$ | Magnetization |
| $M_s$ | Saturation magnetization |
| $N_A$ | Avogadro's number |
| $P$ | Porosity |
| $P_{intra}$ | Intragranular porosity |
| $P_{inter}$ | Intergranular porosity |
| $P_e$ | Eddy-current loss |
| $Q$ | Relative quality factor |
| $T_c$ | Curie temperature |
| $T_n$ | Néel temperature |
| $T_s$ | Sintering temperature |
| $tan\delta$ | Loss factor |
| $Z$ | Complex impedance |
| $\alpha$ | Restoring force coefficient |
| $\beta$ | Viscous damping factor |
| $\gamma$ | Domain wall energy |
| $\omega$ | Angular velocity |
| $\delta_w$ | Domain wall thickness |
| $\mu_i$ | Initial permeability |
| $\mu'$ | Real part of complex permeability |
| $\mu''$ | Imaginary part of complex permeability |
| $\mu_B$ | Bohr magneton |
| $\chi_{spin}$ | Intrinsic rotational susceptibility |
| $\chi_w$ | Domain wall susceptibility |

**pdfMachine - is a pdf writer that produces quality PDF files with ease!**
**Get yours now!**
"Thank you very much! I can use Acrobat Distiller or the Acrobat PDFWriter but I consider your product a lot easier to use and much preferable to Adobe's" A.Sarras - USA

# LIST OF TABLES




**pdfMachine - is a pdf writer that produces quality PDF files with ease!**
**Get yours now!**
"Thank you very much! I can use Acrobat Distiller or the Acrobat PDFWriter but I consider your product a lot easier to use and much preferable to Adobe's" A.Sarras - USA